Utah State University

DigitalCommons@USU

All Graduate Theses and Dissertations | Graduate Studies

12-2009

Quantifying Surface Water and Groundwater Interactions in a High-Gradient Mountain Stream for Solute Transport

Noah M. Schmadel
Utah State University

Follow this and additional works at: https://digitalcommons.usu.edu/etd

 Part of the Environmental Engineering Commons

Recommended Citation

Schmadel, Noah M., "Quantifying Surface Water and Groundwater Interactions in a High-Gradient Mountain Stream for Solute Transport" (2009). *All Graduate Theses and Dissertations*. 486.
https://digitalcommons.usu.edu/etd/486

This Thesis is brought to you for free and open access by the Graduate Studies at DigitalCommons@USU. It has been accepted for inclusion in All Graduate Theses and Dissertations by an authorized administrator of DigitalCommons@USU. For more information, please contact digitalcommons@usu.edu.

QUANTIFYING SURFACE WATER AND GROUNDWATER INTERACTIONS IN A HIGH-GRADIENT MOUNTAIN STREAM FOR SOLUTE TRANSPORT

by

Noah M. Schmadel

A thesis submitted in partial fulfillment
of the requirements for the degree

of

MASTER OF SCIENCE

in

Civil and Environmental Engineering

Approved:

Bethany T. Neilson Major Professor	David K. Stevens Committee Member
Tamao Kasahara Committee Member	Byron R. Burnham Dean of Graduate Studies

UTAH STATE UNIVERSITY
Logan, Utah

2009

Copyright © Noah M. Schmadel

All Rights Reserved

ABSTRACT

Quantifying Surface Water and Groundwater Interactions in a High-Gradient Mountain Stream for Solute Transport

by

Noah M. Schmadel, Master of Science

Utah State University, 2009

Major Professor: Bethany T. Neilson
Department: Civil and Environmental Engineering

A study reach in a mountain stream highly influenced by groundwater was selected to test common data collection strategies used to characterize and quantify groundwater exchange processes necessary to predict solute transport. The data types collected include: high frequency discharge estimates with the use of rating curves, dilution gauging techniques with instantaneous tracer experiments, groundwater table and stream water surface elevations, vertical head gradients, and hydraulic conductivity estimates. The first two data types were categorized as stream gauging and the remaining three data types as site characterization. The stream gauging data were used to quantify net changes in stream discharge at a reach scale with rating curve predictions and dilution gauging. Each method resulted in opposite net changes at this scale. An error analysis regarding rating curve predictions and dilution gauging suggested that neither method detected groundwater exchange at this scale due to discharge estimates being statistically

the same. The error in rating curve predictions was estimated using a 95% joint confidence region of model parameters and the error in dilution gauging was estimated using a first order error analysis. Dilution gauging was also performed at a sub-reach scale to quantify net changes and indicated the groundwater exchange was highly spatially variable, which was not concluded at the reach scale. To quantify a water balance more representative of the exchanges occurring, gross gains and gross losses were quantified by measuring tracer mass recoveries and were found to occur in every sub-reach. However, the error analysis concluded that nearly half of the changes were not significant, which emphasized the importance of quantifying error in stream gauging techniques used to understand surface water-groundwater interactions.

The site characterization data were used to test and verify the water balance results by providing information regarding general trends and spatial variability of surface water-groundwater interactions. This study proved that one data type is not adequate to clearly characterize and quantify surface water-groundwater interactions and researchers must exercise caution when interpreting results from different data types at varying spatial scales.

(189 pages)

ACKNOWLEDGMENTS

I would like to sincerely thank my advisor, Dr. Bethany Neilson, for all her guidance, support, and patience towards my research and education despite her remarkably demanding schedule. You have been a great mentor that has made this work possible. I would also like to thank my committee member, Dr. David Stevens, for his review of my proposal and thesis and for all his expert suggestions. Your support both inside and outside the classroom has invaluably shaped my perspective of research and approach to solving problems. Special thanks to my other committee member, Dr. Tamao Kasahara, for her suggestions, help with field work, and detailed review of my thesis. Others who assisted greatly in the efforts of data collection and discussions include Quin Bingham, Jonathan Bingham, and Andrew Hobson. Thanks to Oscar Marquina, Cami Lyman, and Emily Saad for their help with data collection and to Dr. Jeff Horsburgh for help with equipment troubleshooting and loans. Thanks to Dr. Kenneth Bencala for your helpful research suggestions and collaboration. Thanks to the UDWR and the Hardware Ranch manager, Dan Christensen, for their support and allowing us to conduct research on their management area. Special thanks to the Utah Water Research Laboratory for funding this research and providing me with the opportunity to conduct research on a beautiful mountain stream for this thesis.

Most notably, I would like to thank my family and friends for all their love and support throughout my life. Immense thanks to my kind mother for all your sacrifices made to raise me and to my father for shaping my views and work habits. Their thoughts and prayers throughout my life have made all my progress possible.

Noah M. Schmadel

CONTENTS

LIST OF TABLES

LIST OF FIGURES

CHAPTER 1

INTRODUCTION

Our understanding of the movement and identification of pollutants in the environment continually evolves as new concerns emerge and new theories are developed. Pollutants in the environment are generally defined as substances resulting in health risks to humans, animals, plants, or ecosystems whether sources are connected to human activity or natural processes [*Ramaswami et al.,* 2005]. Pollutants in the environment undergo complex transport and transformation processes depending on physical, chemical, and biological characteristics of a specific system, as well as the chemical composition and molecular structure of a particular pollutant. To better understand the fate and transport of pollutants and the impacts of anthropogenic activities, conceptual and corresponding mathematical models have been developed by scientists and engineers that aid in predicting changes to environmental processes that might occur as a response to human activities [*Ramaswami et al.*, 2005]. In order to use mathematical models for policy development and implementation of appropriate management strategies for environmental quality, field and laboratory studies are often required.

Progress in understanding the transformation and transport processes of pollutants in hydrological systems has been made in past decades. However, the need to better our understanding of these processes becomes more necessary as our demand for safe surface water and groundwater continually grows. Although many types of processes can be equally important to consider in these systems including rivers, streams, and aquifers, this thesis research focuses on physical processes influencing stream pollutant transport. The

dominant physical processes that control the mass movement of a stream solute (any substance that is transported by flowing waters) include bulk stream transport (advection), dispersion, transient storage, and groundwater exchange. Better understanding of how these physical processes influence solute transport is important because of their role in biogeochemical processes [*Harvey and Wagner*, 2000; *Payn et al.*, 2008] that affect water quality and therefore, water uses.

Bulk stream transport (advection) processes are characterized by the concurrent fluid movement in one-direction causing a mass flux driven by the solute concentration gradient and velocity of the bulk fluid movement [*Weber and DiGiano*, 1996]. These processes are commonly estimated by kinematic wave models that simulate dynamic water movement in streams in the simplest form and are developed by combining the advection mass-balance of a stream with Manning's equation, resulting in a mass balance for a conservative solute with time-varying flow [*Chapra*, 1997]. These models typically neglect the effects of other physical processes such as dispersion, transient storage, and groundwater exchange.

Dispersion is caused by small scale mixing that decreases the solute concentration in the water column [*Runkel and Bencala*, 1995]. Solute concentrations in rivers and streams related to advection and dispersion are commonly represented by one-dimensional advection-dispersion models based on conservation of mass and the assumption of a uniform channel with constant flow [*Stream Solute Workshop*, 1990].

While advection and dispersion are the most dominant physical processes affecting solute transport in rivers and streams [*Runkel and Bencala*, 1995], there are other important physical processes that influence solute transport. In past decades,

researchers began looking more thoroughly into the effects of transient storage on solute transport [*Bencala and Walters*, 1983; *Harvey et al.*, 1996; *Runkel and Bencala*, 1995; *Wagner and Harvey*, 1997]. Transient storage is defined as the combined solute storage in the dead zones and hyporheic zone of streams that undergo mass flux with the main channel flow. *Bencala and Walters* [1983] define the dead zones as turbulent eddies, slow moving water relative to the main stream flow, or side pockets that retard main stream flow. Additionally, they define the hyporheic zone as the space where surface water flows into, out of, and through the substrate. *Harvey et al.* [1996] further characterized hyporheic exchange as a streambed flux that occurs in small exchange paths (centimeter to meter) with a timescale of minutes. Later research recognized that the length of hyporheic flow paths range from centimeters to hundreds of meters with substantially different exchange timescales [*Harvey and Wagner*, 2000]. However, it is typically defined as occurring in small exchange paths. In this research, due to residence times of flow paths being highly spatially dynamic, hyporheic exchange is divided into two main types: (1) short flow paths (centimeter to meter exchange paths with residence times of seconds to minutes) and (2) long flow paths (exchange paths of several meters with residence times of hours to days). The reason for the separation is due to long hyporheic flow paths appearing to be a stream loss at the spatial and temporal scale of consideration, but may return to the stream several meters downstream.

To account for transient storage on solute transport, a single lumped transient storage zone has been typically added to the one-dimensional advection-dispersion model assuming first order mass transfer. The combination of mass balances accounting for these physical processes are often referred to as the Transient Storage Model (TSM)

[*Bencala*, 2005; *Ruehl et al.*, 2006; *Schmid*, 2004]. This single storage zone concept assumes one exchange rate to describe both the dead zone and hyporheic zone exchange. Parameter estimation is required for these types of models and is typically performed through stream tracer experiments [*Bencala and Walters*, 1983; *Bencala*, 2005; *Harvey et al.*, 1996; *Wagner and Harvey*, 1997].

Separating the effects of dead zone and hyporheic zone exchange processes on solute transport has been determined to be important due to exchange rates and residence times being substantially different [*Choi et al.*, 2000; *Harvey et al.*, 2005; *Neilson et al.*, 2009a, 2009b, 2009c] resulting in variability in the biogeochemistry [e.g., *Findlay*, 1995; *Payn et al.*, 2008]. *Harvey and Wagner* [2000] confirmed this by finding that storage parameters determined with a one-zone storage model could not be transferred to longer reaches or other flow conditions due to differences in residence times in dead zones and the hyporheic zone. In later research, *Harvey et al.* [2005] recognized the variability in hyporheic flow paths and residence times and used a two-zone modeling approach in wetlands to separate hyporheic exchange into slow exchange and fast exchange. Similarly, *Choi et al.* [2000], *Neilson et al.* [2009a], *Neilson et al.* [2009c], and *Briggs et al.* [2009] used a two-zone modeling approach to separate these processes. However, instead of considering fast and slow exchange, these two-zone models separated out surface (dead zones) and subsurface (hyporheic zone) storage zone exchange processes. *Choi et al.* [2000] used a Monte Carlo analysis of 500 data sets of storage parameters and concluded that the lumped effects with a single storage compartment could reliability characterize the dominant physical processes in most cases (>90%). *Briggs et al.* [2009] and *Neilson et al.* [2009a] collected data in the main channel and dead zones following

solute tracer experiments in order to assist in separating out the effects of each zone. Both studies concluded that the effects of surface and subsurface storage zones need to be quantified separately.

Other than the effects of advection, dispersion, and transient storage on solute transport, many rivers and streams are additionally influenced by lateral inflows from groundwater discharge. To address the effects of these processes on solute transport, the advection-dispersion model with the transient storage added an additional term representing lateral inflows [*Gooseff and McGlynn*, 2005; *Runkel and Bencala*, 1995]. The conceptual TSM with lateral inflow is widely implemented through use of the U.S. Geological Survey modeling code OTIS (One-dimensional Transport with Inflow and Storage) to represent stream and transient storage solute transport where the parameter of lateral inflow is also often calibrated with stream tracer experiments [*Bencala*, 2005; *Runkel*, 1998; *Wagner and Harvey*, 1997]. In some applications, losses to groundwater recharge are neglected. However, *Harvey and Wagner* [2000] estimated groundwater recharge in OTIS by simultaneously considering differential volumetric flow data and tracer experiments.

While these modeling approaches may provide an initial understanding of groundwater exchange, the complexity and extent of these effects are poorly understood and difficult to predict and measure [*Winter et al.*, 1998]. Exchange between stream water and the subsurface system can have flow paths ranging in much larger scales (hundreds of meters) and larger retention time scales (hours to years) than hyporheic flow paths. *Covino and McGlynn* [2007] demonstrated stream water-groundwater interactions can be highly dynamic both spatially and temporally and play an important role in

understanding the impacts on stream solute interactions. *Winter et al.* [1998] describe surface water-groundwater in such systems as being a single resource since they are continuously interconnected. This understanding is important because altering either surface water or groundwater will have a direct effect on the other. Therefore, quantifying groundwater exchange processes are also essential to accurately predict their effects on solute transport.

A variety of approaches have been used to better understand groundwater exchange processes affecting mass movement in a river of stream and include: stream gauging with velocity-area techniques [*Rantz*, 1982], tracer experiments [*Harvey and Wagner*, 2000; *Harvey et al.*, 2005; *Payn et al.*, 2009], hydraulic head from groundwater observation wells and main channel piezometers [*Harvey et al.*, 1996; *Jencso et al.*, 2009], instream vertical head gradients and hydraulic conductivity estimates [*Baxter et al.*, 2003; *Landon et al.*, 2001], stream temperature surveys [*Becker et al.*, 2004; *Kerry et al.*, 2007], or hydrograph separation with isotopic tracer techniques [*Cey et al.*, 1998; *Covino and McGlynn*, 2007].

Stream gauging with velocity-area techniques are often correlated to stage data to develop rating curves used to obtain high frequency stream discharge estimates from continuous stage data [*Kennedy*, 1983]. These data are often used in differential gauging to measure stream net gains and losses. Additionally, dilution gauging completed with tracer experiments can be used to provide groundwater exchange information by quantifying a stream water balance in terms of gains and losses [*Harvey and Wagner*, 2000; *Payn et al.*, 2009]. The error in each discharge estimate with the velocity-area

technique is often reported as 15% [*Cey et al.*, 1998] and for rating curve predictions it is often the residual standard error [*Kennedy*, 1983].

Stream temperature surveys provide reliable information on groundwater influxes, but cannot be used to quantify groundwater recharge [*Becker et al.*, 2004] and may not be appropriate for completing an accurate water balance. Hydrograph separation with isotopic tracer techniques are often used to quantify groundwater inflow to stream water by measuring isotopic concentrations in groundwater, stream water, and storm water. Although, these concentrations must be significantly different to quantify groundwater inflow [*Cey et al.*, 1998].

To quantify surface water-groundwater interactions, a complete water balance is required and can be estimated with accurate discharge measurements. A system water and mass balance assists in model parameter calibration, provides information on flow path residence times, and includes accounting for lateral groundwater discharge, groundwater recharge, and hyporheic exchange as shown by Equation 1-1 [*Harvey and Wagner*, 2000].

$$\frac{dQ}{dx} = q_{L,in} + q_{h,in} - q_{L,out} - q_{h,out} \tag{1-1}$$

where:
Q = the main channel volumetric flow, L s^{-1};
x = longitudinal main channel length in the downstream direction, m;
$q_{L,in}$ = groundwater influx per longitudinal length, L s^{-1} m^{-1};
$q_{h,in}$ = influxes due to hyporheic flow paths, L s^{-1} m^{-1};
$q_{L,out}$ = groundwater recharge (stream loss) per longitudinal length, L s^{-1} m^{-1};
$q_{h,out}$ = outfluxes due to hyporheic flow paths, L s^{-1} m^{-1}.

To better apply this equation, gains and losses throughout a reach must be quantified and the variability over both space and time must be considered. Surface water-groundwater interaction studies have often focused on large spatial scales (several kilometers) [*Covino and McGlynn*, 2007; *Ruehl et al.*, 2006]. However, *Payn et al.* [2009] recently found significant exchanges occurring at much smaller scales (200 m) and, quantified net changes in stream discharge at this scale with dilution gauging techniques. Additionally, to estimate a water balance more representative of exchanges occurring, they quantified gross gains and gross losses by measuring tracer mass recoveries within each reach. Error was not addressed in this research, but is important in order to determine the reliability in water balance estimates. In other dilution gauging studies, error was reported as 10% [*Harvey et al.*, 2003] based on model simulations, but the sources and contributions of the error are currently poorly understood. A better understanding of the components of error in measurements used to quantify a water balance will assist in appropriate experimental design and a reduction of bias in interpretations.

With this understanding, the dominant physical processes affecting solute transport in a mountain stream used for a case study in this research are: bulk stream transport, dispersion, dead zone exchange, hyporheic zone exchange, and groundwater exchange (Figure 1-1).

Although quantifying each of these physical processes individually is important to accurately predict solute mass movement, this research focuses on quantifying groundwater exchange. Researchers have used a variety of approaches to better

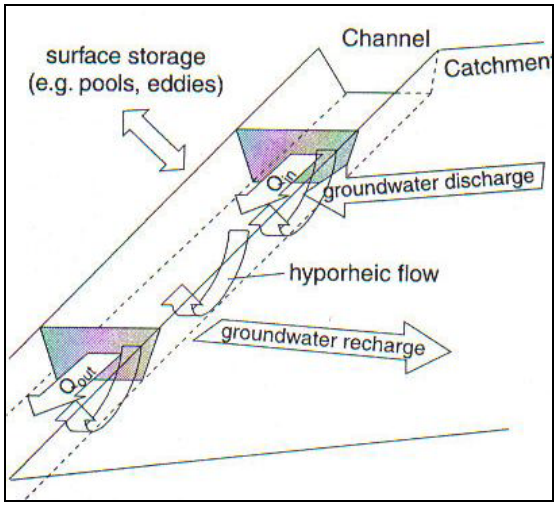

Figure 1-1. Diagram (not to scale) of dominant stream physical processes [*Harvey et al.*, 1996].

understand groundwater exchange; however, often one particular data type and spatial scale have been used.

This research tests the utility and reliability of some common data collection strategies used to quantify and characterize these processes through comparative and uncertainty analyses. This study investigates whether conclusions made from one data type are appropriate and the importance of the spatial scale of consideration in which data are collected.

The common data types collected in this research are: stream gauging using rating curves, dilution gauging with instantaneous tracer experiments, groundwater table and stream water surface elevations, vertical head gradients, and hydraulic conductivity estimates. With rating curves and tracer experiments, net changes in stream discharge were quantified at a reach scale (~500 m) to compare results from two stream gauging approaches. Additionally, a water balance in terms of gross gains and gross losses was quantified at a sub-reach scale (~60 m) similar to *Payn et al.* [2009] to provide information at a finer spatial scale and compare to the reach scale results. Components of

error in these types of calculations were not well understood and therefore, were quantified in detail with a first order error analysis to determine the reliability of this approach to detect significant changes associated with groundwater exchange processes. The remaining data types (groundwater table and stream water surface elevations, vertical head gradients, and hydraulic conductivity estimates) were collected to further investigate the reliability of water balance calculations to capture the complexities of groundwater exchange processes.

This thesis is composed of individual papers that provide details regarding: data collection results and conclusions (Chapter 3 – Data Collection Strategy to Support and Test Water Balance Calculations); and estimated uncertainty in the water balance calculations (Chapter 4 – Uncertainty in Stream Water Balances).

CHAPTER 2

PROJECT BACKGROUND AND OBJECTIVES

This thesis research evolved from the research conducted by *Neilson* [2006] on the Virgin River, a desert river in southern Utah. *Neilson et al.* [2009a], *Neilson et al.* [2009b], and *Neilson et al.* [2009c] developed a two-zone temperature and solute transport model that separates transient storage into surface and subsurface zones. This model approximates energy and mass fluxes in two zones versus one-zone models that lump the effects of transient storage (e.g., OTIS). *Neilson et al.* [2009a] conducted solute tracer experiments and collected data in each zone on the Virgin River to estimate parameters that correspond to storage mechanisms and exchange rates of surface and subsurface storage separately. To test this data collection strategy to measure physical transport processes separately over a broader range of applications (e.g., mountain streams), a portion of Curtis Creek, located in northern Utah, was selected.

This study reach selected is approximately 1.25 km in length and is located near the outlet of the watershed (Figure 2-1) that drains approximately 59.5 square kilometers [*U.S. Geological Survey*, 2007]. The reach is located at Hardware Ranch, a Utah Division of Wildlife Resources (UDWR) operated facility, located approximately 15 miles east of Hyrum, UT. Curtis Creek is a first order perennial stream with ephemeral (seasonal) tributaries during storm and snow melt events. Curtis Creek is a mountain stream tributary to the Blacksmith Fork River which flows into Cutler Reservoir and ultimately the Great Salt Lake.

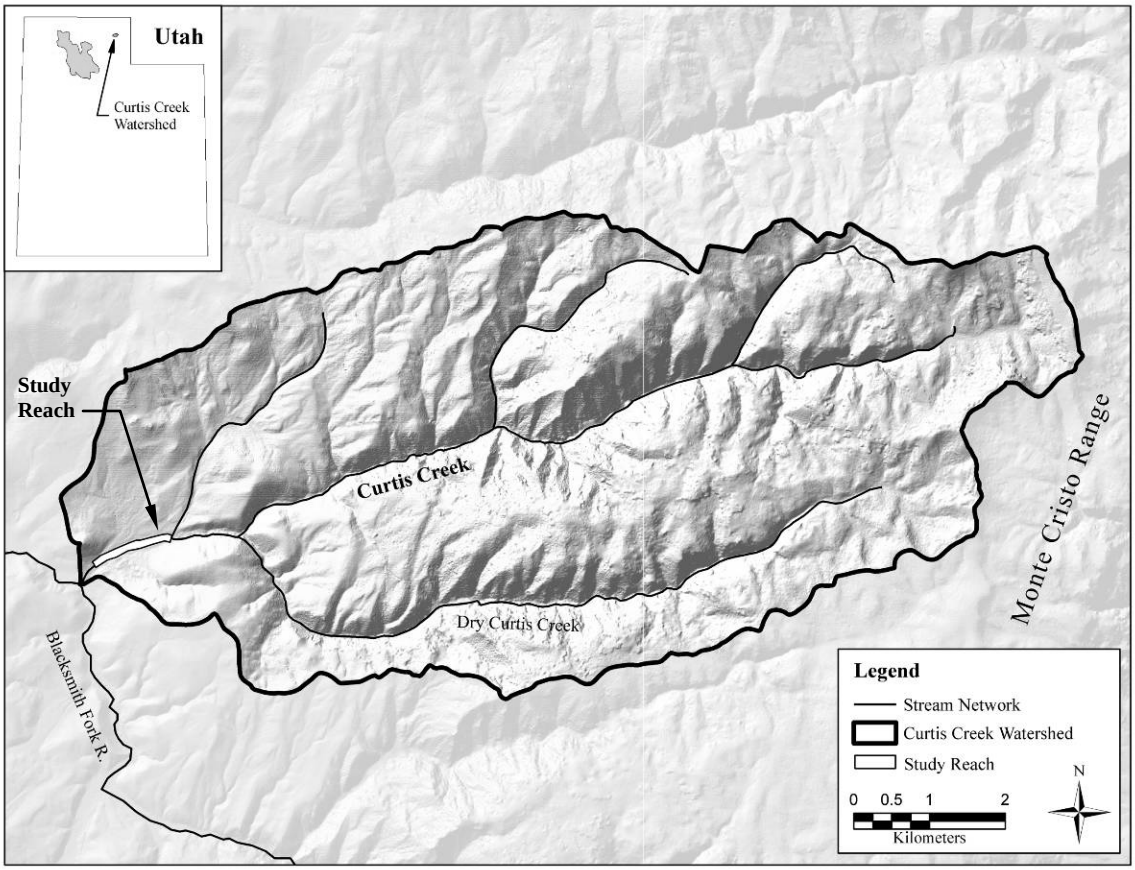

Figure 2-1. Curtis Creek watershed [*U.S. Geological Survey*, 2007] and study reach location. The 5 meter digital elevation model [*Kelson*, 2007] is shown for general topography.

Many of the solute tracer data collection techniques outlined by *Neilson et al.* [2009a] and *Neilson et al.* [2009b] were applied to the selected portion of Curtis Creek, a system with drastically different physical and chemical characteristics. For example, the portion of the Virgin River studied was predominately sand substrate with low gradient bottom slopes (0.001 to 0.004) and minimal groundwater influx. The study portion of Curtis Creek has relatively high gradients (0.010 to 0.032), coarse gravel to large cobble substrate with little sand, and is highly influenced by groundwater exchange. Similar to the data collected by *Neilson et al.* [2009a] and *Neilson et al.* [2009b], solute tracer experiments were performed and samples were collected in the main channel, but given

the different system characteristics, it was determined that additional data collection techniques needed to be developed to more accurately quantify surface water-groundwater exchanges in high gradient systems through a system water balance.

It was found that the effects and dynamics of solute transport in this mountain stream are highly influenced by groundwater exchange processes and therefore, mass movement is challenging to accurately quantify and predict. Based on the general physical characteristics of the study reach and the lack of understanding of groundwater exchange processes in this system, the following research objectives were developed:

1) Implement a data collection strategy for groundwater influenced streams to support and test water balance calculations.
2) Quantify an overall water balance of the entire study reach.
3) Determine the reliability of the water balance calculations.

CHAPTER 3

DATA COLLECTION STRATEGY TO SUPPORT AND TEST WATER BALANCE CALCULATIONS

Abstract

Surface water-groundwater interactions are often poorly understood because they are challenging to predict and measure. However, these interactions must be accurately quantified in order to understand solute mass movement in rivers and streams. This paper describes a comprehensive data collection strategy used to perform water balance calculations and to provide supporting information regarding the groundwater exchange in a study reach highly influenced by groundwater. The specific data types collected were lumped into two main categories: (1) stream gauging and (2) site characterization data. The stream gauging data include discharge estimates using rating curves at a reach scale (515 m and 560 m) and using dilution gauging techniques at a reach and sub-reach scale (lengths ranging from 56 m to 120 m). These data were used to quantify a net water balance through differential gauging to describe groundwater exchange at the two spatial scales. Comparing these two approaches at the reach scale provided conflicting results in terms of net changes. At the sub-reach scale, stream discharge was approximated to have net changes ranging from 3% to 23% of the total discharge. To quantify a more representative water balance, gross gains and gross losses were quantified at the sub-reach scale and ranged from 1% to 28% and -2% to -25% of total stream discharge, respectively. Site characterization data (groundwater table and stream water surface elevations, vertical head gradients, and streambed and aquifer hydraulic conductivities)

were then used to test and verify the water balance results and provided inconsistent information. This indicated that quantifying gains and losses only provides an initial understanding of the complexity of these interactions. Additionally, this study emphasized that one data type is not adequate to describe the extent of surface water-groundwater exchanges and that the spatial scale of consideration is important.

Introduction

Sources, sinks, and residence times of solute mass are important to characterize and quantify in order to predict the fate and transport in a river or stream. These are particularly important because of their role in biogeochemical processes that affect water quality [*Findlay*, 1995; *Payn et al.*, 2008]. Water in a river or stream can have complex flow paths through the main channel, dead zones, hyporheic zone, and surface water-groundwater interface [*Bencala and Walters*, 1983; *Covino and McGlynn*, 2007; *Harvey and Wagner*, 2000; *Payn et al.*, 2009]. The dominant physical processes associated with these flow paths include advection, dispersion, dead zone and hyporheic zone exchange (transient storage), and groundwater exchange. One of the biggest challenges associated with predicting solute transport in a river or stream is attempting to quantify each of these physical processes individually.

Surface water-groundwater interactions are often poorly understood because they are challenging to measure and predict [*Winter et al.*, 1998]. In many stream systems, both gains and losses concurrently occur within the same reach making it challenging to understand the complexity of these interactions. *Winter et al.* [1998] describe surface water-groundwater in such systems as being a single resource since they are continuously

interconnected. This understanding is important because altering either surface water or groundwater will have a direct effect on the other.

To address the effects of groundwater exchange processes on solute transport, some researchers have previously used the advection-dispersion model with the transient storage mass balance and an added term representing lateral inflows [*Gooseff and McGlynn*, 2005; *Runkel and Bencala*, 1995]. This modeling approach, widely implemented through use of the U.S. Geological Survey modeling code OTIS (One-dimensional Transport with Inflow and Storage), often calibrates lateral inflow based on stream tracer experiments [*Bencala*, 2005; *Runkel*, 1998; *Wagner and Harvey*, 1997]. In some applications, losses to groundwater recharge are neglected, however, *Harvey and Wagner* [2000] estimated groundwater recharge in OTIS by simultaneously considering differential volumetric flow data and tracer experiments.

A variety of data collection approaches have been used to better understand stream water-groundwater interactions affecting mass movement and include: stream gauging with velocity-area techniques [*Kennedy*, 1983; *Rantz*, 1982], tracer experiments [*Harvey and Wagner*, 2000; *Harvey et al.*, 2005; *Payn et al.*, 2009; *Ruehl et al.*, 2006], hydraulic head from groundwater observation wells and main channel piezometers [*Harvey et al.*, 1996], instream vertical head gradients and hydraulic conductivity estimates [*Baxter et al.*, 2003; *Landon et al.*, 2001], stream temperature surveys [*Becker et al.*, 2004; *Kerry et al.*, 2007], or hydrograph separation with isotopic tracer techniques [*Cey et al.*, 1998; *Covino and McGlynn*, 2007]. These approaches have additionally been used to support heat and solute transport modeling applications to better describe other physical transport processes (e.g., transient storage) [*Bencala and Walters*, 1983; *Choi et*

al., 2000; *Harvey et al.*, 2005; *Neilson et al.*, 2009a, 2009b, 2009c]. Although many of these methods have additional applications, selecting the appropriate approach to measure and predict groundwater exchange is not always apparent and extracting significant information from each approach may be challenging.

Stream gauging with velocity-area techniques are often correlated to stage data to develop stage-discharge relationships (rating curves) used to obtain high frequency stream discharge estimates from continuous stage data [*Kennedy*, 1983]. These data can be used to quantify stream gains and losses through differential gauging. For example, *Ruehl et al.* [2006] combined high frequency discharge estimates using rating curves and discrete discharge estimates using tracer experiments to quantify net gains and losses in a strongly losing stream at a mean spatial scale of 2 km. Tracer experiments are used for a variety of applications in stream hydrology [*Bencala*, 1983; *Harvey and Wagner*, 2000] including determination of transport characteristics of streams and shallow groundwater interactions of high-gradient streams [*Wagner and Harvey*, 1997], characteristic length and timescales of exchange with storage zones [*Bencala and Walters*, 1983; *Harvey et al.*, 1996; *Harvey and Wagner*, 2000], stream discharges from tracer response curves (dilution gauging) [*Kilpatrick and Cobb*, 1985], and groundwater exchange information by quantifying both net and gross stream gains and losses to quantify a water balance [*Harvey and Wagner*, 2000; *Payn et al.*, 2009].

A complete system water and mass balance assists in model parameter calibration and provides information on flow path residence times [*Harvey and Wagner*, 2000]. While most studies have focused efforts at relatively larger spatial scales [e.g., *Covino and McGlynn*, 2007; *Ruehl et al.*, 2006], *Payn et al.* [2009] recently found significant

exchanges occurring at much smaller scales (200 m). Using dilution gauging techniques, they estimated a complete water balance by quantifying gross gains and losses through tracer mass recoveries within each reach.

A number of additional data types have been used to better understand and support quantifying surface water-groundwater interactions. Groundwater observation wells have been used to form transects with stream channels by installations on both sides of the channel to monitor the direction of groundwater flow and shifts during events through three-point triangulation [*Jencso et al.*, 2009]. Vertical head gradient (VHG), defined by *Baxter et al.* [2003], is a unitless measure where a positive value suggests upwelling conditions and a negative suggests downwelling conditions and can be used to quantify groundwater fluxes together with hydraulic conductivity estimates. Saturated hydraulic conductivity (*K*) is often measured in the streambed and shallow aquifer to characterize spatial variability [*Landon et al.*, 2001] and permeability [*Winter et al.*, 1998] of the stream substrate and aquifer materials. Additionally, *K* estimates can be used for model simulations (e.g., MODFLOW and MODPATH) used to predict gains and losses to the stream and long hyporheic exchange [*Kasahara and Wondzell*, 2003].

To better understand the effects of surface water-groundwater interactions on solute stream transport and to test the utility and reliability of common data collection strategies, specific data types were collected in this study and lumped into two main categories representing: (1) stream gauging and (2) site characterization data. The stream gauging data were used to quantify net surface water-groundwater exchanges at a reach scale (515 m to 560 m) through differential gauging similar to *Ruehl et al.* [2006] with two separate methods: (1) high frequency discharge estimates with the use of rating

curves and (2) dilution gauging techniques with the use of instantaneous tracer experiments. These two methods were compared at the reach scale to test the reliability of each method to detect surface water-groundwater exchanges. Similar to methods presented by *Payn et al.* [2009], net and gross water balances were then quantified by segmenting the study reach into sub-reaches (lengths ranging from 56 m to 120 m) to provide groundwater exchange information at a finer spatial scale and test if the information provided at the reach scale was representative. The site characterization data (groundwater table and stream water surface elevations, vertical head gradients, and hydraulic conductivity estimates) were then used to verify and test the accuracy of the water balance calculations and provide supporting information regarding the complexity of interactions by estimating groundwater flow directions and spatial variability.

Site Description

The selected study portion of Curtis Creek, UT is approximately 1.25 km in stream length near the outlet of the watershed (refer to Figure 2-1) that drains approximately 59.5 km^2 [*U.S. Geological Survey,* 2007]. Curtis Creek is a first order perennial mountain stream with ephemeral (seasonal) tributaries during storm and snowmelt events. It is a tributary to the Blacksmith Fork River which flows into Cutler Reservoir and ultimately the Great Salt Lake.

The site of this project is located on Curtis Creek at Hardware Ranch, a Utah Division of Wildlife Resources (UDWR) operated facility, located approximately 15 miles east of Hyrum, UT. The land area just to the north of the study site is used to grow animal feed to supply an elk refuge during winter months and the southern side is

bordered by a road (Figure 3-1). The northern area is irrigated for most of the summer months by flood irrigation from Curtis Creek water diverted upstream of the study site (Christensen, personal communication, 2008).

The average stream discharge for July 2007 to November 2008 was approximately 200 L s^{-1} (~7 cfs) with a range of 142 L s^{-1} to 1841 L s^{-1} (~5 to 65 cfs). Baseflow occurs during late summer into late winter (August to February) and peaks during late spring into early summer (April to June). The average channel width is approximately 3.7 m (12 ft) with a bottom slope of 0.010 to 0.032.

The overall experimental reach selected was segmented into two separate reaches, an Upper (~0.515 km) and Lower (~0.560 km) Reach (Figure 3-1). The Upper Reach has had little influence of anthropogenic activities (e.g., altering of channel location or geometry) and is dominantly a pool-riffle system with varying storage characteristics (i.e., woody debris, slow moving water, plunge pools, large cobble substrate, and vegetation in shallow pools). There are visible surface seeps (i.e., groundwater that surfaces in marsh areas prior to flowing into the stream) along the right edge of water contributing to gains in stream discharge. The channel of the Lower Reach was altered in 2001 by the UDWR [*Utah Division of Wildlife Resources*, 2001] resulting in different physical characteristics than the Upper Reach. The Lower Reach has more swift riffles, less pool-riffle features, more uniform channel geometry, and similar coarse gravel to large cobble substrate. The Lower Reach is also influenced by groundwater influxes from surface seeps along the right edge of water. The Upper and Lower Reaches are hypothesized to have highly variable stream water gains and losses.

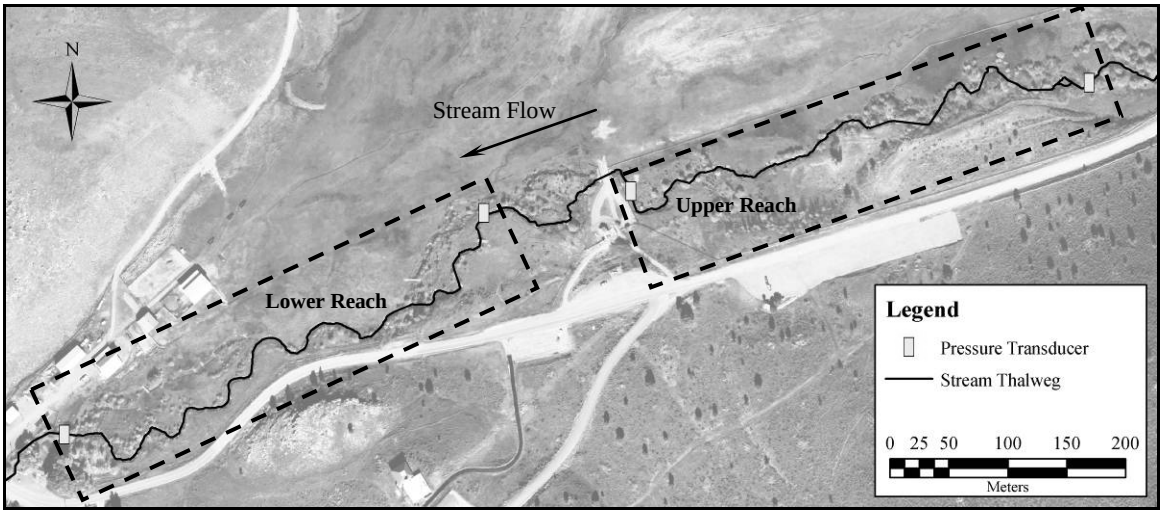

Figure 3-1. Upper and Lower Reaches. Locations of pressure transducers installed are shown to indicate reach boundaries.

The watershed feeding the study reach of Curtis Creek includes a combination of hard rock (Paleozoic and Precambrian bedrock that is strongly indurated (hardened)) and very dense soil deposits in valleys consisting of coarse-grained deposits with gravel, cobble, or boulders that include alluvial fan deposits [*McCalpin et al.*, 2001]. The headwater of Curtis Creek originates in the Monte Cristo Range (a sub-range of the Wasatch Range) in northern Utah and flows southwesterly through narrow canyons into broad valleys (Figure 2-1).

Methods

To test the utility of common data types to quantify and characterize surface water-groundwater interactions, comprehensive data sets were collected in the study reaches, streambed, and surrounding aquifer. A majority of the data sets were collected during July 2008 during a period where stream and groundwater flow conditions were assumed to be steady state. The pasture to the north of the overall study reach was not

irrigated for two weeks prior to conducting tracer experiments in order to eliminate the influences of irrigation (Christensen, personal communication, 2008). The travel time of irrigation water to the stream channel is unknown, but was assumed to reach steady state.

Stream Gauging Data

Rating Curves

In order to establish rating curves at reach boundaries, stage-discharge observations were required [*Kennedy*, 1983]. With this information rating curves can be developed in the form of Equation 3-1 [*Cey et al.*, 1998; *Rantz*, 1982].

$$Q = aZ^{b} \tag{3-1}$$

where:
Q = predicted stream discharge, cfs;
a and b = the regression parameters;
Z = the stage reading, ft.

To increase the accuracy of the discharge predicted from the rating curves, discharges were measured during both high and low flows periods to provide a reliable rating curve for a wide range of stream discharges. Total stream discharge, Q, was calculated by the velocity-area method according to *Rantz* [1982]. Stream velocity at the reach boundaries were measured with a Marsh McBirney Inc.® Flo-Mate™ (Model 2000, Frederick, Maryland) velocity meter. The accuracy of the sensor to measure velocity is ±2% of the reading [*Marsh-McBirney*, 1990]. Each velocity recorded was a 40 second average of each position to reduce noise caused by fluid turbulence and therefore, is assumed that instrumental error is negligible relative to the noise. All

velocities were measured at 60% of the water column depth with no depths exceeding 0.61 m (2 ft) [*Rantz*, 1982].

Reach boundaries were selected at stream distances of 0 m (station PT 0) and 515 m (station PT 515) for the Upper Reach and 692 m (station PT 692) and 1252 m (station PT 1252) for the Lower Reach (Figure 3-1). The exact locations of the reach boundaries were selected based of the uniformity of the channel geometry necessary to measure more accurate stream discharges [*Rantz*, 1982]. Using the discharge and stage data acquired at each station, a nonlinear regression based on the least residual sum of squares was performed to estimate the parameters *a* and *b* in Equation 3-1. The resulting rating curves were constructed at each station to obtain high frequency discharge estimates from continuously monitored water levels (stage) recorded using KWK Technologies® SPXD™ 600 and 610 (0-5 psig) pressure transducers (PT) (Spokane, Washington) with vented cables and Campbell Scientific® CR-206 data loggers (Logan, UT) at 5-minute intervals. Pressure transducers were installed at stations PT 0 and PT 1252 in July 2007 and at stations PT 515 and PT 692 in June 2008.

With high frequency discharge estimates at the reach boundaries, net changes in stream discharge were estimated at this reach scale by difference. Additionally, information regarding diel fluctuations was provided by these high frequency estimates to test a steady state assumption required for dilution gauging techniques.

Dilution Gauging Techniques

In Curtis Creek, tracer experiments were used for stream gauging and tracer mass recoveries were used to quantify a gross water balance similar to *Payn et al.* [2009]. There are three common types of tracer experiments which are: instantaneous tracer slug

injection where a known mass of tracer is instantaneously injected into the stream and measured downstream; a rapid pulse tracer injection where a tracer is injected at a constant rate for a longer time interval (several minutes) and measured downstream; and a constant-rate tracer injection where a constant flow of known concentration is injected into the stream and measured downstream until a plateau (steady-state) in solute concentration is reached [*Wagner and Harvey*, 1997]. Instantaneous and constant-rate stream tracer experiments were compared by *Payn et al.* [2008] and it was concluded that constant-rate tracers were more accurate in sandy substrate, but differ by only 0.3% in larger cobble substrate when calculating stream discharge. Instantaneous tracer experiments were selected to be used in Curtis Creek rather than constant-rate injection experiments due to the potential to overload the stream with solute mass required to reach steady-state concentrations.

There are a variety of tracers commonly used in rivers and streams and each have their advantages and disadvantages (refer to Appendix B for more information regarding commonly used tracers). In Curtis Creek, chloride was selected and used as a conservative solute tracer for all instantaneous experiments which was concluded by *Zellweger* [1994] to be conservative. The source of chloride was sodium chloride (NaCl). The equipment used to measure responses from pre-dissolved tracer injections were four YSI® sondes (models 600 LS and 600 XLM, Yellow Springs, Ohio) which were measured in situ with specific conductance (SC) at one second intervals. To correlate the response curves to chloride concentrations, calibration curves were constructed using each instrument and chloride concentration standards made with creek water [*Gooseff and McGlynn*, 2005] from two locations (one in the Upper Reach and one

in the Lower Reach). The background SC was subtracted from each response curve prior to establishing the correlations [*Gooseff and McGlynn*, 2005; *Payn et al.*, 2009].

The procedure used to estimate stream discharge from tracer injections (dilution gauging) was:

1) Inject an instantaneous slug just upstream from a measurement location,
2) Measure the response of the injection downstream with SC (Figure 3-2),
3) Correct background SC to zero,
4) Translate the SC response curve to chloride concentrations,
5) Integrate the calibrated chloride concentration response curve, and
6) Divide the mass of chloride injected by the integrated curve (Equations 3-2 and 3-3) [*Kilpatrick and Cobb*, 1985].

Figure 3-2 provides an illustration of how instantaneous tracer experiments were conducted within each sub-reach to quantify a net change in stream discharge. The stream discharge (Q_1) at the downstream boundary (Location 1) of a sub-reach is first calculated from a tracer slug (Slug #1) injected just above Location 1. The stream discharge (Q_2) was then calculated at the upstream boundary (Location 2) from a second slug (Slug #2) injection. A net change in discharge, net ΔQ, can be calculated by $Q_1 - Q_2$ for one sub-reach based on Equations 3-2 and 3-3 [*Kilpatrick and Cobb*, 1985].

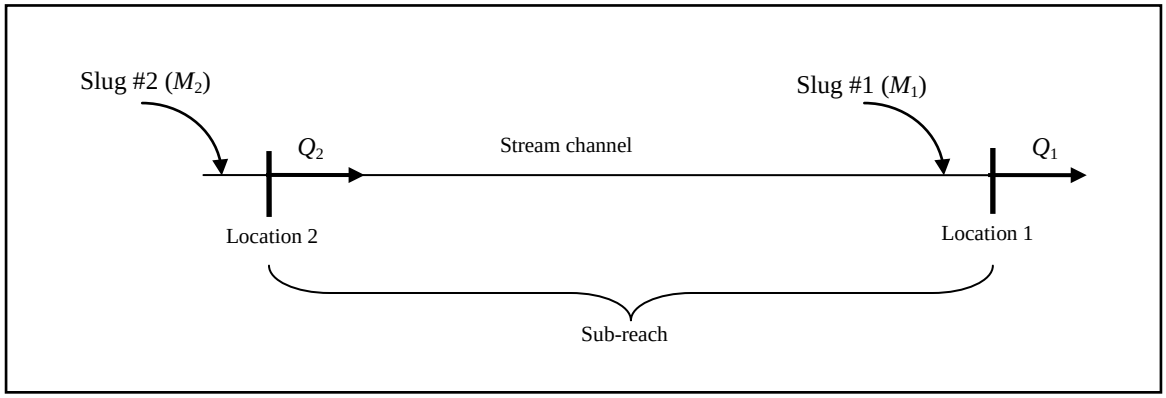

Figure 3-2. Diagram (not to scale) illustrating the method used to calculate a net ΔQ within an individual sub-reach. Monitoring equipment was placed at Locations 1 and 2 (sub-reach boundaries) to obtain two individual tracer response curves.

$$Q_1 = \frac{M_1}{\int_0^t (C_1(t) - C_{b1})dt} \tag{3-2}$$

$$Q_2 = \frac{M_2}{\int_0^t (C_2(t) - C_{b2})dt} \tag{3-3}$$

where:
Q_2 = the calculated stream flow at Location 2, L s^{-1};
Q_1 = the calculated stream flow at Location 1, L s^{-1};
M_1 = the known mass of the tracer Slug #1 injected just above Location 1, mg;
M_2 = the known mass of the tracer Slug #2 injected just above Location 2, mg;
$C_2(t)$ = the measured solute tracer concentration at Location 2, mg L^{-1};
$C_1(t)$ = the measured solute tracer concentration at Location 1, mg L^{-1};
C_{b2} = the measured solute background concentration at Locations 2, mg L^{-1};
C_{b1} = the measured solute background concentration at Location 1, mg L^{-1}.

The denominators of Equations 3-2 and 3-3 were calculated using a trapezoidal approximation [*Stewart*, 1998]. For an accurate stream discharge calculation to be obtained, the following assumptions must be met:

1) The tracer slug instantaneously injected must become completely mixed before the measurement location;

2) No tracer is lost between the injection location and the measurement location; and
3) The stream flow remains constant during the tracer measurement time.

If the required assumptions are not met, then inaccurate discharge calculations will result. An important note is that if tracer mass is lost before the measurement location, discharges will be overestimated [*Payn et al.*, 2008].

Dilution gauging was first performed at the reach scale to provide a comparison to rating curve discharge predictions. Net changes were then quantified from the discharges estimated at each reach boundary using the two stream gauging methods to test if groundwater exchange could be detected at this spatial scale. However, preliminary data of groundwater table and stream water surface elevations along with visual signs of surface seeps indicated gains and losses were occurring at a smaller spatial scale than the reach scale. These data and visual signs of influxes were used to select sub-reaches that were hypothesized to be dominantly gaining or losing. The Upper and Lower Reaches were segmented into 13 sub-reaches (six in the Upper and seven in the Lower) based on the data sets mentioned above (Figure 3-3). The sub-reaches are numbered continuously from the upstream end of the Upper Reach.

Dilution gauging was performed at each sub-reach boundary. To quantify the variability of stream discharge associated with groundwater exchange at this scale, a total of 15 instantaneous tracer injections were performed within two consecutive days at the same time period each day. Seven injections were performed in the Upper Reach (Figure 3-3 (a)) and eight in the Lower Reach (Figure 3-3 (b)) during assumed steady state conditions. To avoid injecting into poorly mixed pools or at locations of visual inflows, the distances between injection locations and measurement locations varied and ranged

from 23 m to 77 m. The first slug injection was measured at stream distance 1291 m and the following were measured consecutively moving upstream to the next sub-reach boundary (Figure 3-3 (b)) to prevent error caused by measuring residual solute.

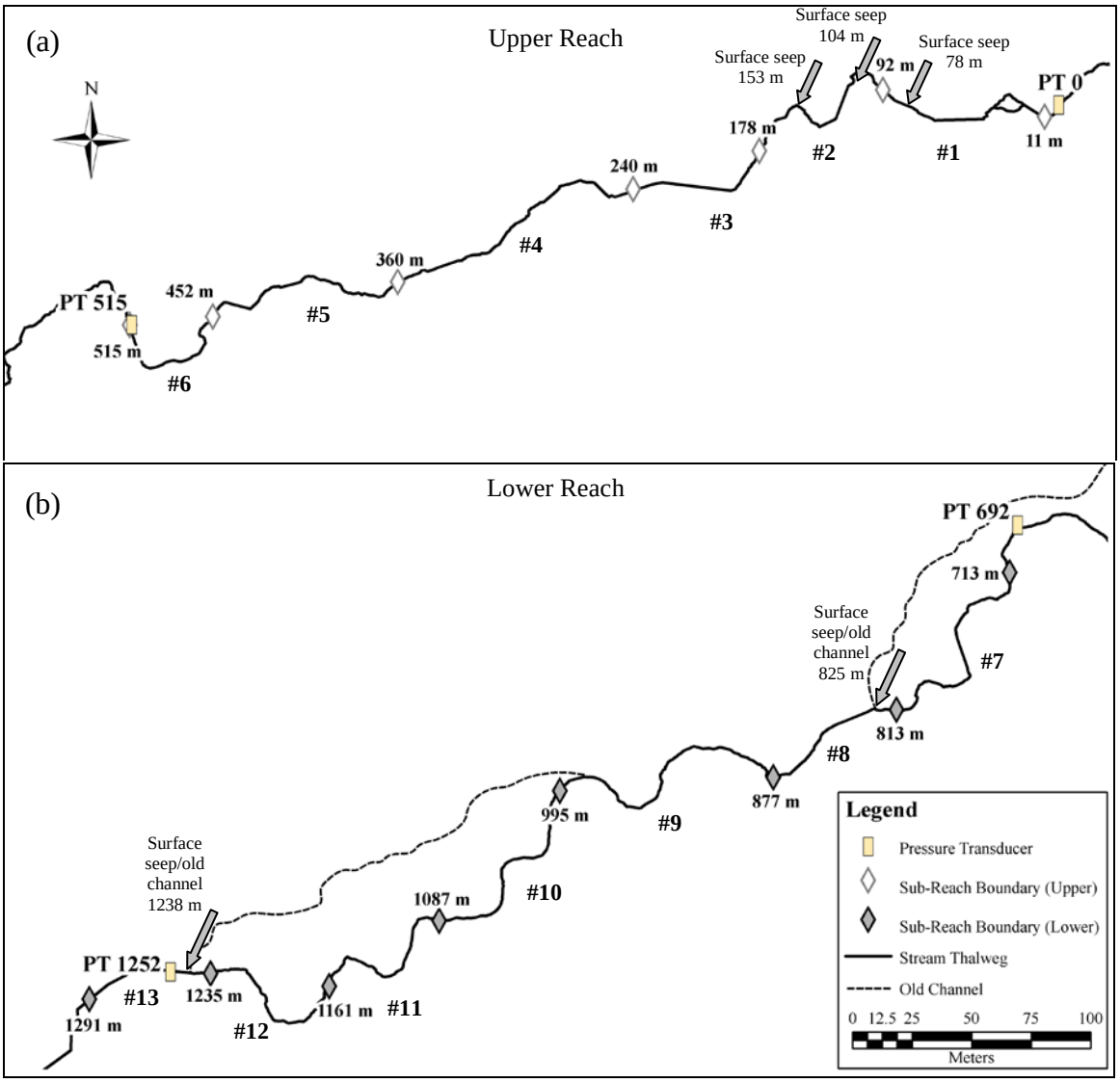

Figure 3-3. (a) Upper and (b) Lower Reach sub-reach boundaries. Surface seep locations are shown with large arrows. Dashed lines show the approximate location of the old stream channel before 2001.

While the net ΔQ of each sub-reach estimates a water balance from an overly simplified perspective, it does not provide an understanding of the extent of sub-reach exchanges occurring. For example, this approach does not account for gains and losses that may occur simultaneously within the same sub-reach. Therefore, gross gains and gross losses that contribute to a net ΔQ need to be quantified separately at the sub-reach scale based on tracer mass recoveries according to *Payn et al.* [2009].

Tracer Mass Recovery

The movement of stream water was analyzed from a Lagrangian perspective in which the fluid passes through a control volume (a sub-reach in this study). For each sub-reach, the two slug injections used to quantify a net ΔQ were also used to quantify mass recoveries. With the discharge, Q_1, estimated at Location 1 from Slug #1, the tracer mass recovered, M_{12}, was calculated from the tracer response at Location 1 from Slug #2, $C_{12}(t)$, using Equation 3-4 (refer to Figure 3-2) [*Dierberg and DeBusk*, 2005].

$$M_{12} = Q_1 \int_0^t \left(C_{12}(t) - C_{b1}(t)\right) dt \qquad (3\text{-}4)$$

where:
M_{12} = the calculated tracer mass recovered, mg of Chloride;
Q_1 = the calculated stream flow from Slug #1 injection, L s^{-1};
$C_{12}(t)$ = the observed tracer response in chloride concentrations at Location 1 from Slug #2, mg L^{-1};
$C_{b1}(t)$ = the background chloride concentration at Location 1, mg L^{-1};
$\int (C_{12}(t) - C_{b1}(t))dt$ = the integral calculated from the tracer response curve measured at Location 1 from Slug #2, mg s L^{-1}.

The mass loss (unrecovered mass), M_{loss}, was calculated by difference from the mass injected above Location 2, M_2, and the recovered mass shown in Equation 3-5.

Finally the percent of mass change, $\%\Delta M$, was found using Equation 3-6. Estimating the net ΔQ and ΔM provided the necessary information to quantify gross gains and losses separately.

$$M_{loss} = M_{12} - M_2 \tag{3-5}$$

$$\%\Delta M = \frac{M_{loss}}{M_2} \times 100\% \tag{3-6}$$

where:
M_{loss} = unrecovered mass, mg of chloride.

Gross Gains and Gross Losses

As previously mentioned, quantifying the net ΔQ for each sub-reach provides a limited, but necessary understanding of the quantity of groundwater exchange occurring. However, there are several contributors to the net ΔQ (e.g., hyporheic flow, a gain from groundwater discharge, and a loss from groundwater recharge). To include each of these possible contributors, a stream mass balance for surface water-groundwater exchange processes was proposed by *Harvey and Wagner* [2000]. They looked at groundwater exchange as a distributed source, assumed that the stream discharge was steady state, and assumed the reach length was long enough to include many hyporheic flow paths. Assuming hyporheic exchanges occur in short flow paths at a sub-reach scale and any flow out of the stream into the hyporheic zone returns back within the same sub-reach may or may not be a valid assumption.

In Curtis Creek, the contributors to a net ΔQ are hypothesized to be groundwater recharge (Q_R), groundwater discharge (Q_{GW}), long hyporheic flow (Q_{hL}), short hyporheic

flow (Q_{hS}), dead zone exchange (Q_{DZ}), and surface seeps (Q_{SS}) (Figure 3-4). Identifying these possible sources and sinks of stream water is important to understand all surface water-groundwater interactions occurring. Assuming that the net $\Delta Q = f(Q_{SS}, Q_{GW}, Q_R, Q_{hL}, Q_{hS}, Q_{DZ})$, the water balance becomes Equation 3-7. However, only gross gains and gross losses can be quantified with these methods and even though important to indentify, each individual contributor cannot be quantified.

$$Q_1 - Q_2 = Q_{SS} + Q_{GW} - Q_R \pm Q_{hL} \pm Q_{hS} \pm Q_{DZ} \quad (3\text{-}7)$$

where:
Q_2 = the stream discharge at Location 2, L s^{-1};
Q_1 = the stream discharge at Location 1, L s^{-1};
$Q_1 - Q_2$ = net ΔQ, L s^{-1}.

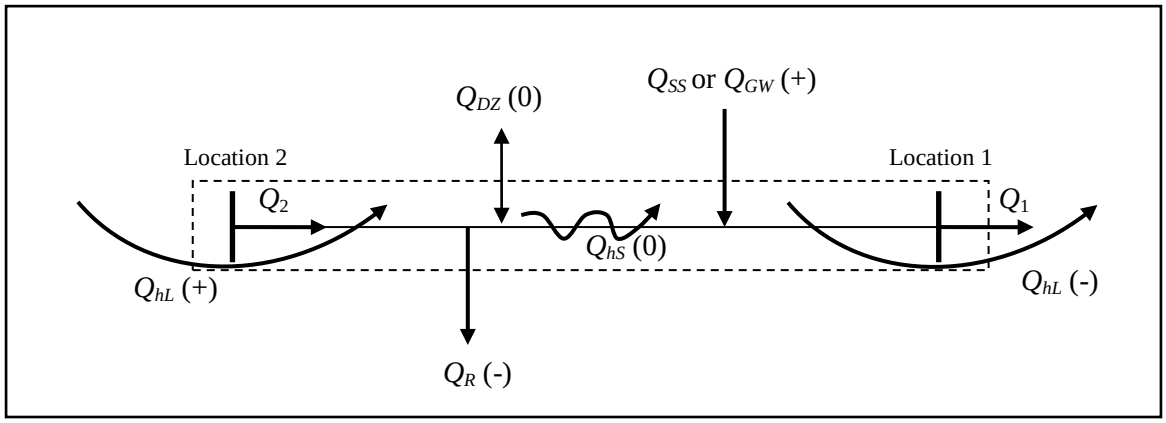

Figure 3-4. Diagram (not to scale) of contributors to a net ΔQ in one sub-reach [adapted from *Payn et al.*, 2009].

In order to estimate the water balance of a sub-reach in terms of a gross gain, Q_{gain}, and a gross loss, Q_{loss}, the water balance shown in Equation 3-7 must be simplified. The following assumptions are applied to lump together the contributors as either a gross gain or gross loss:

(1) $Q_R = Q_R + Q_{hL}$;

(2) $Q_{GW} = Q_{GW} + Q_{hL}$;

(3) Q_{hS} and Q_{DZ} have a net contribution of zero to ΔQ;

(4) $Q_{gain} = Q_{SS} + Q_{GW}$; and

(5) $Q_{loss} = Q_R$.

Groundwater discharge, Q_{GW}, and recharge, Q_R, were lumped together with Q_{hL} because hyporheic flow traveling in long flow paths (several meters) behaves similar to groundwater with potentially similar concentrations and temperature. Additionally, Q_{hS} is assumed to occur in short enough flow paths such that any water leaving a sub-reach into the hyporheic zone will return to the stream within the same reach. Q_{DZ} is assumed to behave similarly with any main channel water entering dead zones, an equal amount of water and solute is returned back to the main channel within a relatively short time period.

With these assumptions applied, a Q_{gain} or a Q_{loss} are treated as point flows rather than distributed flows, although, the location within a sub-reach where these gains and losses occur is not understood. To account for this uncertainty, calculations were completed based on two idealized situations. As suggested by *Payn et al.* [2009] these are: (1) a loss occurs before a gain and (2) a gain occurs before a loss (refer to Appendix B for diagrams of these situations (Figures B-4 and B-5)). The assumption of which

situation occurs in a sub-reach will affect the mass balance because the solute concentration of Q_{loss} during a tracer injection is a function of the stream location it occurs within (i.e., in a sub-reach with a Q_{loss}, the solute concentration will be higher if it occurs before a gain).

With the estimate of the mass recovered, Q_{loss} and Q_{gain} may then be estimated by completing the mass balance with the injection of Slug #2 shown by Equation 3-8.

$$M_2 = Q_{gain}\int_0^t C_{gain}(t)dt - Q_{loss}\int_0^t C_{loss}(t)dt - Q_1\int_0^t C_{12}(t)dt \qquad (3\text{-}8)$$

The unknowns in Equation 3-8 are Q_{gain}, $\int_0^t C_{gain}(t)dt$, Q_{loss}, and $\int_0^t C_{loss}(t)dt$. The background concentrations, $\int_0^t C_b dt$, are not shown in Equation 3-8 for simplicity because the background specific conductance (SC) is subtracted from each response curve measured prior to correlating to chloride concentrations. Additionally, any mass contributed from C_{gain} is assumed to be subtracted from the mass balance by subtracting off the background concentrations, and therefore, the term $Q_{gain}\int_0^t C_{gain}(t)dt$ is eliminated from Equation 3-8. To clarify, if C_{gain} becomes completely mixed with stream water before it reaches Location 1, then the background concentration measured in the response contains all contribution of C_{gain} to the mass balance. This means that in a purely gaining reach, $\%\Delta M = 0$. Applying this assumption, Equation 3-8 is simplified to Equation 3-9.

$$M_2 = Q_{loss}\int_0^t C_{loss}(t)dt - Q_1\int_0^t C_{12}(t)dt \qquad (3\text{-}9)$$

The unknowns in Equation 3-9 are now Q_{loss} and $\int_0^t C_{loss}(t)dt$. To solve for Q_{loss}, *Payn et al.* [2009] suggested that if a loss is assumed to occur before a gain (Situation 1), the C_{loss} can be set equal to the concentrations of the response curve at Location 2, that is $\int_0^t C_{loss}(t)dt = \int_0^t C_2(t)dt$. For a gain to be assumed to occur before a loss (Situation 2), they suggested the assumption that the concentration leaving the control volume, C_{loss}, is set equal to the concentration of the measured response curve at Location 1 from Slug #2, that is $\int_0^t C_{loss}(t)dt = \int_0^t C_{12}(t)dt$. With Q_{loss} quantified, Q_{gain} is then quantified using Equation 3-10 [*Payn et al.*, 2009].

$$Q_{gain} = \Delta Q - Q_{loss} \tag{3-10}$$

Quantifying Q_{loss} and Q_{gain} for Situations 1 and 2 separately is important because an assumption regarding the order contributes error to these calculations.

While quantifying Q_{loss} and Q_{gain} provides a more complete understanding of the stream water balances, it should be noted that contributions from long hyporheic flow cannot be determined with this method and therefore, add to the error in these calculations. This error is not quantified in this research, but it is important to understand this bias when interpreting the results. Additionally, gains and losses are assumed to behave as points sources, but may occur as both point and distributed sources. Applying the assumptions for C_{loss} may or may not be valid. To better understand the complexity of these interactions and test the water balance results, the site characterization data was used to provide information regarding locations of gains and losses and the heterogeneity of the streambed and aquifer.

Site Characterization Data

Groundwater Table and Stream Water Surface Elevations

To establish the horizontal and vertical coordinates of the stream thalweg, stream water surface measurement locations, and groundwater observation well locations, a land survey was conducted using a Trimble® R8 (Dayton, Ohio) GNSS (Global Navigation Satellite System) receiver and rover in July 2008 with an accuracy relative to the start location of sub-centimeter (5 mm horizontal and 5 mm vertical) [*Trimble*, 2009]. A total of 44 groundwater observation wells were installed throughout the overall experimental reach in June 2008 to measure the relative discrete elevations of the shallow groundwater table in close proximately to (3 m to 25 m normal to) the channel. The observation wells were constructed of half inch (1.27 cm) diameter polyvinyl chloride (PVC), 2 m in length, and have 40 cm of perforation covered with 2 mm flexible screen to exclude soil. The discrete groundwater table elevations were determined by measuring the distance from the top of each well (which were surveyed) to the groundwater table with a Solinst® electronic well sounder (Model 101 Mini, Georgetown, Ontario, Canada). By subtracting this distance from the surveyed well elevation, the elevation of the groundwater table was established at these discrete locations. The stream water surface elevations were also measured at 25 locations. In order to establish the vertical and horizontal coordinates of the stream water surface at these locations, 1.5 m lengths of rebar were first installed in the main channel and the tops were surveyed. The distance from the tops of the rebar lengths to the water surface were then measured and subtracted from the elevations of the surveyed rebar.

The Upper Reach had 24 observation wells and 15 locations where stream water surface elevations were measured (Figure 3-5 (a)) and the Lower Reach had 18 observation wells and 10 stream water surface locations (Figure 3-5 (b)). The wells were numbered from the upstream end of the reach following the letter 'W' (e.g., W1). Stream water surface measurement locations were selected to form a transect with surrounding wells normal to the direction of stream flow for both the Upper and Lower Reach. The nomenclature for these locations is represented by the distance downstream from the top of the Upper Reach boundary. The old stream channel (shown as a dashed line in Figure 3-5 (b)) has water constantly present and additionally had five water surface elevation measurement locations to provide additional information regarding old and active channel interactions.

To provide more information regarding surface water-groundwater interactions, parameters of chloride concentration, specific conductance, and temperature were measured in a subset of wells and surface seeps on July 16, 2008 to qualitatively determine the spatial variability of groundwater flow paths. Chloride concentrations were measured with a Dionex® ion chromatograph (Model AS4A, Sunnyvale, California) according to EPA Method 300.0. Specific conductance was analyzed according to Standard Methods (SM) 2510B [*American Public Health Association*, 1999] with a Fisher Scientific Accumet® conductivity meter (Model 30, Waltham, Massachusetts) calibrated in the laboratory. The quality assurance and quality control (QA/QC) of all grab samples analyzed for chloride concentration were analysis of replicate samples, sample spikes and replicates, calibration curve verifications, blanks, and trip blanks.

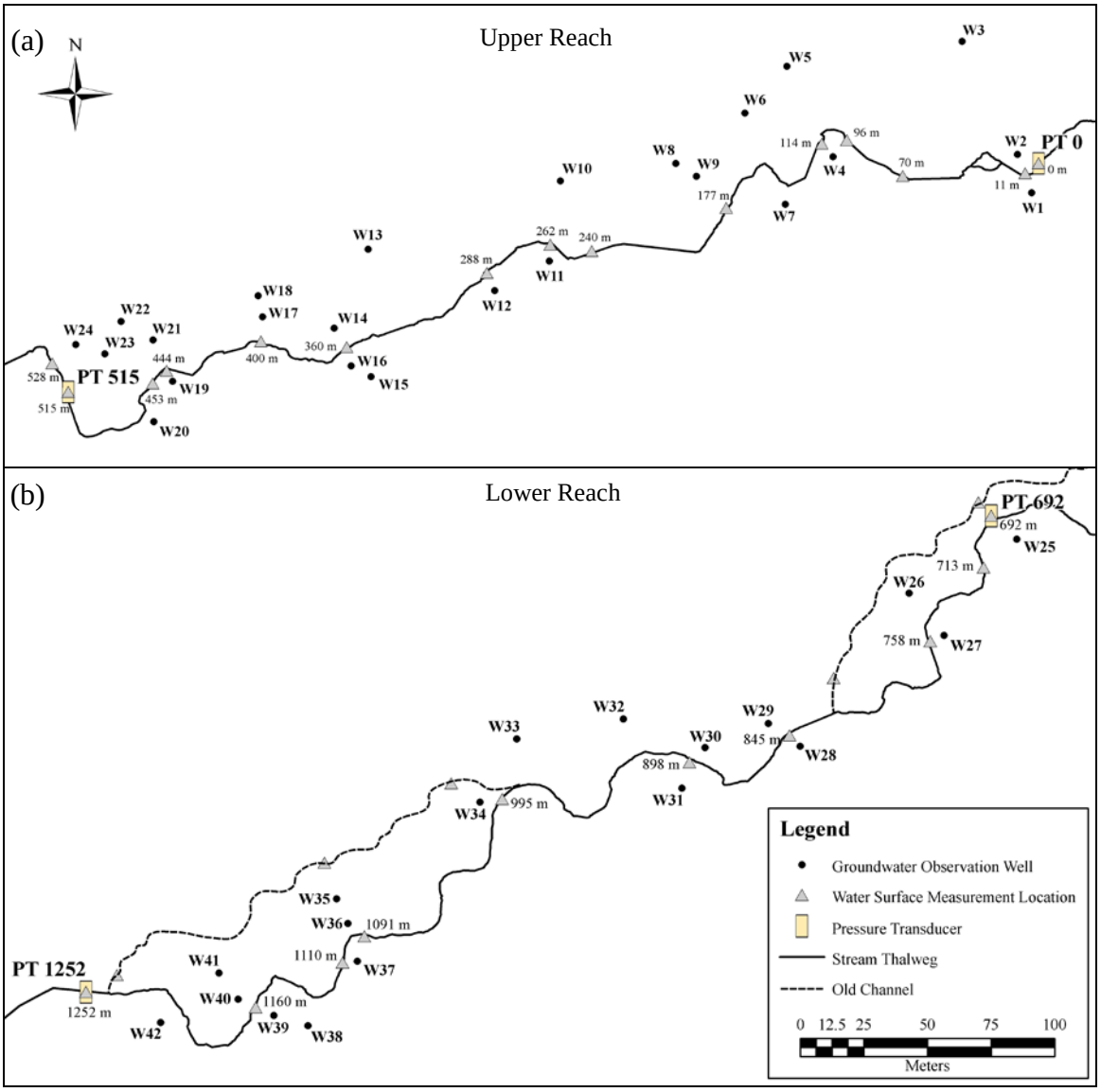

Figure 3-5. (a) Upper and (b) Lower Reach observation well, stream water surface measurement, and pressure transducer locations. The dashed lines show approximately where the original (old) stream channel was before 2001.

Vertical Head Gradients

Instream piezometers were installed in the stream substrate and vertical head gradient (VHG) was estimated. Due to the substrate in Curtis Creek dominantly consisting of large cobble, a method for installing piezometers that minimizes substrate disturbance proposed by *Baxter et al.* [2003] was implemented. Piezometers were

installed at six locations in the main channel (three locations in the Upper Reach and three locations in the Lower Reach) at depths of 9 cm and 20 cm at each location to represent different head conditions in the hyporheic zone. The piezometers were installed at downstream distances of 96, 240, 713, and 1160 m in July 2007 and additionally of 360 and 995 m in July of 2008 (refer to Figure 3-5 for locations). Half inch (1.27 cm) diameter PVC was selected for the piezometers and 2 mm flexible screen was used to cover the perforation. Eight inches (20.3 cm) of perforation was used for each piezometer. For comparison purposes, VHG was estimated on July 11, 16, and 18, 2008. The uncertainty in the VHG estimates was approximated by taking one standard deviation of triplicate measurements.

Hydraulic Conductivity Estimates

Similar to *Baxter et al.* [2003], hydraulic conductivity (*K*) was estimated in the main channel of the stream by conducting slug tests in which piezometers were filled with water to a target height and head-time curves were constructed. Equation 3-11 (Hvorslev equation) [*Baxter et al.*, 2003] was then used to calculate *K*.

$$K = \frac{\left(r^2\right)\ln\left(L_p / R\right)}{2L_p T_0} \quad for \quad L_p / R > 8 \tag{3-11}$$

where:
r = piezometer radius, cm;
L_p = length of perforations, cm;
R = radius of perforated interval, cm;
T_0 = the basic time lag to 37% of normalized water level, s.

This equation only estimates *K* in the horizontal direction and groundwater fluxes are expected to have both horizontal and vertical components that will be highly complex

[*Landon et al.*, 2001], therefore, this method has limitations. However, vertical hydraulic conductivity is often used to estimate the flux through the streambed with a form of Darcy's equation [*Cey et al.*, 1998].

Hydraulic conductivity (*K*) was estimated in the hyporheic zone at the six locations where piezometers were installed at depths of both 9 cm and 20 cm below the streambed. *K* was also estimated in a subset of the groundwater observation wells in the saturated zone of the shallow aquifer. These data provided measured information regarding the potential for hyporheic fluxes and surface water-groundwater exchange. Additionally, these data provided information regarding the variability and complexity of groundwater flow paths influencing surface water-groundwater exchange to support water balance results.

Results

Stream Gauging Data

Reach Scale

The parameters *a* and *b* of the rating curve model, $Q = aZ^b$, for each station (PT 0, PT 515, PT 692, and PT 1252) were estimated by nonlinear regression based on the least residual sum of squares (refer to Appendix A for plots of the rating curves and outputs for the model parameter estimates (Figures A-2, A-6, A-10, and A-14 and Table A-5)) assuming normality, independence, and constant variance of residual distribution.

Predicted stream discharge from the rating curves and continuous stage data are shown for five days at the Upper and Lower Reach boundaries (Figure 3-6). The highlighted sections indicate the time intervals when tracer experiments were conducted

to quantify a sub-reach scale water balance. These data suggest that the steady state assumption may not have held for the water balance representing the Upper Reach. However, varying stream discharge at the Upper Reach boundary is assumed to not contribute error to each sub-reach water balance due to relatively short travel times in each sub-reach.

From Figure 3-6, groundwater exchange appears to occur at the reach scale with Upper Reach gaining 0% to 32% and Lower Reach losing -2% to -12% from upstream discharge when considering one diel cycle (7/17 0:00 to 7/18 0:00). These types of high frequency estimates provide valuable information regarding diel fluctuations and seasonal variations at this scale, but do not provide detailed information regarding the extent of groundwater exchange occurring. To show seasonal variations, eighteen months (July 2007 to November 2008) of high frequency discharge estimates for the Upper and Lower Reach boundaries are shown in Appendix C (Figure C-1).

For comparison purposes, the time interval (~9 hours) dilution gauging was performed (within the shaded regions of Figure 3-6) near the PT stations was selected to predict discharge from each rating curve (Table 3-1). The rating curves at stations PT 0 and PT 515 estimated an increase of 16.6% in the Upper Reach through differential gauging. The rating curves at stations PT 692 and PT 1252 estimated a decrease of -11.2% in the Lower Reach.

Dilution gauging at the reach scale was conducted at location 11, 515, 713, and 1291 m (Figure 3-3). Three of the four distances are not at the exact locations of PT stations due to selecting measurement locations for appropriate slug travel distances that were not of consideration for PT station locations. However, significant changes in

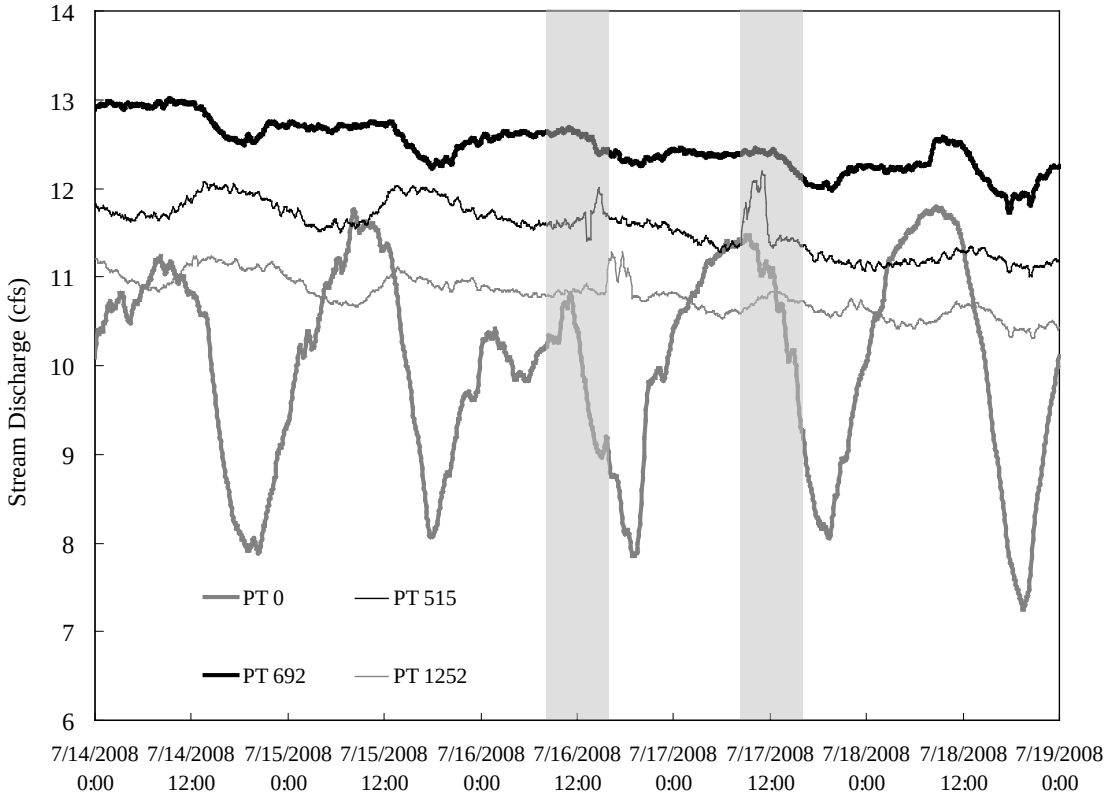

Figure 3-6. Five days of high-frequency discharge estimates using rating curves at the reach boundaries. The gray bars indicate when tracer experiments were performed.

Table 3-1. Rating Curve Predictions at the Reach Boundaries at the Time Intervals Dilution Gauging was Performed

Reach	Station	Date and time interval	Stage, *Z* (ft)	*Q* (cfs)	*Q* (L s^{-1})	Net %Δ*Q* from upstream *Q*
Upper	PT 0	7/17/08 13:30 to 13:40	0.47	10.5	296.5	
	PT 515	7/17/08 9:40 to 9:50	0.52	12.2	345.8	**16.6**
Lower	PT 692	7/16/08 15:20 to 15:30	0.72	12.1	343.6	
	PT 1256	7/16/08 9:45 to 9:55	0.56	10.8	305.0	**-11.2**

stream discharge are assumed to be negligible for the short distances between the corresponding dilution gauging and PT station locations. Dilution gauging near the reach boundaries show a decrease of -1.6% in the Upper Reach and an increase of 20.0% in the Lower Reach (Table 3-2) (refer to Appendix B for the calibration curves representing the Upper and Lower Reaches separately used to correlate SC to chloride concentrations (Figure B-3)).

At the reach scale, rating curves predictions resulted in an increase in discharge and dilution gauging estimated a decrease for the Upper Reach (Figure 3-7). The opposite occurred in the Lower Reach where the rating curve predictions show a decrease and dilution gauging show an overall increase. This conflicting information indicates that neither method was capable to detect groundwater exchanges at the reach scale. Therefore, surface water-groundwater exchange information is required at a smaller spatial scale to better understand the exchanges occurring.

Table 3-2. Reach Scale Dilution Gauging Results and Net %Δ*Q*

Reach	Injection distance downstream (m)	Measurement location downstream (m)	Slug travel distance (m)	*M* (g)	$\int C(t)dt - \int C_b dt$ (mg s L^{-1})	*Q* (L s^{-1})	Net %Δ*Q* from upstream *Q*
Upper	-48	11	60	364	1075.9	338.3	
	452	515	63	364	1093.5	333.0	**-1.6**
Lower	636	713	77	364	1220.2	298.3	
	1252	1291	39	364	1018.4	357.8	**20.0**

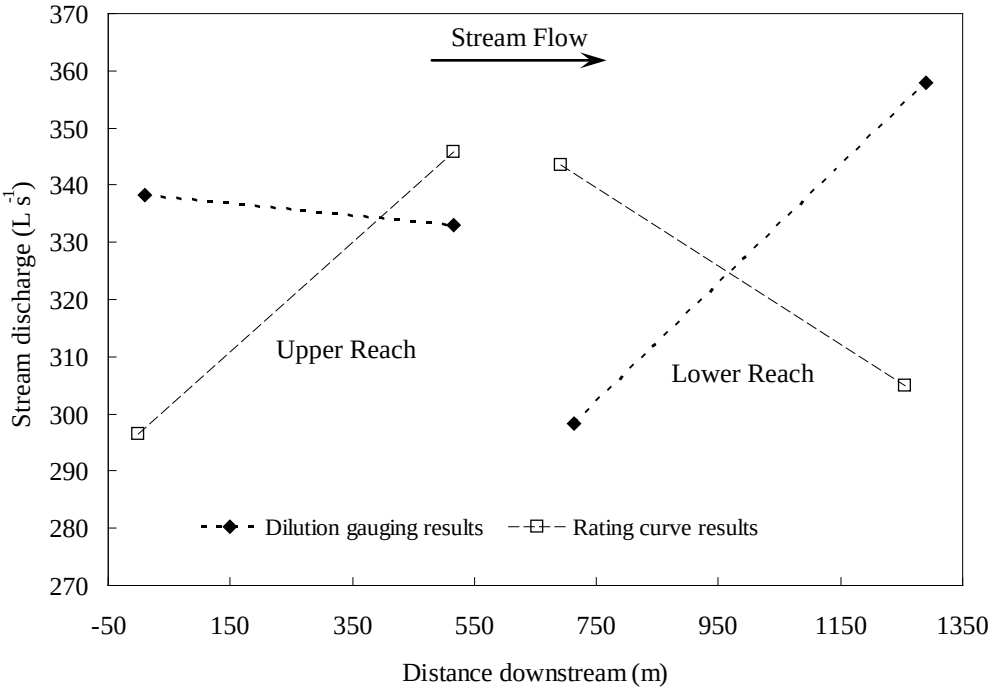

Figure 3-7. Dilution gauging results compared to rating curve results at the reach scale of the Upper and Lower Reach boundaries.

Sub-Reach Scale

The stream discharges estimated at the sub-reach boundaries with dilution gauging techniques in the Upper Reach indicate there are varying changes to discharge with a range from 297 L s^{-1} to 381 L s^{-1} (Figure 3-8). In the Lower Reach there are also varying changes to discharge between each sub-reach boundary with a range from 298 L s^{-1} to 358 L s^{-1} (Figure 3-8) (refer to Appendix B for response curve information used to quantify each stream discharge (Tables B-1 and B-2)). The variability in discharge estimates range from approximately 5% to 20% of the upstream discharge and these were not detected at the reach scale (Figure 3-8). The sub-reach results confirm that gains and losses are highly spatially dynamic.

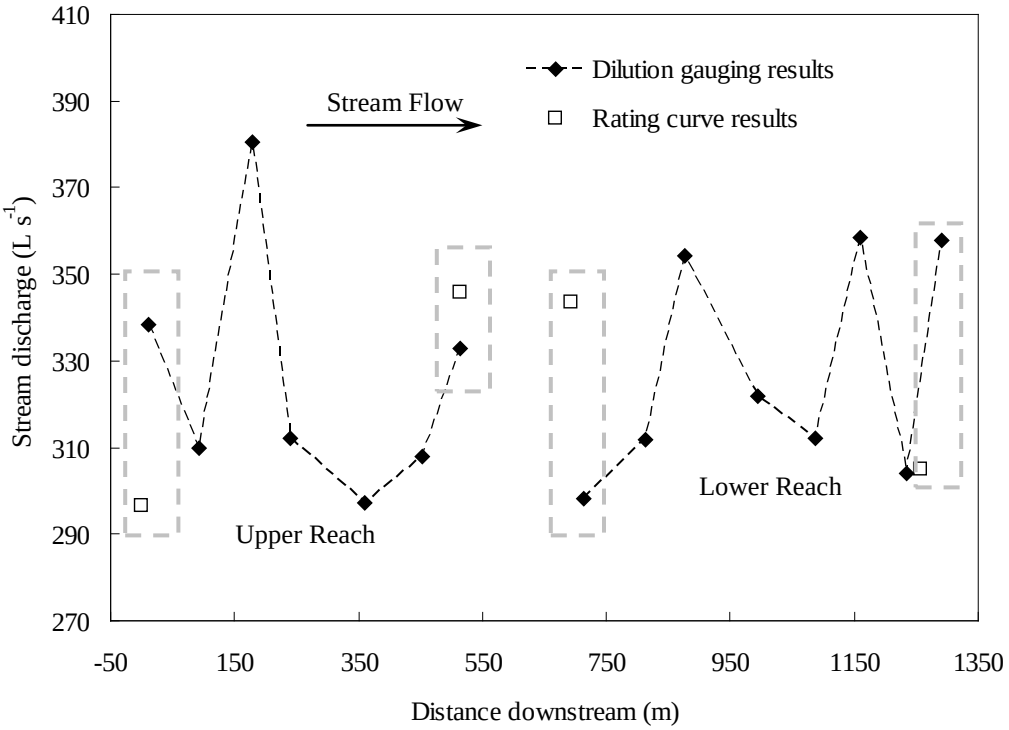

Figure 3-8. Sub-reach scale dilution gauging results compared to reach scale rating curve predictions. The dashed boxes show the estimates that are compared in Figure 3-7.

Using the discharge estimates at the sub-reach boundaries, net change in stream discharge was quantified. The net $\%\Delta Q$ ranges from -18.0% to 22.8% of the discharge at the upstream end of each sub-reach for the Upper Reach (Table 3-3) and -15.2% to 17.7% for the Lower Reach (Table 3-4). This suggests that stream water is variably gaining from groundwater discharge and losing to groundwater recharge in both reaches. The percent tracer mass lost, $\%\Delta M$, for each sub-reach ranged from -24.8% to 22.2% for the Upper Reach (Table 3-3) and -18.1% to 8.5% for the Lower Reach (Table 3-4). This is an important parameter to measure because some sub-reaches were found to have a positive net ΔQ and a negative ΔM (Tables 3-3 and 3-4). This type of occurrence indicates gains and losses are occurring simultaneously within the same sub-reach (refer to Appendix B for all mass recovery calculations (Tables B-3 and B-4)).

Table 3-3. Net Percent Change in Stream Discharge and Mass for the Upper Reach

Sub-reach number	Sub-reach interval (m)	Length of sub-reach (m)	Net ΔQ ($L\ s^{-1}$)	Net $\%\Delta Q$ from upstream Q	$\%\Delta M$
1	11 to 92	80	-28.4	**-8.4**	**-5.9**
2	92 to 178	86	70.6	**22.8**	**22.2**
3	178 to 240	62	-68.4	**-18.0**	**-4.4**
4	240 to 360	119	-15.0	**-4.8**	**-16.7**
5	360 to 452	93	10.7	**3.6**	**-24.8**
6	454 to 515	63	25.1	**8.2**	**-1.8**

Table 3-4. Net Percent Change in Stream Discharge and Mass for the Lower Reach

Sub-reach number	Sub-reach interval (m)	Length of sub-reach (m)	Net ΔQ ($L\ s^{-1}$)	Net $\%\Delta Q$ from upstream Q	$\%\Delta M$
7	713 to 813	100	13.4	**4.5**	**-1.7**
8	813 to 877	64	42.7	**13.7**	**-6.0**
9	877 to 995	118	-32.5	**-9.2**	**-12.9**
10	995 to 1087	92	-9.9	**-3.1**	**-18.1**
11	1087 to 1161	74	46.4	**14.9**	**8.5**
12	1160 to 1235	74	-54.5	**-15.2**	**-14.0**
13	1235 to 1291	56	53.9	**17.7**	**-4.7**

In the Upper Reach, positive net $\%\Delta Q$ was observed in Sub-reaches #2, #5, and #6 and a negative $\%\Delta M$ observed in Sub-reaches #5 and #6 (Figure 3-9 and Table 3-3). This indicates gains and losses are occurring simultaneously in Sub-reaches #5 and #6. Another indication of gains and losses occurring together is in Sub-reach #3 having a large negative net $\%\Delta Q$ relative to a small negative $\%\Delta M$ while Sub-reach #4 had a small negative net $\%\Delta Q$ with a relative large negative $\%\Delta M$. A positive net $\%\Delta Q$ was observed in Sub-reach #2 (highlighted with a dashed box in Figure 3-9); however, a positive $\%\Delta M$ (22.2% in Table 3-3) was also observed. Any gain in mass was assumed to have been subtracted from the mass balance (refer to Equation 3-9) and a positive $\%\Delta M$ observed indicates an error occurred somewhere in this experiment when measuring tracer response curves. This indicates an error because in a purely gaining

reach, Δ*M* should be zero and a net Δ*Q* should be positive based on the mass balance shown in Equation 3-9. With Sub-reach #2 showing a substantial gain in mass, the significance of this error highlights limitations in these methods.

In the Lower Reach, Sub-reaches #7, #8, #11, and #13 had observed positive net Δ*Q* with negative Δ*M* in Sub-reaches #7, #8, and #13 (Figure 3-10 and Table 3-4). Again, this indicates gains and losses are occurring together in these sub-reaches. Additionally, Sub-reaches #9, #10, and #12 have negative net Δ*Q* with negative Δ*M* of different relative magnitudes. Not only do these results provide evidence of simultaneous gains and losses, but complex surface water-groundwater interactions are occurring. Similar to Sub-reach #2 in the Upper Reach, a positive Δ*M* was observed in Sub-reach #11 indicating an error occurred in the experiment for this sub-reach (highlighted with a dashed box in Figure 3-10).

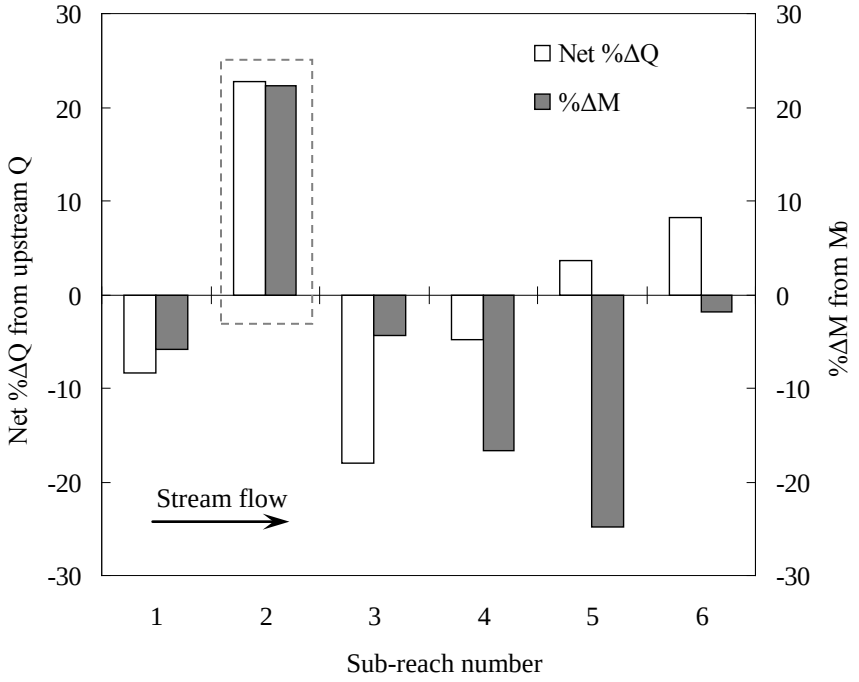

Figure 3-9. Percent net change in upstream discharge and injected tracer mass for the Upper Reach. The dashed box indicates an error occurred in Sub-reach #2.

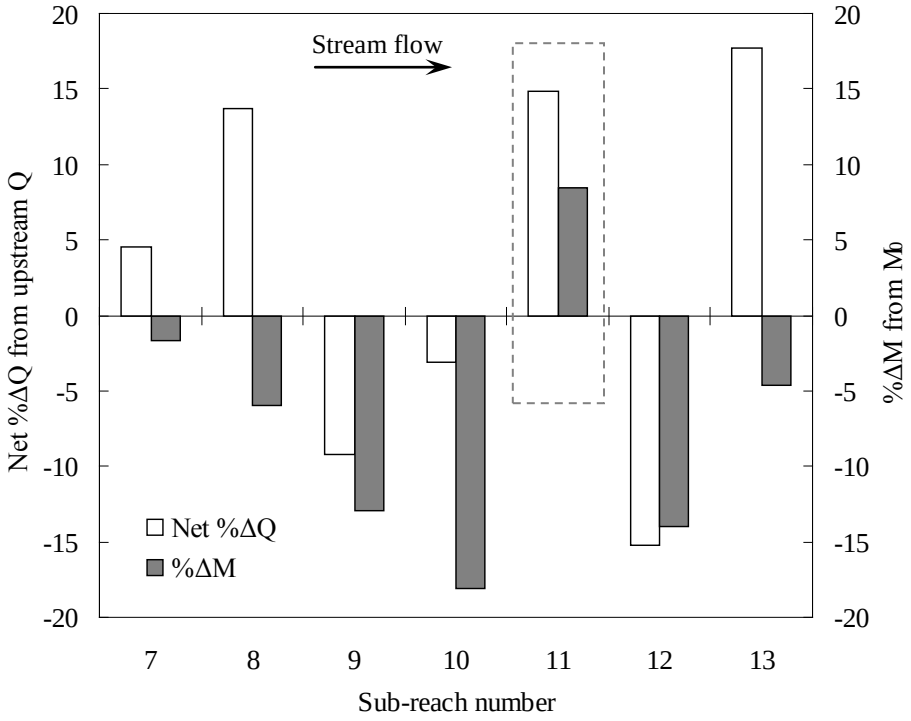

Figure 3-10. Percent net change in upstream discharge and injected tracer mass for the Lower Reach. The dashed box indicates an error occurred in Sub-reach #11.

The percent gross gain, $\%Q_{gain}$, and percent gross loss, $\%Q_{loss}$, were quantified for both situations where a loss is assumed to occur before a gain (Situation 1) and a gain is assumed to occur before a loss (Situation 2) to determine the range of error associated with this assumption. These values were calculated as a percent change (gain or loss) for each sub-reach from the upstream discharge at the top of each corresponding sub-reach. The Upper Reach had $\%Q_{loss}$ ranging from -1.8% to -24.8% with the positive value of +22.2% treated as an error in the method (Table 3-5). However, the magnitude of this error suggests a significant error occurred in the method and again illustrates limitations that may arise to detect real exchanges. The $\%Q_{gain}$ ranged from 10.0% to 28.4% with the negatives values (-2.5% and -13.6% in Table 3-5) indicating that the error in Sub-reach #2 was carried over to the gross exchange calculations for Sub-reaches #1, #2, and

#3. The $\%Q_{loss}$ and $\%Q_{gain}$ were then calculated for Situation 2 to represent the error associated with the assumption of the locations of gains and losses (Table 3-5). The largest error (±9.40%) associated with the assumption of the order of gains and losses as point sources occurred in Sub-reach #5 indicating this assumption can result in great uncertainty. Recall that $Q_{gain} = \Delta Q - Q_{loss}$ (Equation 3-10) was calculated with net ΔQ remaining constant for both Situations 1 and 2. Therefore, the error based on the order assumption is the same for both Q_{loss} and Q_{gain}.

In the Upper Reach, Sub-reaches #4 and #5 show a relatively small net $\%\Delta Q$ (Figure 3-9), but have large $\%Q_{gain}$ and $\%Q_{loss}$ occurring that were not shown in the net water balance (Figure 3-11). Quantities shown are for Situation 1 with errors bars indicating the variability due to assuming Situation 2. The error observed in Sub-reach #2 resulted in inconclusive values for the surrounding sub-reaches (highlighted with a dashed box in Figure 3-11).

Table 3-5. Percent Gross Gains and Losses for the Upper Reach

Sub-reach number	Sub-reach interval (m)	Situation 1		Situation 2		Error in $\%Q_{loss}$ and $\%Q_{gain}$ from assumption
		$\%Q_{loss}$ before gain	$\%Q_{gain}$ after loss	$\%Q_{loss}$ after gain	$\%Q_{gain}$ before loss	
1	0 to 92	-5.9	-2.5	-5.7	-2.7	±0.2
2	92 to 178	22.2	0.6	22.3	0.5	±0.1
3	178 to 240	-4.4	-13.6	-3.7	-14.2	±0.6
4	240 to 360	-16.7	11.9	-19.0	14.2	±2.4
5	360 to 454	-24.8	28.4	-34.2	37.8	±9.4
6	452 to 515	-1.8	10.0	-2.0	10.2	±0.2

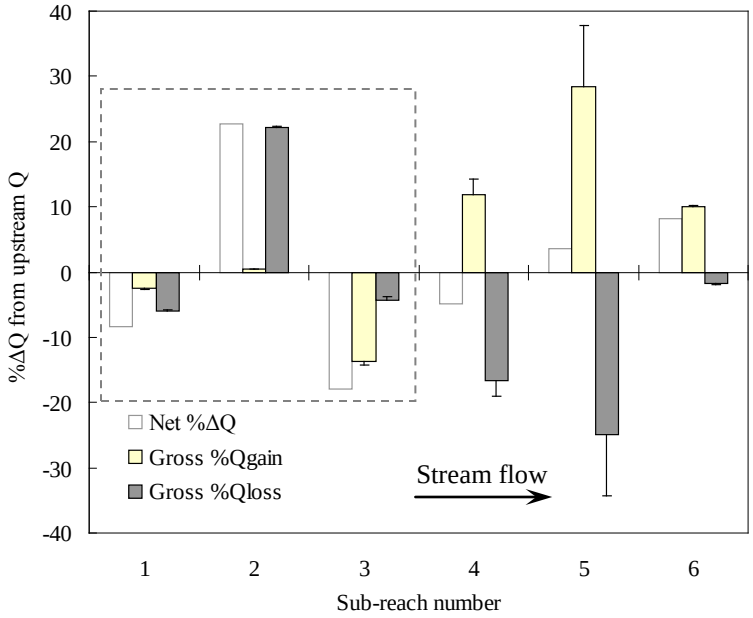

Figure 3-11. Percent gross gains and losses for Situation 1 in the Upper Reach. Error bars indicate values based on the Situation 2 assumption. Net changes are also shown. The dashed box indicates inconclusive results based on a positive ΔM in Sub-reach #2.

The Lower Reach had $\%Q_{loss}$ range from -1.7% to -18.6% and $\%Q_{gain}$ range from 3.8% to 22.6% (Table 3-6). However, the negatives value (-1.3% in Table 3-6) for $\%Q_{gain}$ shows the error causing the positive ΔM to occur in Sub-reach #11 may have been carried over to these calculations. The $\%Q_{loss}$ and $\%Q_{gain}$ were then calculated for Situation 2 to represent the error associated with the assumption of the order of gains and losses.

Table 3-6. Percent Gross Gains and Losses for the Lower Reach

Sub-reach number	Sub-reach interval (m)	Situation 1		Situation 2		Error in $\%Q_{loss}$ and $\%Q_{gain}$ from assumption
		$\%Q_{loss}$ before gain	$\%Q_{gain}$ after loss	$\%Q_{loss}$ after gain	$\%Q_{gain}$ before loss	
7	713 to 813	-1.7	6.1	-1.8	6.2	±0.1
8	813 to 877	-6.0	19.7	-7.2	20.9	±1.3
9	877 to 995	-12.9	3.8	-13.5	4.3	±0.6
10	995 to 1087	-18.1	15.0	-21.4	18.3	±3.3
11	1087 to 1160	8.5	6.4	9.0	5.9	±0.5
12	1160 to 1235	-13.9	-1.3	-13.7	-1.5	±0.2
13	1235 to 1291	-4.8	22.6	-6.0	23.7	±1.2

In the Lower Reach, Sub-reach #10 shows a relatively small net %Δ*Q* (Figure 3-10) with a large %Q_{gain} and %Q_{loss} occurring together (Figure 3-12). Sub-reaches #8 and #13 have substantial gross gains. Even with visual evidence of gains in two sub-reaches (Figure 3-2), every sub-reach has gains and losses that occur together. However, the error in Sub-reach #11 caused results for Sub-reaches #11 and #12 to be inconclusive (highlighted with a dashed box in Figure 3-12).

Quantifying %Q_{gain} and %Q_{loss} provide a better understanding of the extent of surface water-groundwater interactions occurring. However, the complexity of these interactions (e.g., locations of gains and losses (both laterally and longitudinally), flow paths, and spatial distributions) are not understood based on the gross water balance information.

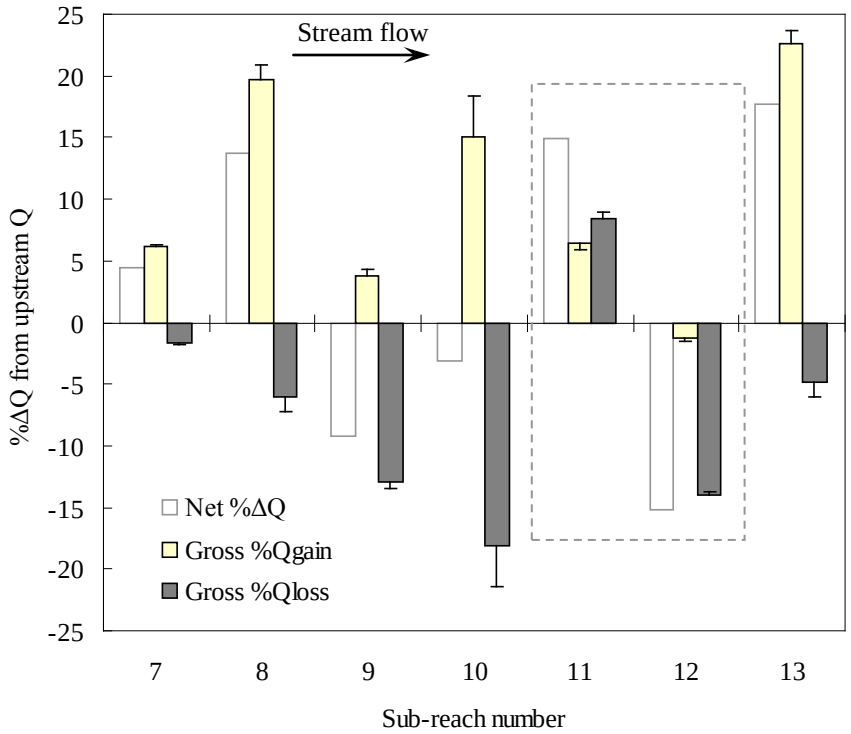

Figure 3-12. Percent gross gains and losses for Situation 1 of the Lower Reach. Errors bars indicate values based on the Situation 2 assumption. Net changes are also shown. The dashed box indicates inconclusive results based on a positive Δ*M* in Sub-reach #11.

Site Characterization Data

Groundwater Table and Stream Water Surface Elevations

The average bottom slope of the Upper Reach is 0.023 and 0.016 of the Lower Reach (refer to Tables D-1 and D-2 in Appendix D for the bottom slope of each sub-reach). The Upper Reach has a steeper slope than the Lower Reach by 33%, but has more variability at the sub-reach scale based on the standard deviation (located in Tables D-1 and D-2) of the sub-reach bottom slopes. The thalweg elevation profile shows the variability of the bottom slope in the Upper Reach (Figure 3-13) and Lower Reach (Figure 3-14). The profile for the Upper Reach shows there are more distinct changes than the Lower Reach, indicating there are more pool-riffle features while the variability of the Lower Reach is more constant. There are distinct surface seeps in the Upper Reach at distances of 78, 104, and 153 m and in the Lower Reach at distances of 825 m and 1238 m with all occurring along the right edge of water (Figures 3-13 and 3-14). In the Lower Reach, the surface seeps appear to be a combination of surfacing groundwater and water flowing through the old channel.

The measured aquifer depth is shallow with a mean depth from the ground surface to the groundwater table of ~0.9 m (~3 ft) indicating a high potential for surface water-groundwater interactions. The discrete groundwater table and stream water surface elevations measured on July 11, 2008 provided information regarding possible locations that were gaining or losing. These elevations, shown with the profiles, are separated into the groundwater table along the right and left side of the channel, the water surface in the active stream channel, and the water surface in the old channel (Figures 3-13 and 3-14).

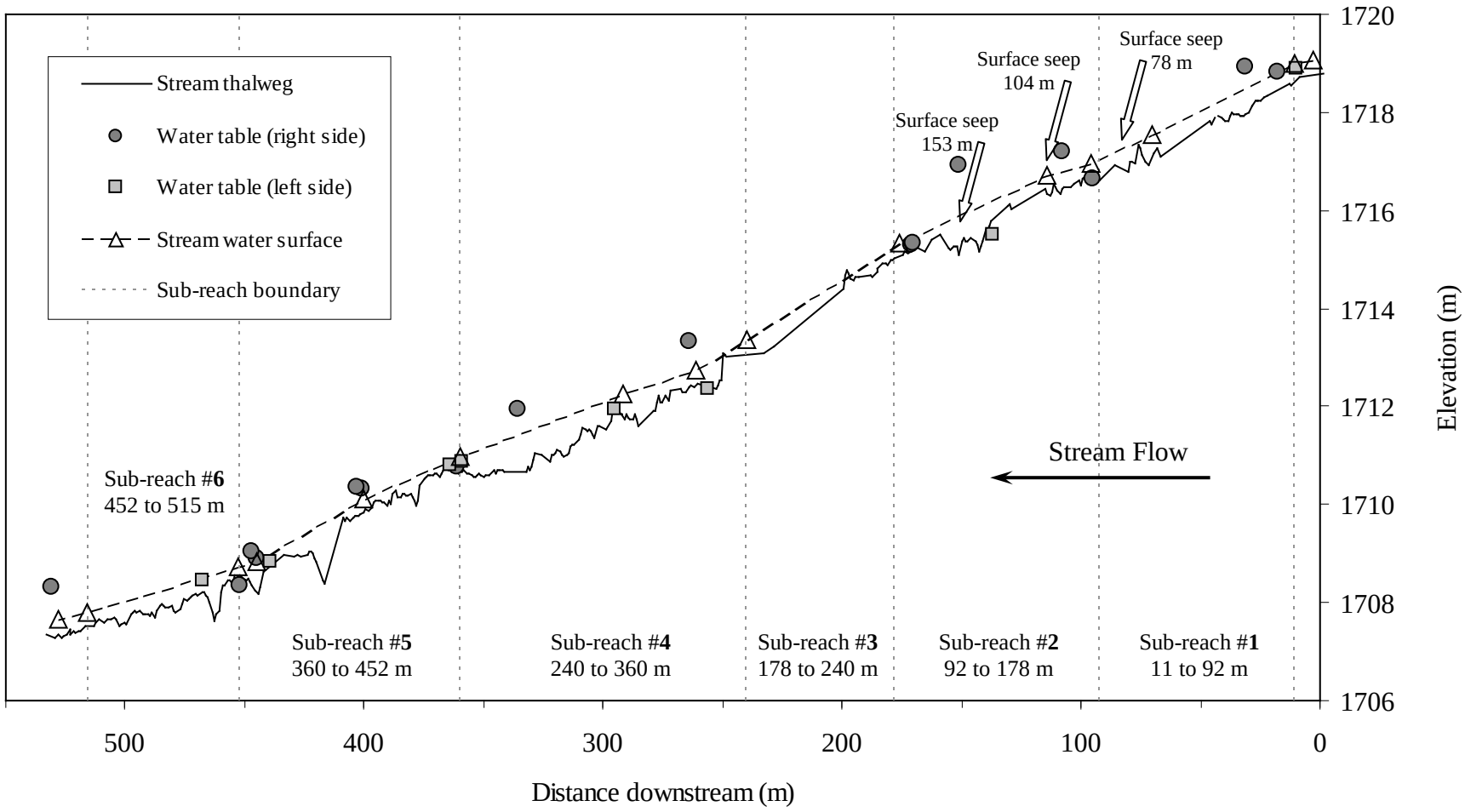

Figure 3-13. Elevation profile of stream thalweg, groundwater table, and stream water surface for the Upper Reach measured on July 11, 2008. The arrows indicate stream locations where visual surface seeps are present.

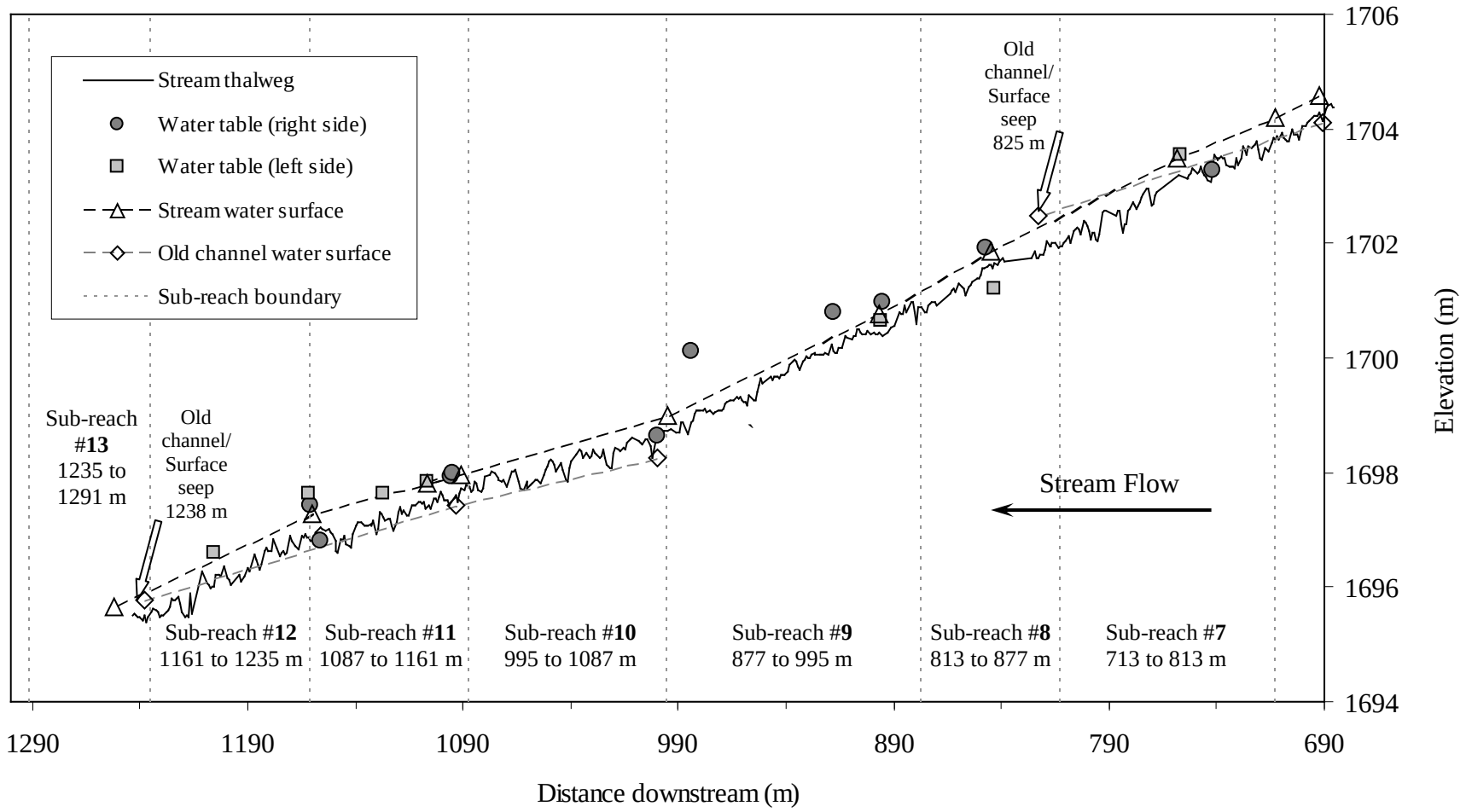

Figure 3-14. Elevation profile of stream thalweg, groundwater table, and stream water surface for the Lower Reach measured on July 11, 2008. The arrows indicate stream locations where visual surface seeps are present.

From these elevation data and signs of surface seeps, the Upper and Lower reaches have varying groundwater exchange occurring and the selected sub-reaches have either gains or losses dominantly occurring. However, the spatial resolution of discrete elevation information is coarse, resulting in limited information regarding the complexity of surface water-groundwater interactions. To provide more information from the discrete elevation data, 0.25 m groundwater table contours were constructed using ESRI® ArcGIS™ (Version 9.3, Redlands, California) software and creating a triangulated irregular network (TIN) surface by interpolating between the discrete elevation data for the Upper Reach (Figure 3-15) and the Lower Reach (Figure 3-16). The estimated direction of groundwater flow is perpendicular to the groundwater table contours.

The overall groundwater table gradient estimated from the groundwater table and stream water surface elevation data is 0.029 for the Upper Reach and 0.023 for the Lower Reach. The groundwater table gradient is approximately 32% higher in the Upper Reach than the Lower Reach while the average stream bottom slope for the Upper Reach is 33% higher than the Lower Reach. Refer to Appendix D for additional discrete elevation measurements measured on July 16, 2008 (Figures D-1 and D-2) and August 22, 2008 (Figures D-3 and D-4) with groundwater table contours constructed from these data. The fluctuations of the water table remained stable for July 2008 through August 2008.

For the Upper Reach, the groundwater table contours indicate that Sub-reaches #1 and #2 are gaining along the right edge of water and also losing along the left edge (Figure 3-15) while the profile information suggests dominant gains along the right edge of water (Figure 3-13). Evidence of gains and losses concurrently occurring along the right edge and left edge of water indicate the assumption that a loss occurs before a gain

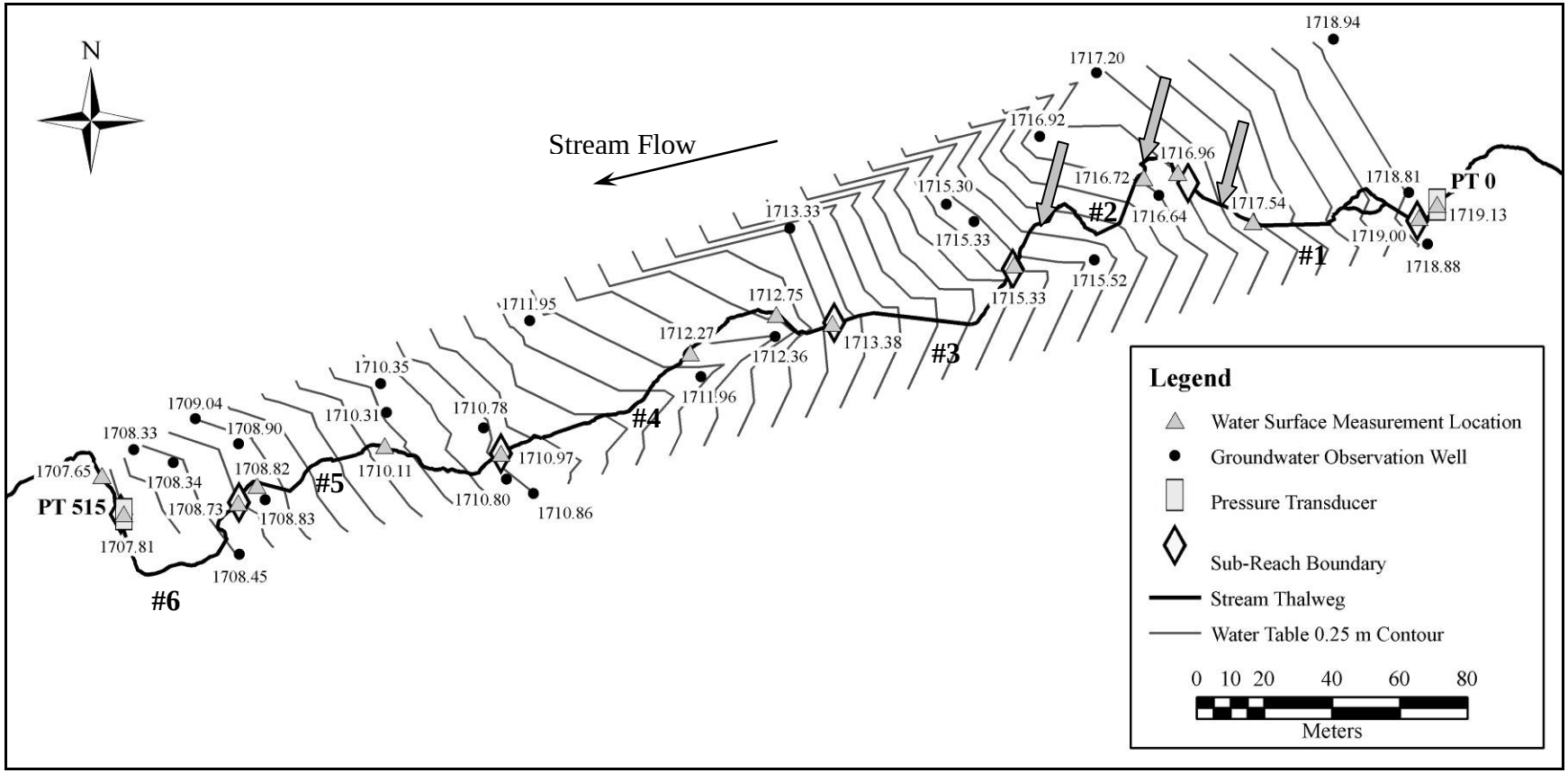

Figure 3-15. Upper Reach discrete head information (elevations in meters) measured on July 11, 2008 and 0.25 m groundwater table contours. Sub-reach boundaries and pressure transducer locations are also shown. The arrows show surface seep locations.

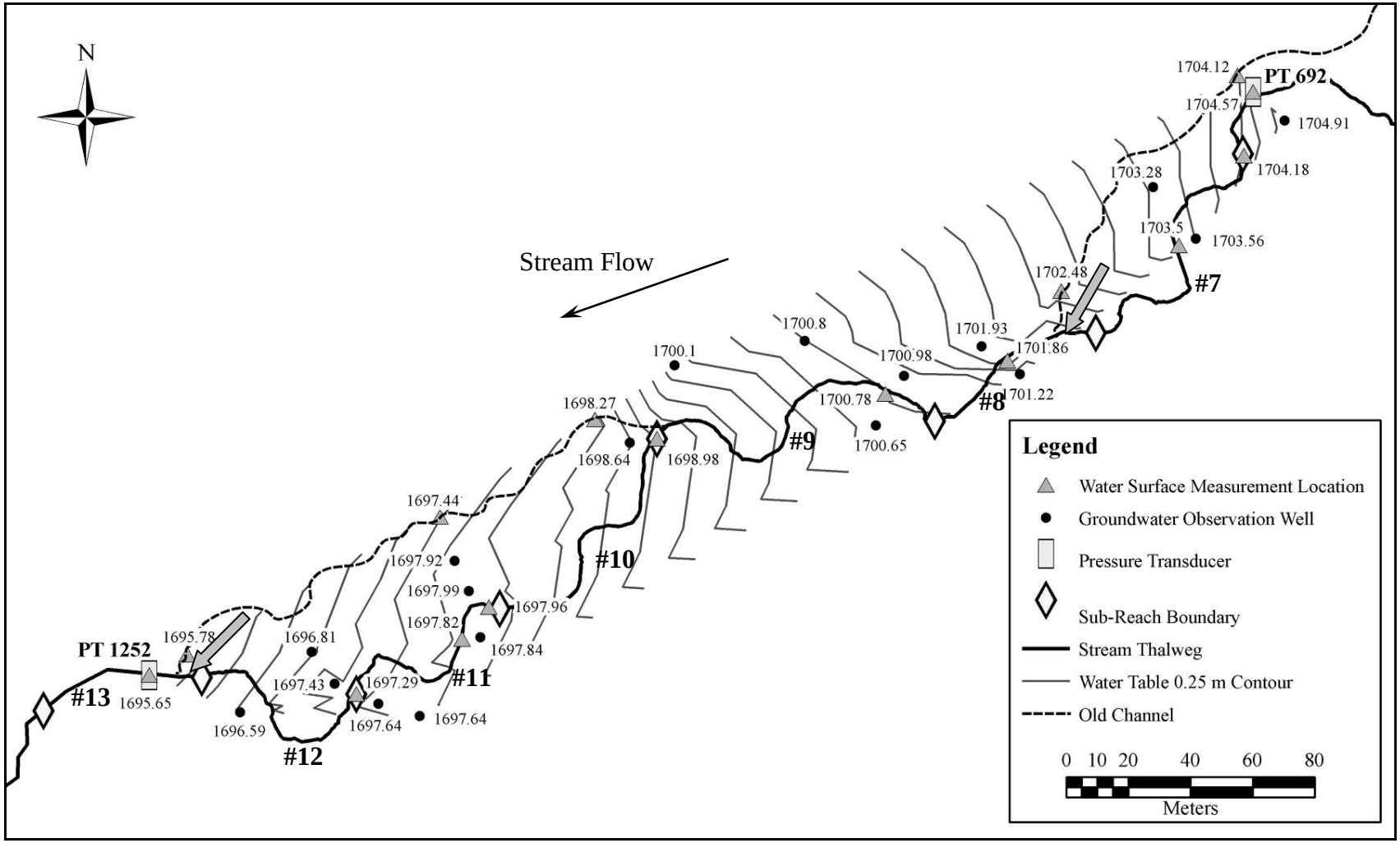

Figure 3-16. Lower Reach discrete head information (elevations in meters) measured on July 11, 2008 and 0.25 m groundwater table contours. Sub-reach boundaries and pressure transducer locations are also shown. The arrows indicate surface seeps and the dashed lines show approximately the location of the old stream channel before 2001.

or a gain occurs before a loss as point flows is invalid. Sub-reaches #3 and #4 are shown to be gaining along the right edge and left edge of water which is not consistent with the profile information. This indicates dominant gains along the right edge of water and slightly losing along the left edge of water relative to the right edge. Sub-reach #5 is neither significantly gaining nor losing. Sub-reach #6 is slightly gaining, which is not consistent with the profile information.

For the Lower Reach, these data indicate Sub-reach #7 is gaining along the left edge of water and losing along the right edge of water (Figures 3-16) which is consistent from the profile information (Figure 3-14). The opposite is occurring in Sub-reach #8 with a loss on the left edge and a gain on the right edge which is consistent with the profile information. The groundwater table contours indicate that Sub-reach #9 is also losing along the left edge for the upper portion of the sub-reach and gaining on the lower portion. The profile shows only dominant gaining is occurring. Information is provided that Sub-reach #10 is gaining along the left edge of water from the groundwater contours that was not provided from the profile and losing water into the old stream channel along the right edge of water that is consistent with the profile. Sub-reaches #11 and #12 are indicated to have complex interactions with gains and losses occurring along the right and left edges of water. Stream water is shown to be gaining along the left edge, losing along the right edge, and returning to the stream. Altering the stream channel may have induced complexity of interactions between the active channel and the old channel. The groundwater contours are consistent with the profile information for Sub-reaches #10, #11, and #12. Similar to the Upper Reach, the elevation information along the south side of the Lower Reach is coarse causing a limitation in understanding locations of some

gains and losses. The elevation data of the groundwater table and stream water surface provided useful information regarding potential flow paths and locations of gains and losses. However, the spatial complexity and heterogeneity of the surface water-groundwater interactions is not understood from these data.

To further investigate the spatial complexity and variability of surface water-groundwater interactions in this system, chloride concentrations, specific conductance (SC), and temperature were measured in a subset of the groundwater observation wells (refer to Figure 3-5) and surface seeps (refer to Tables E-1 and E-2 in Appendix E). The variability, measured as one standard deviation (StDev) of the data set, in chloride concentrations for the Upper Reach and Lower Reach is 5.42 mg L^{-1} (Table E-1) and 92.09 mg L^{-1} (Table E-2) with averages of 12.18 mg L^{-1} and 73.54 mg L^{-1}, respectively. The indication of variability in the two reaches is also shown by the SC measurements with a standard deviation of 88.3 μS cm^{-1} for the Upper Reach and 327 μS cm^{-1} for the Lower Reach with average of 560 μS cm^{-1} and 733 μS cm^{-1}, respectively (Tables E-1 and E-2). The variations in temperature measurements are less with standard deviations of 2.3 °C for the Upper Reach and 1.3 °C for the Lower Reach. There is significant spatial variation of concentrations in the Upper Reach. However, there is also a high degree of spatial variation in the Lower Reach with some observations more that are an order of magnitude different. These data provide additional evidence that the interactions in this system are highly spatially complex and are challenging to measure and predict.

The error in chloride concentration is 0.12 mg L^{-1} based on one standard deviation of triplicates. From the QA/QC results, all percent recoveries (%R) and relative percent differences (RPD) from spikes and replicate spikes are within precision and accuracy

requirements according to EPA Method 300.0 (refer to Appendix B for RPDs (Table B-5) and a quality control chart of %Rs (Figure B-1)).

Vertical Head Gradients

Vertical head gradient (VHG) was estimated within the same time period for each day and the error bars in these estimates is 0.025 cm cm^{-1} determined by taking one standard deviation of triplicate estimates at one piezometer (Figure 3-17). The VHG estimates show that all the locations are locally downwelling with the exception of 1160 m which is slightly upwelling (Figure 3-17 (a) and (c)). The localized VHG estimates significantly fluctuate within the one week period and at locations 96, 360, and 995 m and the VHG is significantly different at depths of 9 and 20 cm. At location 995 m, the depth of 9 cm shows slight upwelling and slight downwelling at the 20 cm depth on July 16 (Figure 3-17 (b)). Compared to the information collected on July 18 (Figure 3-17 (c)), both the 9 cm and 20 cm depths show downwelling, although, the VHG is an order of magnitude higher at 20 cm. The VHG at 9 cm transitioned from upwelling to downwelling within two days illustrating that small variations in stream discharge can have large impacts on VHG estimates. The mechanisms affecting groundwater discharge and recharge measured with groundwater table and stream water surface elevation data is at a different scale than the VHG estimates and information provided by the two data types cannot be directly compared. The VHG of the shallow streambed is controlled by channel-unit scale morphology because 20 cm is the deepest piezometer. For example, the groundwater table and stream water surface elevations suggested dominant gaining in Sub-reaches #1 and #2 while the VHG indicated downwelling at the boundary (distance 96 m).

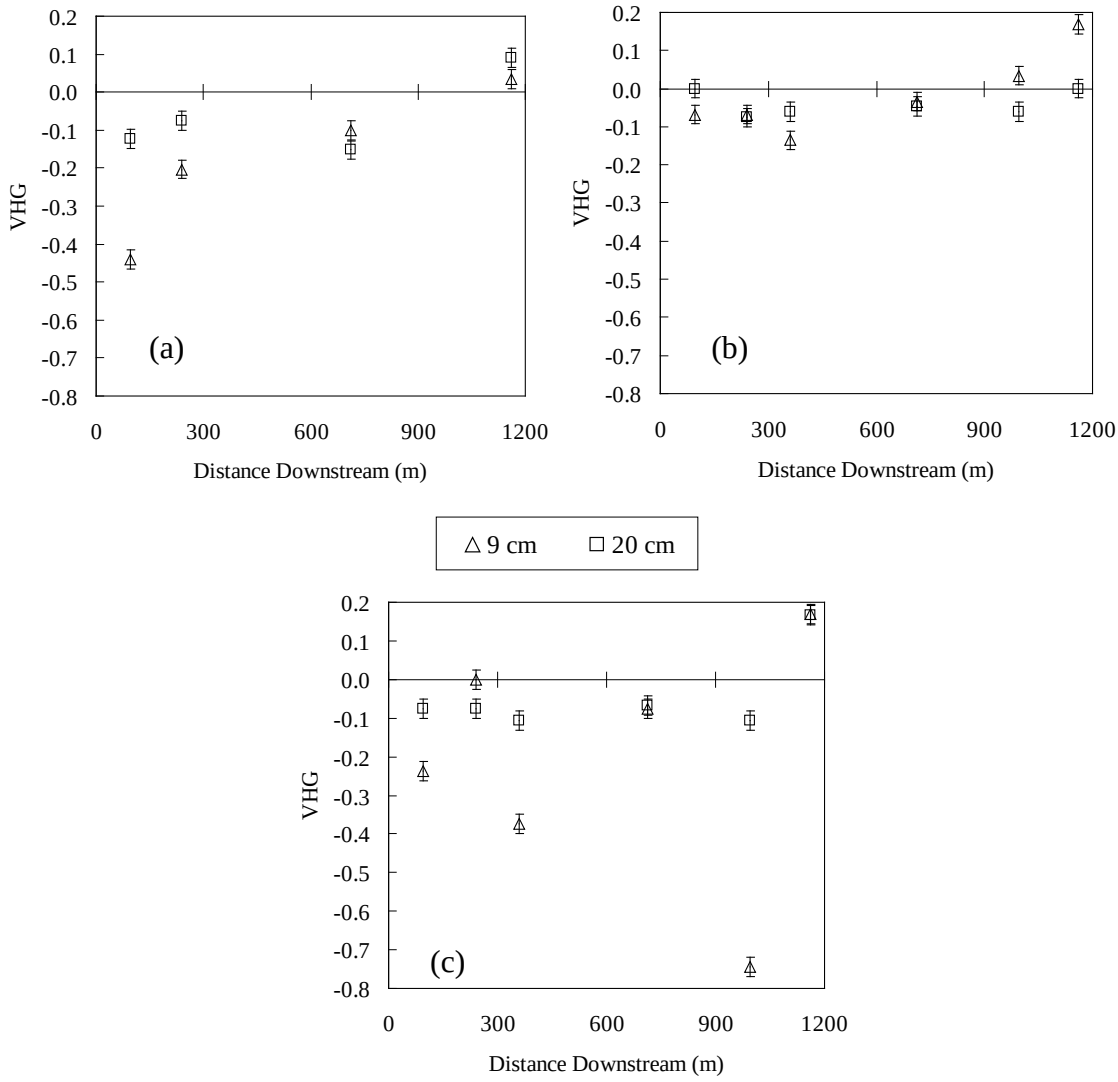

Figure 3-17. VHG estimates at depths of 9 cm and 20 cm observed on (a) 7/11/09, (b) 7/16/09, and (c) 7/18/09.

Hydraulic Conductivity

The saturated hydraulic conductivity (*K*) estimates in the streambed suggest hyporheic exchange is highly variable within a short distance downstream and between depths (Table 3-7). The only location measured at two different times of the year in the streambed was at 240 m. This location had a large decrease in *K* from 3/20 to 9/23 at 9 cm and a large increase in *K* at 20 cm (refer to Appendix E for example plots of

normalized head versus time curves from two slug tests used to estimate *K* (Figures E-1 and E-2)).

The *K* estimates in the surrounding aquifer from the subset of wells also show high spatial variability (Table 3-8). *K* was estimated at a different time period in the aquifer than instream, but *K* values in the aquifer are assumed to not have significantly changed over time. Of the subset of wells tested in the Upper Reach, seven wells had a high *K*, making estimates with slug tests impossible. Additionally, the Lower Reach had six of the 14 wells in the subset that were too high to estimate. For the *K* values able to be estimated with slug tests, the Lower Reach had more variability than the Upper Reach based on one standard deviation of the data set shown in Table 3-8.

Table 3-7. Streambed Hydraulic Conductivity Estimates at Depths of 9 cm and 20 cm

Reach	Sampling Date	Stream Location	Depth in Streambed	
			9 cm	20 cm
			K	*K*
	(mm/dd/yyyy)	(m)	(m d^{-1})	(m d^{-1})
Upper	3/20/2008	96	5.94	0.77
		240	2.33	2.05
		360	-	-
	9/23/2008	96	-	-
		240	0.56	4.58
		360	7.37	1.44
Lower	3/20/2008	713	-	-
		995	-	-
		1160	2.31	7.29
	9/23/2008	713	7.02	2.00
		995	3.34	0.09
		1160	-	-

Table 3-8. Upper and Lower Reach Hydraulic Conductivity Estimates and Chloride Concentrations in Well Subsets

Reach	Well name	*K* ($m\ d^{-1}$)	Chloride conc. ($mg\ L^{-1}$)		Reach	Well name	*K* ($m\ d^{-1}$)	Chloride conc. ($mg\ L^{-1}$)
Upper	W1	0.27	13.63		Lower	W25*	-	252.20
	W2	0.80	8.07			W26*	-	61.49
	W3	1.31	-			W27*	-	295.50
	W4	0.14	7.23			W28	0.04	-
	W8*	-	17.26			W30*	-	22.43
	W9	0.30	-			W31*	-	40.35
	W10*	-	-			W32	0.91	-
	W11*	-	6.12			W33	1.19	20.80
	W12*	-	-			W34	0.42	11.90
	W14	0.12	-			W36	1.50	34.25
	W16	0.36	7.51			W37	0.07	160.15
	W17*	-	10.58			W38	5.78	-
	W19	0.20	9.87			W40	3.42	15.92
	W23	0.27	8.34			W42*	-	13.60
	Average	0.31	10.14			Average	1.67	84.42
	StDev	0.21	3.45			StDev	1.99	103.09

*Wells with high hydraulic conductivities that could not be estimated

The *K* estimates in the subset of wells and in the streambed do not show a clear trend (Figure 3-18). In the Upper Reach, the varying chloride concentrations indicate groundwater exchange is highly influencing mass movement (Figure 3-18). This supports the information provided by the gross water balance that gains and losses are occurring throughout the study reach. Similar to the Upper Reach, the *K* estimates in the Lower Reach vary between the streambed and surrounding aquifer. This illustrates that the spatial scale of consideration is important because the channel unit scale measurements describe the potential for hyporheic exchange and aquifer scale describe the potential for groundwater exchange.

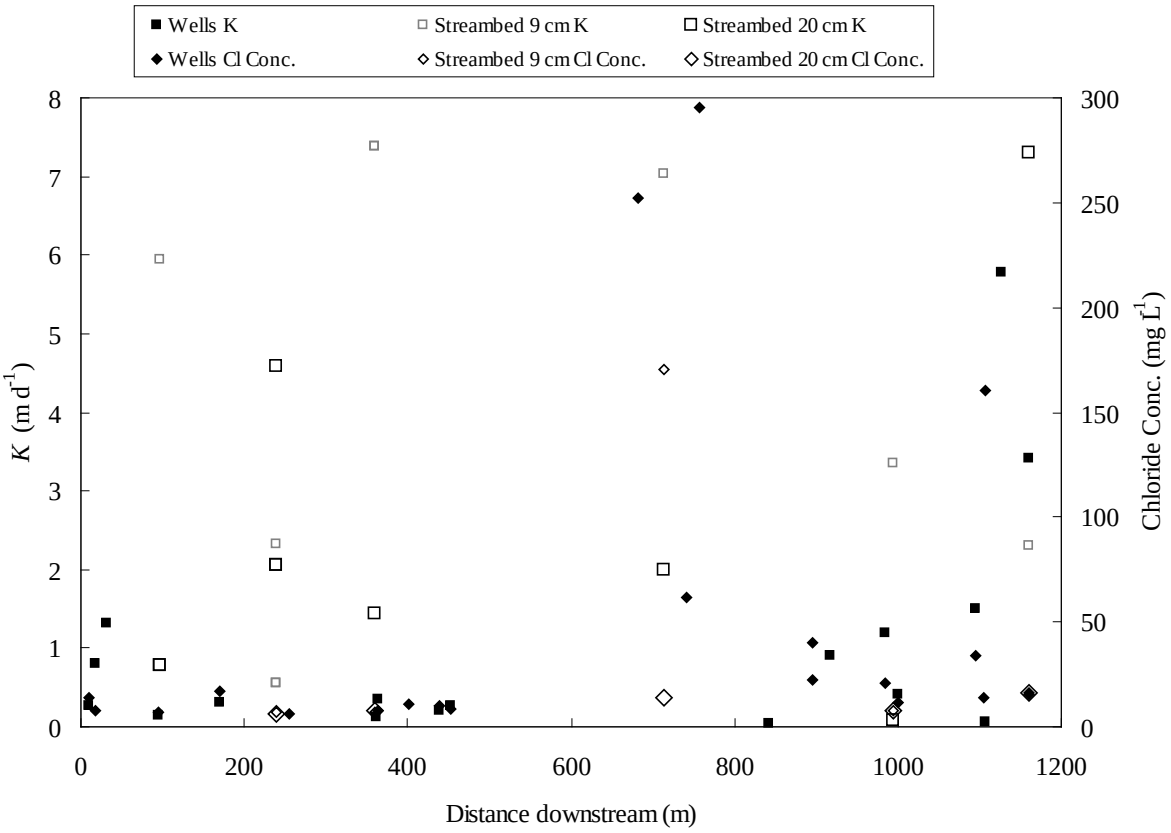

Figure 3-18. Upper and Lower Reach aquifer and instream hydraulic conductivities. Groundwater and streambed chloride concentrations are also shown.

Discussion

Dilution gauging results were compared to rating curve predictions to provide a check to verify if the required assumptions for dilution gauging were reasonably met. When compared at the reach scale, conflicting information resulted with one method suggesting net gaining while the other suggests net losing (Figure 3-7). The error in each method was not addressed in this study and therefore, verifying assumptions was difficult. This conflicting information is significant because when stream gauging is applied at the reach scale, many of the surface water-groundwater interactions occurring may be overlooked and confirms the need to quantify a water balance at a finer spatial

scale. Additionally, this illustrates the need to complete an error analysis for each stream gauging method to understand the reliability to detect significant changes in stream discharge due to small net gains and losses. Quantifying a gross water balance resulted in gross gains and losses concurrently occurring in every sub-reach longitudinally (Figures 3-21 and 3-22), confirming that the spatial scale of consideration is important when studying these processes.

While gross gains and losses provide more information, these calculations require assumptions regarding the locations of exchanges and whether they behave as point flows. Varying if assumptions are appropriate is important because if they are inappropriate, then inaccurate water balance calculations will result and they may also be the largest contributor of error in those calculations. To test and verify the effects of these assumptions on this study, the site characterization data can be used to provide insight regarding the locations (both lateral and longitudinal) of gaining and losing sections. For example, lateral inflows and outflows occur in Sub-reaches #1, #2, and #3 (Figure 3-15) and in Sub-reaches #8, #9, and #10 (Figure 3-16). This information implies that the assumption that gains and losses behave as point flows may not be valid due to exchanges behaving more like distributed flows occurring both laterally and longitudinally. Looking at Sub-reaches #1, #2, and #3 as one combined reach and applying the assumption that a loss is a function of the concentration at either the top of the reach (Situation 1) or at the bottom of the reach (Situation 2), the stream concurrently gains 11.6% to 14.4% and loses -19.3% to -22.1% (Table 3-9). According to observation wells W2 and W8 (Figure 3-5 (a)), the source water of gains had chloride concentrations ranging from 8.07 mg L^{-1} to 17.26 mg L^{-1}, respectively (Table 3-8). Comparatively, the

water leaving the stream (according to wells W1, W4, and W11) had concentrations of 13.63 mg L^{-1}, 7.23 mg L^{-1}, and 6.12 mg L^{-1}, respectively with a mean of 9.0 mg L^{-1}. The top of Sub-reach #1 had a concentration of 5.51 mg L^{-1} and a concentration of 5.17 mg L^{-1} at the bottom of Sub-reach #3 (refer to Table B-7 in Appendix B). The current water balance calculations assume that C_{loss} in Equation 9 is either the concentration at the top or bottom of a sub-reach. The large difference between stream and groundwater concentrations indicates this assumption associated with Situation 1 or 2 may not be valid and the true distribution of concentrations throughout a sub-reach was not necessarily represented.

To further test how applying this assumption changes water balance calculations, additional tracer response curves were measured at stream locations 92 m and 178 m from the slug injection just upstream of 11 m (upstream boundary of Sub-reach #1) (Figure 3-2 (a)). Using these additional response curves, new gain and loss estimates can be calculated resulting in a larger range of concurrent gains of 10.3% to 14.4% and losses of -18.0 to -22.1% (Table 3-9). This illustrates that applying the assumptions for the current water balance, gains and losses can be poorly estimated and the distribution of sources and sinks is not described.

Table 3-9. Tracer Response Curves Measured at Two Additional Locations and Used to Calculate Gross Gains and Losses for Testing Assumptions

Sub-reach number	Measurement location (m)	$\int C(t)dt - \int C_b(t)dt$ (mg L^{-1} sec)	Q (L s^{-1})	$\%\Delta Q$	$\%Q_{loss}$	$\%Q_{gain}$	Situation assumed
	11	1075.9	338.3		**-19.3**	**11.6**	1 (loss before gain)
1	92	1105.4		-7.7	-18.8	11.1	
2	178	1156.4			-18.0	10.3	
3	240	940.7	312.1		**-22.1**	**14.4**	2 (gain before loss)

While this example shows the importance of collecting various types of information at varying spatial scales to better understand surface water-groundwater interactions, there is still limited information regarding the true concentrations leaving the stream. However, a better understanding of the concentration of a loss is important to calculate a more accurate water balance. A better representation of the water balance may use distributed flows similar to *Harvey and Wagner* [2000] and would likely require a better known distribution of concentrations leaving the control volume. To confirm this and better estimate concentrations entering and leaving the stream channel, a longitudinal concentration profile, deep piezometers, or more well transects would be necessary.

Other assumptions required for quantifying a water balance using dilution gauging techniques that are challenging to meet and verify are the completely mixed and the steady state assumptions. The stream discharge at station PT 0 was found to change by ~10% during the time interval tracer experiments were performed (Figure 3-6). This indicated that the assumption of steady state conditions was not met for dilution gauging in the Upper Reach and may have added error to the overall water balance, but the water balance for each sub-reach is assumed to not have been affected by this do to negligible changes in flow during slug travel times for each sub-reach. The discharge fluctuations during tracer experiments in the Lower Reach appeared to be a negligible source of error in water balance estimates. Another advantage of using high frequency discharge estimates together with dilution gauging is that seasonal flow variation information can be used to determine optimal time periods to conduct tracer experiments to capture a wider range of flow conditions and how the surface water-groundwater interactions may vary.

This study proved that extracting comprehensive information from a variety of common data types used to characterize and quantify groundwater exchange processes affecting stream solute transport is challenging. Data collected at larger spatial scales did not detect smaller scale interactions occurring. Smaller scale data were used to understand the complexities of interactions, but some small scale processes are so spatially variable they are difficult to predict or anticipate. In larger reach scale modeling, extrapolation of processes may be assisted by some insight of the small scale processes occurring and are therefore, important to understand. This study provided evidence that collecting one data type is not enough to effectively describe smaller scale stream water-groundwater interactions occurring in order to predict and model solute mass movement. Researchers must be careful about what data types are collected (and at which spatial and temporal scales) to describe these interactions.

Even with a gross water balance shown to be a better representation of groundwater exchange than a net water balance, some shortcomings were observed. Gross gain and gross loss calculations were inconclusive in Sub-reaches #1, #2, and #3 of the Upper Reach (Figure 3-11) and in Sub-reaches #11 and #12 of the Lower Reach (Figure 3-22) due to positive mass recoveries observed in Sub-reaches #2 and #11 (Figures 3-9 and 3-10, respectively) that are assumed to be caused by errors in the data collection methods. A positive calculated ΔM likely occurred due to: (1) the tracer slug not completely mixing before measurements were taken and (2) the background specific conductance (SC) measured in the response curves was not representative of the actual instream background SC due to a lack of lateral mixing. For example, surface seeps proved to have a higher background solute concentration on average than instream and

this input may not have completely mixed where the response curves were measured. Sub-reach #2 had two distinct surface seeps flowing into the stream (refer to Figure 3-2) that may have caused an error in response curves and background SC measured. Sub-reach #11 does not have visual evidence of a surface seep inflow, but the tracer slug travel distance was only 32 m which suggests the slug did not become completely mixed.

Sub-reaches #1, #2, and #3 were combined and treated as one sub-reach by measuring the response of the slug injected upstream of Sub-reach #1 and measured at the downstream boundary of Sub-reach #3. The ΔM for each of the four sub-reaches are now negative suggesting that the influence of the surface seeps was not detected because the travel distance is long enough to have the influxes fully incorporated in the stream water (Figure 3-19). Sub-reaches #11 and #12 were also combined and treated as one sub-reach. The ΔM for each of the now six sub-reaches are negative, suggesting that the error in the data collection was omitted (Figure 3-20).

The newly calculated gross gains and losses appear to be more representative of the exchanges occurring in the Upper and Lower Reaches (Figures 3-21 and 3-22). This shows the importance of observing tracer responses at more than one sub-reach boundary in case of the event of an error in the data collection. Combining sub-reaches may still provide enough information regarding a water balance to be used to support solute transport modeling. However, while these results appear to be more probable, it is possible that in combining sub-reaches some exchanges may not be detected.

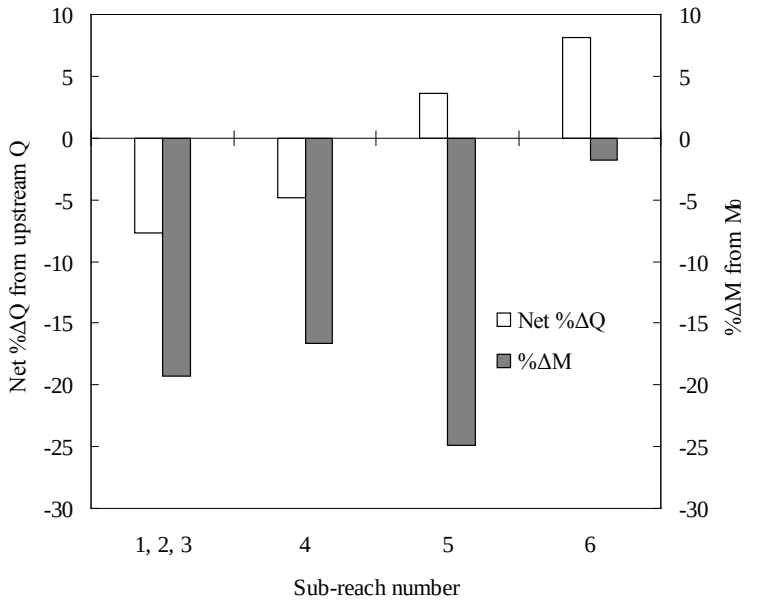

Figure 3-19. Percent net change in discharge and tracer mass for Sub-reaches #1, #2, and #3 combined in the Upper Reach.

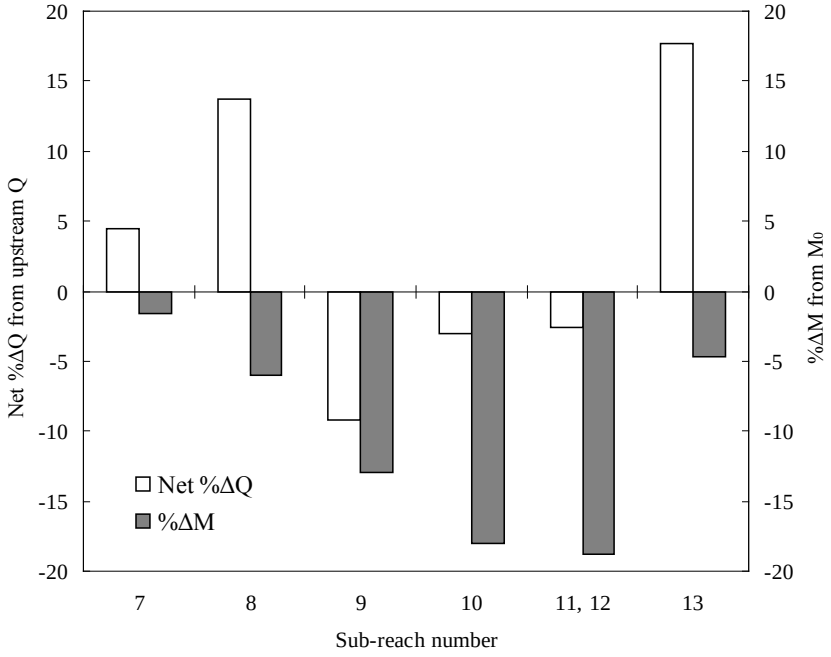

Figure 3-20. Percent net change in discharge and tracer mass for Sub-reaches #11 and #12 combined in the Lower Reach.

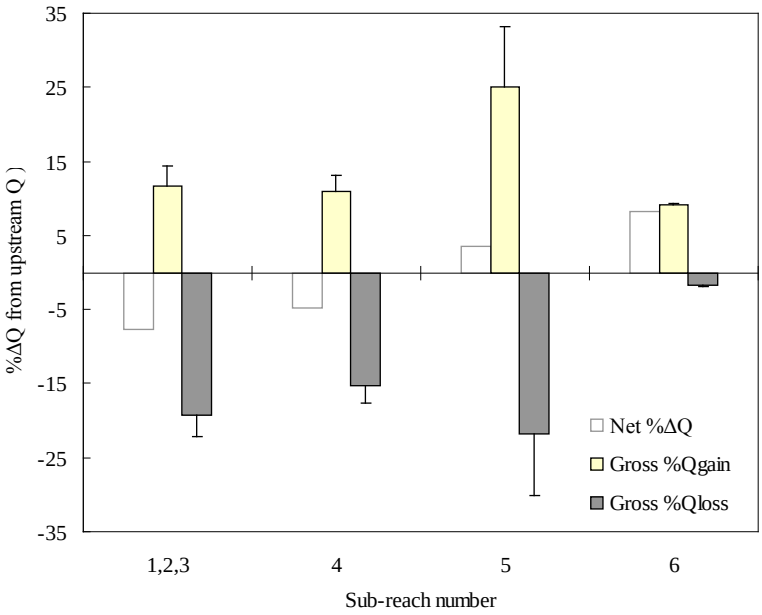

Figure 3-21. Gross gains and losses for the Upper Reach with Sub-reaches #1, #2, and #3 combined. Net changes are also shown.

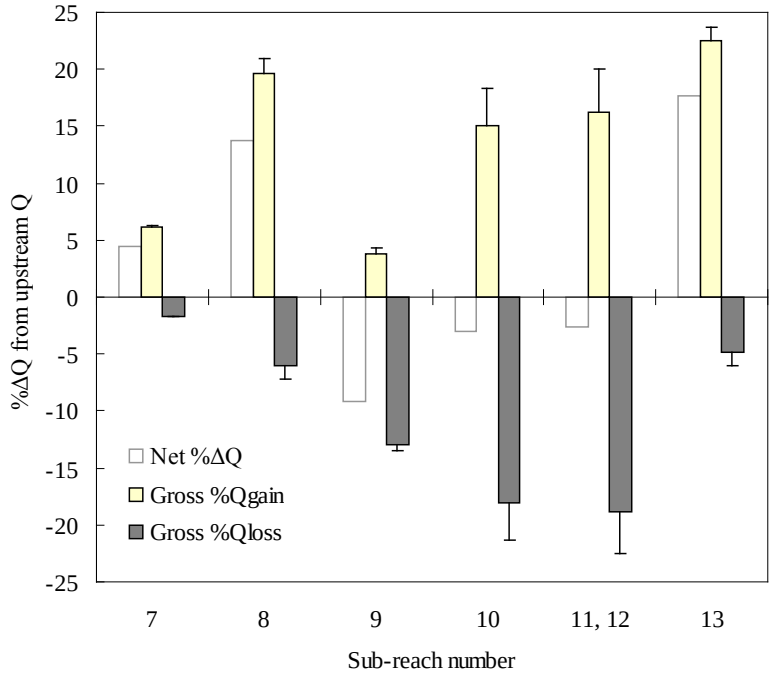

Figure 3-22. Gross gains and losses for the Lower Reach with Sub-reaches #11 and #12 combined. Net changes are also shown.

Conclusions

The surface water-groundwater interactions in the two study reaches at Curtis Creek were shown to be highly spatially variable and complex. The spatial scale in which data were collected proved to be important when attempting to understand and predict solute mass movement. This study also provided evidence that collecting one data type is not adequate to effectively describe stream water-groundwater interactions occurring. Researchers must be careful about what data types are collected, and at which spatial scale, to describe these interactions.

A reach scale net water balance with the two methods of rating curve predictions and dilution gauging techniques provided limited information regarding surface water-groundwater exchanges and did not represent all exchanges that occurred in the system. Establishing sub-reaches was necessary to examine the extent of surface water-groundwater exchange. The sub-reaches were shown to have highly spatially dynamic groundwater exchange processes where gains and losses were concurrently occurring.

The water balance quantified in terms of gross gains and losses provided information used to support solute transport predictions. However, assumptions applied to quantify the water balance were proven to be challenging to test and verify. Assuming that gains and losses occur as point flows was found to provide reasonable estimates of gains and losses, but may not be appropriate to accurately represent all groundwater exchange processes occurring based on the groundwater table and stream water surface elevation data. Although an estimate of groundwater exchange was determined, the uncertainty in the distribution of concentrations entering and leaving the stream channel contribute to the error in water balance calculations and the effects of the assumptions on

these calculations should be further investigated. To confirm and test this importance, a higher spatial resolution of both instream concentration data is required.

CHAPTER 4

UNCERTAINTY IN STREAM WATER BALANCES

Abstract

Throughout the stream reach in this study, gains and losses are highly spatially dynamic and are attributed to groundwater exchange processes. Stream water balances were quantified to describe these processes because of their role in solute mass movement through surface water bodies. Net changes in stream discharge were first estimated at a reach scale for two separate portions of the stream with lengths of 515 m and 560 m, respectively, by applying two separate methods: (1) high frequency discharge estimates using rating curves and (2) dilution gauging techniques with instantaneous tracer experiments. To determine the reliability of each method to detect changes, errors in rating curve predictions were quantified using 95% joint confidence regions and errors in dilution gauging were estimated with a first order error analysis. Neither method was found to be capable of detecting surface water-groundwater exchanges occurring at this scale with the mean error in rating curve predictions estimated to be 10% and 8% with dilution gauging. To better understand exchanges at a smaller spatial scale using dilution gauging, a net system water balance in terms of net changes was estimated at a sub-reach scale (lengths ranging from 56 m to 120 m). At this scale, changes ranged from 3% to 23% of the total discharge and occurred in all sub-reaches. When considering that the 95% confidence interval in these estimates is ±8%, significant net changes were observed in only half of the sub-reaches. Gross gains and gross losses that contribute to these net changes were quantified and an error analysis was additionally performed for these

estimates. Some sub-reaches that did not have significant net changes did show significant gross gains and losses concurrently occurring. The results highlight the importance of estimating error to determine the reliability of detecting surface water-groundwater exchanges at different spatial scales.

Introduction

A better understanding of surface water-groundwater interactions is essential for appropriate management strategies and policy because of their role in solute transport. These interactions are often poorly understood because they are challenging to predict and measure [*Winter et al.*, 1998]. Stream water will either be gaining from groundwater discharge or losing to groundwater recharge, can often be highly spatially and temporally dynamic, and plays an important role on stream solute interactions [*Covino and McGlynn*, 2007]. In many systems, both gains and losses occur within the same reach making it challenging to measure and predict the complexity of these interactions. *Winter et al.* [1998] describe surface water-groundwater in such systems as being a single resource, that is they are continuously interconnected. This understanding is important because altering either surface water or groundwater will have a direct effect on the other.

Previous approaches used to estimate and characterize surface water-groundwater interactions include: stream gauging with velocity-area techniques [*Rantz*, 1982], tracer experiments [*Harvey and Wagner*, 2000; *Payn et al.*, 2009; *Ruehl et al.*, 2006], stream temperature surveys [*Becker et al.*, 2004; *Kerry et al.*, 2007], or hydrograph separation with isotopic tracer techniques [*Cey et al.*, 1998]. The results of these studies are typically used to support heat and solute transport modeling applications that more

completely describe other physical transport processes (e.g., transient storage) [*Bencala and Walters*, 1983; *Choi et al.*, 2000; *Harvey et al.*, 2005].

Stream gauging with velocity-area techniques are often correlated to stage data to develop rating curves used to obtain high frequency stream discharge estimates from continuous stage data [*Kennedy*, 1983]. Error in velocity-area techniques has been expressed as ±15% of the discharge observation [*Cey et al.*, 1998]. Uncertainty in rating curves predictions is often determined by taking the standard deviation of the residuals and applying a constant error to all the predictions [*Kennedy*, 1983].

Dilution gauging, completed with tracer experiments, also provides flow estimates at point locations on a stream. This approach can additionally be used to provide groundwater exchange information by quantifying both net and gross stream gains and losses used to estimate a water balance [*Harvey and Wagner*, 2000; *Payn et al.*, 2009]. Error in dilution gauging has been reported as 10% and is expressed as the residual standard error between observations and model simulations [*Harvey et al.*, 2003]. However, the components of uncertainty in dilution gauging are currently poorly understood.

To predict and model stream transport processes at a small spatial scale, a complete water balance estimated with accurate discharge measurements is required. This information will assist in model parameter calibration and provide information regarding flow path residence times [*Harvey and Wagner*, 2000]. In order to determine a water and mass balance, gains and losses throughout a reach must be quantified. This may require reach segmentation to capture spatial variability in streams highly influenced by groundwater. Surface water-groundwater interaction studies have often focused on

large spatial scales (several kilometers) [*Covino and McGlynn*, 2007; *Ruehl et al.*, 2006]. However, *Payn et al.* [2009] recently quantified net changes in stream discharge of 200 m sub-reaches with dilution gauging techniques and found gross gains and losses occurring at this scale. However, the ability to determine whether these exchanges were significant was limited.

In this paper, methods are presented to complete error analyses of both rating curves and dilution gauging used to estimate a net water balance at a reach scale. To provide groundwater exchange information at a finer spatial scale, net and gross water balances are estimated with dilution gauging techniques at a sub-reach scale. The error analyses are used to test the reliability of the two approaches and to detect significant changes in stream discharge at the two spatial scales.

Site Description

The selected study portion of Curtis Creek, UT is approximately 1.25 km in length near the outlet of the watershed (Figure 2-1) that drains approximately 59.5 km^2 [*U.S. Geological Survey*, 2007]. Curtis Creek is a first order perennial mountain stream with ephemeral (seasonal) tributaries during storm and snow melt events. Curtis Creek is a tributary to the Blacksmith Fork River which flows into Cutler Reservoir and ultimately the Great Salt Lake.

The site of this project is located on Curtis Creek at Hardware Ranch, a Utah Division of Wildlife Resources (UDWR) operated facility, located approximately 15 miles east of Hyrum, UT. The land area just to the north of the study site is used to grow

animal feed (Figure 4-1) and is irrigated for most of the summer months by flood irrigation from Curtis Creek water that is diverted upstream of the study site.

The average stream discharge for July 2007 to November 2008 was approximately 200 L s^{-1} (~7 cfs) with a range of about 142 L s^{-1} to 1,841 L s^{-1} (~5 to 65 cfs) where base flow occurred during late summer into late winter (August to February) and peaked during late Spring into early Summer (April to June). The average channel width is approximately 3.7 m (12 ft) with a gradient of 0.010 to 0.032.

The overall experimental reach selected was divided into two separate reaches, an Upper (~0.515 km) and Lower (~0.560 km) Reach (Figure 4-1). The Upper Reach has had little influence of anthropogenic activities (e.g., altering of channel location or geometry) and is dominantly a pool-riffle system with varying storage characteristics (i.e., woody debris, slow moving water, plunge pools, large cobble substrate, and vegetation in shallow pools). There are at least four visible surface seeps (i.e., groundwater that surfaces in marsh areas prior to flowing into the stream) contributing to gains in stream flow along the right edge of water. The Lower Reach channel was altered in 2001 by the UDWR [*Utah Division of Wildlife Resources,* 2001] resulting in different physical characteristics than the Upper Reach. The Lower Reach has more swift riffles, less pool-riffle features, more uniform channel geometry, and similar coarse gravel to large cobble substrate. The Lower Reach is also influenced by groundwater influxes from surface seeps in two distinct locations along the right edge of water. The overall experimental reach (which includes the Upper and Lower Reach) has stream water gains and losses, due to groundwater exchanges and long hyporheic flow paths, which are highly spatially dynamic that affect solute transport.

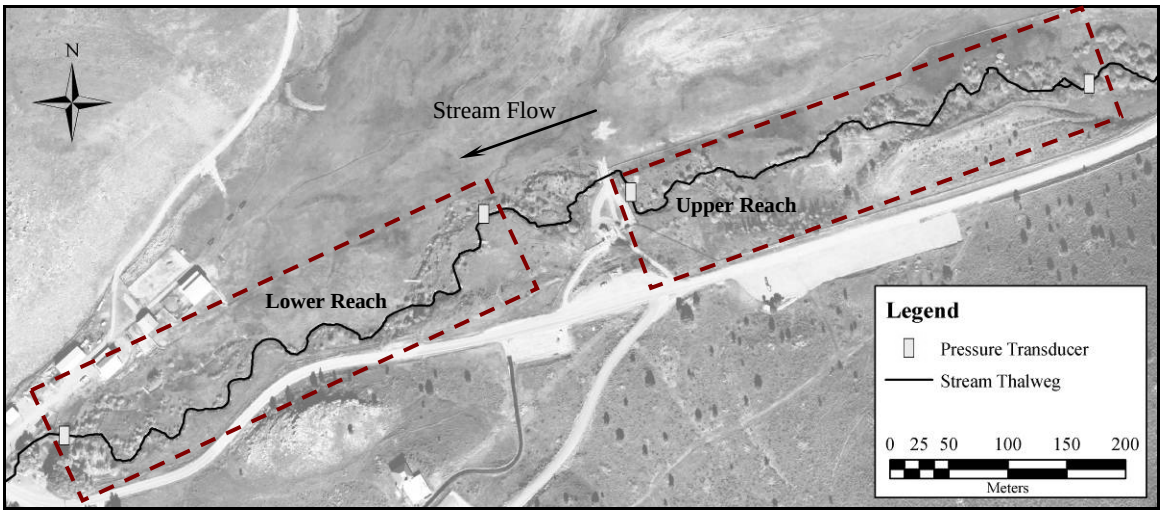

Figure 4-1. Upper and Lower Reaches. Locations of pressure transducers installed are shown to provide locations of reach boundaries.

The watershed feeding the experimental reach of Curtis Creek includes a combination of hard rock (Paleozoic and Precambrian bedrock that is strongly indurated (hardened)) and very dense soil deposits in valleys consisting of coarse-grained deposits with gravel, cobble, or boulders that include alluvial fan deposits [*McCalpin et al.*, 2001]. The headwater of Curtis Creek originates in the Monte Cristo Range that is part of the Wasatch Range in northern Utah and flows southwesterly through narrow canyons into wider valleys (refer to Figure 2-1). A general understanding of the watershed geology is important because water chemistry is influenced by the type of geological material and contact times [*Winter et al.*, 1998].

Methods

Rating Curves

In order to establish rating curves at reach boundaries, stage-discharge observations were required [*Kennedy*, 1983]. With this information rating curves were developed in the form of Equation 4-1 [*Cey et al.*, 1998; *Rantz*, 1982].

$$Q = aZ^{b} \quad (4\text{-}1)$$

where:
Q = predicted stream discharge, cfs;
a and b = the regression parameters;
Z = the stage reading, ft.

Reach boundaries were selected at stream distances of 0 m (station PT 0) and 515 m (station PT 515) for the Upper Reach and 692 m (station PT 692) and 1252 m (station PT 1252) for the Lower Reach (Figure 4-1). The exact locations of the reach boundaries were selected based of the uniformity of the channel geometry necessary to measure more accurate stream discharges [*Rantz*, 1982].

Using the discharge and stage data acquired at each station, a nonlinear regression based on the least residual sum of squares was completed to estimate the parameters *a* and *b* in Equation 4-1 resulting in high frequency discharge estimates from continuously monitored water levels (stage). Stage was recorded using KWK Technologies® SPXD™ 600 and 610 (0-5 psig) pressure transducers (PT) (Spokane, Washington) with vented cables and Campbell Scientific® CR-206 data loggers (Logan, UT) at 5-minute intervals.

The error associated with each of the four rating curves was estimated by sampling from the estimated 95% joint confidence region (JCR) of the parameters *a* and *b* computed according to *Beale* [1960]. This method consists of generating a random sample of paired parameter values using Latin hypercube techniques centered on the nonlinear least sum of squares estimate and rejecting the parameter values whose residual sum of squares do not verify the Beale criterion (95% JCR).

Assumptions required to estimate error in rating curve predictions using this approach are: observations are random, observations are independent, variance is

constant, and residuals are normally distributed. To test these assumptions, the residuals of each rating curve were analyzed with a probability plot and histogram to test normality and the constant variance assumption.

Dilution Gauging Techniques

Dilution gauging techniques with the use of instantaneous tracer experiments were used to quantify stream discharge at a reach scale and provide a comparison to rating curve discharge predictions. Additionally, using an approach similar to *Payn et al.* [2009], dilution gauging was completed at a sub-reach reach to provide more information on groundwater exchanges at a finer spatial scale.

Chloride was selected and used as a conservative solute tracer [*Zellweger*, 1994] for all instantaneous experiments and rhodamine WT was used as a visual indicator for qualitatively testing mixing assumptions. The source of chloride was sodium chloride (NaCl). Tracer response curves were measured in situ with specific conductance (SC) in the main channel following an instantaneous pre-dissolved chloride tracer injection with YSI® sondes (models 600 LS and 600 XLM, Yellow Springs, Ohio) at one second intervals. To correlate the response curves to chloride concentrations, external chloride concentration standards were made with creek water [*Gooseff and McGlynn*, 2005] from two locations (one in the Upper Reach and one in the Lower Reach). Four calibration curves between SC and chloride concentrations were then made for comparison purposes by measuring the SC response from each field instrument in each standard and the SC of each standard was measured according to Standard Methods 2510B [*American Public Health Association*, 1999].

Once the SC tracer response curves were translated to chloride concentrations, these data were used to estimate stream discharge using Equation 4-2 [*Kilpatrick and Cobb*, 1985]. Refer to Chapter 3 for more detail regarding the procedure.

$$Q = \frac{M}{\int_0^t \left(C(t) - C_b\right)dt} = \frac{M}{\int_0^t C(t)dt - \int_0^t C_b dt} \tag{4-2}$$

where:
Q = the main channel volumetric flow, L s^{-1};
M = mass of solute tracer slug injected, mg;
$C(t)$ = observed solute tracer concentration, mg L^{-1};
C_b = background solute tracer concentration, mg L^{-1};
t = time, s.

For an accurate stream discharge calculation to be obtained from Equation 4-2, the following assumptions must be met:

1) The tracer slug instantaneously injected must become completely mixed before measurements are observed;
2) No mass of the slug is lost between the injection location and the measurement location; and
3) The stream flow remains constant during the tracer measurement time period.

Instream background concentrations of chloride were measured with a Dionex® ion chromatograph according to EPA Method 300.0. The quality assurance and quality control (QA/QC) for measured grab samples was analysis of replicate tests, replicate specimens, spikes and duplicate spikes, calibration curve verifications (CCVs), blanks, and trip blanks. The background SC was subtracted from each response curve and therefore, the slope of the calibration curve was used to correlate SC to chloride concentrations [*Gooseff and McGlynn*, 2005; *Payn et al.*, 2009].

To quantify the variability of stream discharge associated with groundwater exchange at a smaller scale, 13 sub-reaches were selected with six in the Upper Reach (Figure 4-2 (a)) and seven in the Lower Reach (Figure 4-2 (b)). Fifteen instantaneous tracer slug injections were performed to estimate stream discharge at each sub-reach boundary. Seven injections were completed in the Upper Reach (Figure 4-2 (a)) and eight in the Lower Reach (Figure 4-2 (b)) during minimal stream discharge variations (assumed to be steady state conditions). To avoid completing injections into poorly mixed pools or at locations of visual inflows and to meet the assumptions of complete mixing and no loss of tracer mass, the travel distances (distances between injections locations and measurement locations) varied and ranged from 23 m to 77 m.

Dilution gauging was completed by measuring the response curve at stream distance 1291 m first and then moving upstream to the next sub-reach boundary (Figure 4-2). This approach was used to prevent experimental error caused by measuring residual solute. The uncertainty in dilution gauging was analyzed in two separate parts: (1) variance in data collection and (2) variance in the field injection method.

Variance in Data Collection Method

There is variance in each piece of information used to estimate stream discharge from dilution gauging techniques. The total variance in these estimates can be attributed to:

1) The measured tracer mass injected;
2) The integrated response curve; and
3) The measured background concentration.

Additional sources of error are assumed to be random.

The contribution of each individual error to the variance was determined by estimating the variance of each variable in Equation 4-2. Each individual variance results in a weighted contribution to the total variance and can be estimated with a first order error analysis through error propagation [*Berthouex and Brown*, 2002]. To apply error

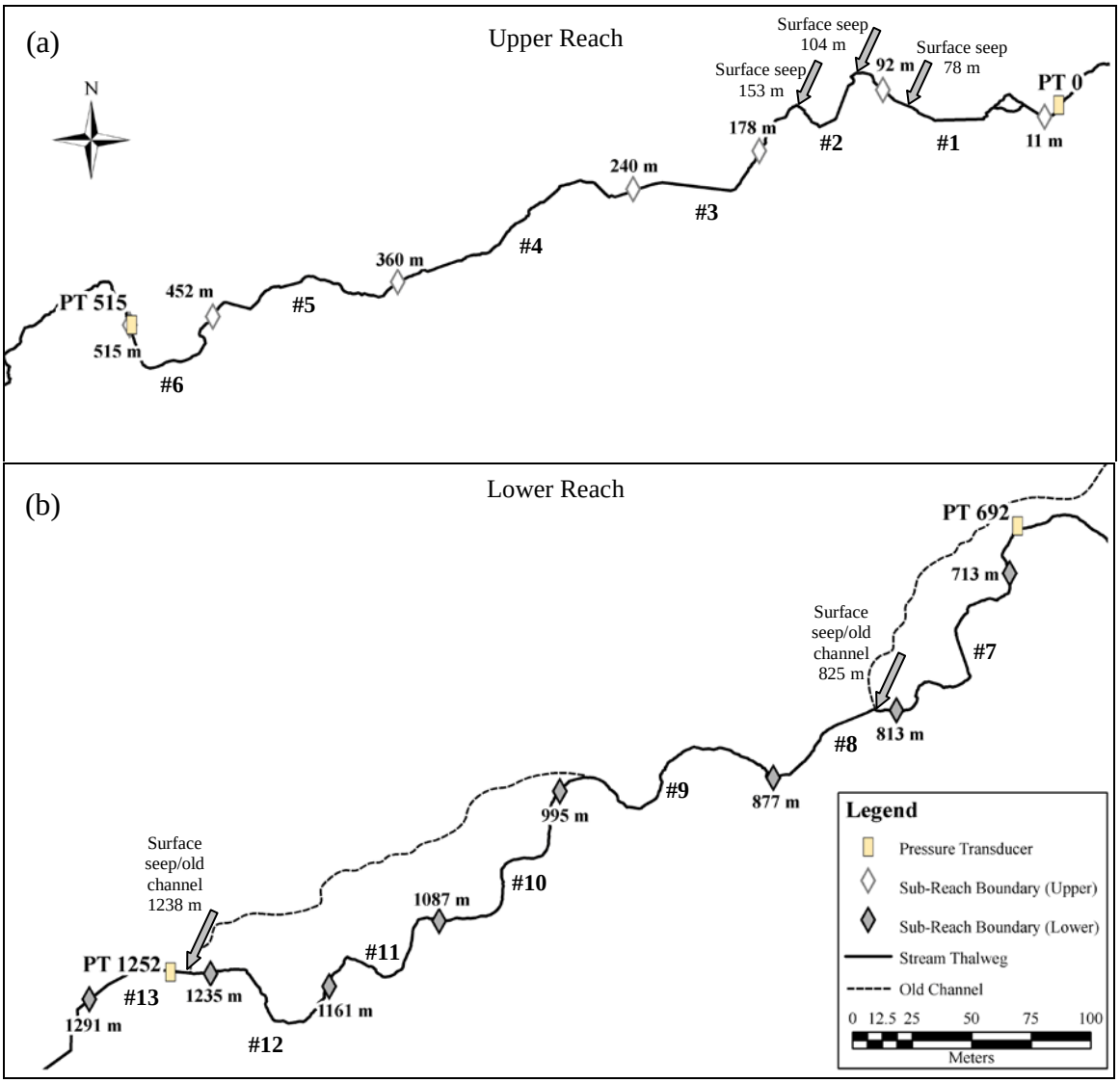

Figure 4-2. (a) Upper and (b) Lower Reach sub-reach boundaries. Surface seep locations are shown with large arrows. Dashed lines show the approximate location of the old stream channel before 2001.

propagation, Equation 4-2 must be linearized to determine how much a unit change of each variable will affect the discharge estimate (Equation 4-3). This sums together all the variance components (based on their respective sensitivity coefficients) associated with the data collection method (Equation 4-4). These sensitivity coefficients (i.e., weighting factors), θs in Equation 4-3, are estimated by taking the partial derivative of Q with respect to each variable shown in Equation 4-2 (refer to Appendix B for calculating the sensitivity coefficients). In Equation 4-4, covariance is assumed negligible due all measurements being taken independently of each other.

$$Q = \theta_0 + \theta_M (M - \overline{M}) + \theta_{\int C(t)} \left(\int C(t)dt - \int \overline{C}(t)dt \right) + \theta_{\int C_b dt} \left(\int C_b dt - \int \overline{C}_b dt \right) \quad (4\text{-}3)$$

where:
the values with bars indicate the center value;
$\theta_0 = Q$ from the centered value = $\dfrac{\overline{M}}{\int \overline{C}(t)dt - \int \overline{C}_b dt}$, L s^{-1};
θ_M, $\theta_{\int C(t)}$, and $\theta_{\int Cbdt}$ = the *sensitivity coefficients* shown in Equation 4-4.

$$\sigma^2_{Q,Data} = \theta^2_M \sigma^2_M + \theta^2_{\int_0^t C(t)dt} \sigma^2_{\int_0^t C(t)dt} + \theta^2_{\int_0^t C_b dt} \sigma^2_{\int_0^t C_b dt} \quad (4\text{-}4)$$

where:
σ^2_M = the variance of the tracer mass injection, mg^2;
$\sigma^2_{\int_0^t C(t)dt}$ = the variance in the integrated response curve, mg^2 s^2 L^{-1};
$\sigma^2_{\int_0^t C_b dt}$ = the variance in the integrated background concentration, mg^2 s^2 L^{-1};

Variance in Mass Injected

The variance in the injected mass is comprised of the purity of the NaCl used and the laboratory measurement. The NaCl (CASRN 7647-14-5) used for all tracer injections has an estimated purity of 99.8%. An Ohaus® Navigator™ (Model N18110, Pine Brook, New Jersey) digital scale was used to measure out the tracer mass for each injection. The repeatability of replicate measurements is 0.1 g [*Ohaus*, 2002] based on one standard deviation. To determine the amount of chloride in the tracer slug, the reaction of NaCl in an aqueous solution is $NaCl \rightarrow Na^{+} + Cl^{-}$ and therefore, $1\ mol\ NaCl = 1\ mol\ Cl^{-}$. The variance for each chloride tracer mass injected, σ_M^2, is shown by Equation 4-5.

$$\sigma_M^2 = \left[\left(0.1\ g + (1 - 0.998(Mass\ of\ \ NaCl\ in\ g)\right) \left(\frac{35.5\ g/mol\ Cl^{-}}{58.4\ g/mol\ \ NaCl} \right) \right]^2 \qquad (4\text{-}5)$$

Variance in Integrated Response Curves

The variance in the integrated tracer response curve is due to instrumental and calibration curve error. Instrumental error contributing to uncertainty in discharge estimates is reported to be ±0.5% of the specific conductance (SC) reading of the instrument [*YSI*, 2006] and was added to the confidence bounds of each chloride concentration response curve.

Error in the chloride concentration predictions from the calibration curves was estimated by first constructing Working-Hotelling 95% confidence bands for 90% of future observations shown by Equation 4-6 and 4-7 [*Berthouex and Brown*, 2002].

$$b_0 + b_1 x \pm \sqrt{2F_{2,\nu,\alpha} s^2 \left(\frac{1}{n} + \frac{(x - \bar{x})^2}{\sum (x_i - \bar{x})^2} \right)} \quad (4\text{-}6)$$

$$s^2 = \sum \frac{(y_i - \hat{y})^2}{n - 2} \quad (4\text{-}7)$$

where:
$F_{2,\upsilon,\alpha}$ = the 95% percentage point of the F distribution for υ degrees of freedom;
s^2 = the mean residual sum of squares, $\mu S^2\ cm^{-2}$;
y_i = the SC reading, $\mu S\ cm^{-1}$;
$\hat{y}$ = the predicted SC for each known chloride standard concentration, $\mu S\ cm^{-1}$.

To use the Working-Hotelling confidence region to determine the confidence interval of the predicted chloride concentration, a 100P% (P = 0.90) confidence interval of the true concentration for a future observation of SC was computed using Equation 4-8 [*Berthouex and Brown*, 2002]. Two degrees of freedom are lost to estimate the two parameters of the straight line model.

$$y \pm z_p \sqrt{\frac{\nu s^2}{\chi^2_{\nu,\alpha/2}}} \quad (4\text{-}8)$$

where:
$z_{p=0.9}$ = the standard normal deviate for P = 0.9;
$\chi^2_{\nu,\alpha/2}$ = the lower percentile point of the chi square distribution [*Lapin*, 1997];
υ = the degrees of freedom (n – 2).

The confidence limits that contain the true value of SC 90% of the time are calculated using $z_{p\,=\,0.9}$ = 1.28 [*Berthouex and Brown*, 2002]. Note that only the slope of the calibration curve is used to translate SC to chloride concentrations because the SC baseline of each response curve is corrected to zero. The variance in measured

background concentrations is assumed to contribute only to the variance in the discharge calculations.

With the combined errors of the instrument response and calibration curve, the variance in the tracer response, $\int_0^t C(t)dt$, is estimated by Equation 4-9.

$$\sigma^2_{\int_0^t C(t)dt} = \frac{\sum_{i=1}^{N} (y_i - \hat{y})^2 \Delta t}{n-1} \quad (4\text{-}9)$$

where:
y_i = the upper or lower bound chloride concentration from the Working-Hotelling confidence bands, mg s L^{-1};
$\hat{y}$ = the predicted chloride concentration from the calibration curve, mg s L^{-1};
n = the number of observations.

Variance in Background Concentrations

To account for variance associated with correcting each tracer response curve to zero prior to calculating stream discharge, the variance in background chloride concentrations was estimated. Within each measured background chloride concentration, there are three components of variation (variation between specimens (grab samples at the same location), variation between tests (replicates of one grab sample), and variation between locations) that combine to give a total variation in each measured chloride concentration. An analysis of variance (ANOVA) was completed to determine each variance component of the background chloride concentration, σ_y^2 (Equation 4-6), assuming error is random, observations are independent, variance is constant, and residuals are normally distributed [*Berthouex and Brown*, 2002].

$$\sigma_y^2 = \sigma_T^2 + \sigma_S^2 + \sigma_L^2 \qquad (4\text{-}10)$$

The subscripts *T*, *S*, and *L* identify the variance components of the tests, specimens, and site locations, respectively. Refer to Appendix B for the equations used to estimate each variance component of the background chloride measurement (Equations B-1, B-2, and B-3) [*Berthouex and Brown*, 2002].

With the variance in the measured background concentrations shown by Equation 4-10, the variance in the integrated background concentration for time 0 to t, $\int_0^t C_b dt$, is estimated similarly to the integrated response curve shown in Equation 4-9.

Variance in the Tracer Injection Method

An additional source of error that must be considered to determine the overall variance in the dilution gauging results is related to the injection method and the associated assumption of complete mixing. The variance in the mixing of the injection was estimated by placing three instruments laterally across the stream resulting in three response curves at one transect from a slug injection. To test how this variance differs over representative mixing lengths, this procedure was duplicated with one slug injected in the Lower Reach and one injection in the Upper Reach. Each of the two slugs were injected at different travel distances resulting in two independent data sets. Variances of each data set were determined and then these estimates were pooled to get an overall variance associated with this method (refer to Appendix B for equations used to calculate variances and standard error). To obtain the 95% confidence interval of the mean *Q*, the standard error is multiplied by the 95% probability value of the *t* distribution for υ degrees of freedom (Equation 4-11). It should be noted that this component of

uncertainty is dependent on the system of consideration and flow conditions (e.g., channel width, stream bottom slopes, substrate, volumetric flow, and stream velocities).

$$Q - s_{\bar{Q}} t_{\nu,\alpha/2} < \eta < Q + s_{\bar{Q}} t_{\nu,\alpha/2} \quad (4\text{-}11)$$

where:
Q = the calculated stream discharge, L s^{-1};
$s_{\bar{Q}}$ = the standard error, L s^{-1};
$t_{\upsilon,\alpha/2}$ = the probability value of the t distribution where $\alpha = 0.05$ and $\upsilon = 4$;
η = the true value of Q, L s^{-1}.

Total Variance and Error in Dilution Gauging

The total variance of dilution gauging is determined by summing the variance associated with the data collection method and the pooled variance associated with the injection method. To get an estimated 95% confidence interval of the discharge estimate, the square root of the variance estimate from the data collection method is multiplied by 2 and summed with the 95% confidence interval from the injection method as shown in Equation 4-12. This is used later to determine the error in net changes in stream discharge quantified from the dilution gauging.

$$Q \pm \left(2\left(\sigma_{Q,Data}\right) + s_{\bar{Q}} t_{\nu,\alpha/2}\right) \quad (4\text{-}12)$$

Net Change in Stream Discharge and Tracer Mass

To complete a representative system water balance, gross gains and losses need to be quantified using net changes and mass recoveries. The net change in stream discharge, net ΔQ, was calculated within each sub-reach by difference of the discharges

estimated at the downstream boundary (Location 1 in Figure 4-3) and at the upstream boundary (Location 2 in Figure 4-3). Therefore, a net $\Delta Q = Q_1 - Q_2$ where the subscripts 1 and 2 correspond to the boundary locations. The error in a net ΔQ is a direct result of the error in Q_1 and Q_2 and can be calculated with an independent *t*-test using a pooled variance [*Berthouex and Brown*, 2002] from the injection method. This is completed by first quantifying the standard error of the difference between Q_1 and Q_2 and the 95% confidence interval of the true difference is estimated by using the probability value of the *t* distribution. To include the variance contribution from the data collection method with 95% confidence, the mean of the variances of Q_1 and Q_2 are used. Therefore, the estimated 95% confidence interval for the net ΔQ is shown by Equation 4-13.

$$(Q_1 - Q_2) \pm \left[\left(\frac{2\sigma_{Q_1,Data} + 2\sigma_{Q_2,Data}}{2} \right) + s_{\overline{Q_1} - \overline{Q_2}} t_{\nu,\alpha/2} \right] \tag{4-13}$$

To quantify the mass recovered from each tracer slug injection mass, M_2, for each sub-reach, the second slug injection (Slug #2) at the upstream sub-reach boundary (used to quantify Q_2) was additionally measured at Location 1 (Figure 4-3). With this response curve and the previously quantified Q_1, the mass recovered is calculated with Equation 4-14 [*Dierberg and DeBusk*, 2005]. With M_{12} quantified, a change in mass (also referred to as unrecovered mass), ΔM, is determined by $M_{12} - M_2$. For all cases, ΔM should be negative due to subtracting off background concentrations. This information is used along with net ΔQ to quantify gross gains and gross losses.

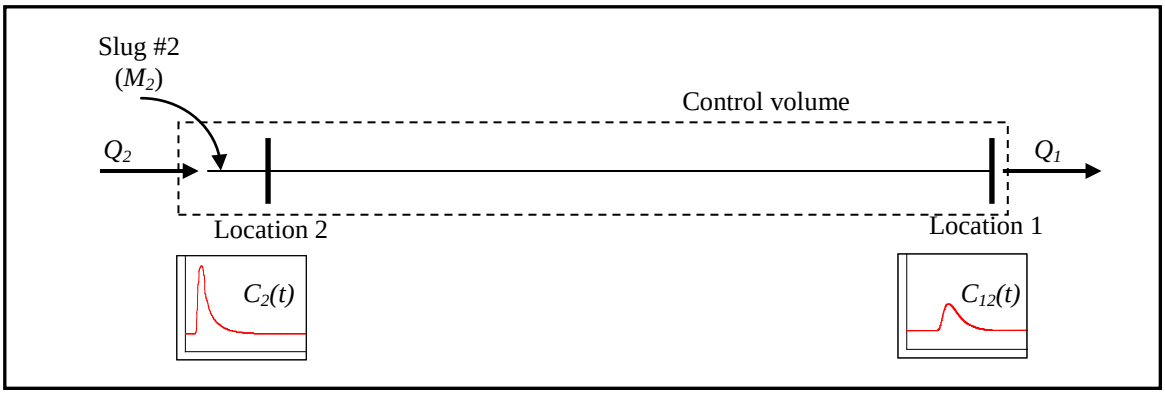

Figure 4-3. Diagram (not to scale) of the method used to determine tracer mass recoveries for each sub-reach by measuring responses at the upstream and downstream sub-reach boundary from one slug injection at the upstream end.

$$M_{12} = Q_1 \int_0^{\infty} (C_{12}(t) - C_{b1})dt \qquad (4\text{-}14)$$

where:
M_{12} = the calculated tracer mass recovered, mg of chloride;
Q_1 = the calculated stream flow from previous tracer injections, L s^{-1};
C_{12} = the observed solute tracer concentration at Location 1, mg L^{-1};
C_{b1} = the solute background concentration at Location 1, mg L^{-1};
$\int (C_{12}(t) - C_{b1})dt$ = the integral calculated from the tracer response curve measured at Location 1 from Slug #2, mg s L^{-1}.

Due to variance in discharge calculations, SC to chloride concentration calibration curves, and measured background concentrations, variance in the mass recovery calculations is created. This variance can be determined similar to the error propagation applied to dilution gauging. Equation 4-15 shows that the variances estimated for the discharges are carried over to the variance in the measured mass recovery (refer to Appendix B for calculating θs). The variance in the ΔM is then estimated with Equation 4-16. The estimated 95% confidence interval for ΔM is shown in Equation 4-17.

$$\sigma^2_{M_{12}} = \theta^2_Q \sigma^2_Q + \theta^2_{\int C(t)_{12}\,dt} \sigma^2_{\int C(t)_{12}dt} + \theta^2_{\int C_b dt} \sigma^2_{\int C_b dt} \qquad (4\text{-}15)$$

$$\sigma_{\Delta M}^2 = \frac{\left(\sigma_{M_2}^2 + \sigma_{M_{12}}^2\right)}{2} \tag{4-16}$$

$$\Delta M \pm 2\left(\sigma_{\Delta M}\right) \tag{4-17}$$

Gross Gains and Gross Losses

With this additional information of tracer mass loss, gross gains and losses to stream discharge are then calculated to complete a more representative water balance. There are a number of contributors to a net ΔQ described in Chapter 3, but this method can only be used to quantify a gross gain, Q_{gain}, and a gross loss, Q_{loss}. The method of quantifying Q_{gain} and Q_{loss} occurring within each sub-reach is similar to the methods presented by *Payn et al.* [2009]. Q_{loss} and Q_{gain} are estimated by completing the mass balance with the injection of Slug #2 shown by Equation 4-18.

$$M_2 = Q_{loss}\int_0^t C_{loss}(t)dt + Q_1\int_0^t C_{12}(t)dt - Q_{gain}\int_0^t C_{gain}(t)dt \tag{4-18}$$

The unknowns in Equation 4-18 are Q_{gain}, $\int_0^t C_{gain}(t)dt$, Q_{loss}, and $\int_0^t C_{loss}(t)dt$. The background concentrations, $\int_0^t C_b dt$, are not shown in Equation 4-18 for simplicity because the background specific conductance (SC) is subtracted from each response curve measured prior to correlating to chloride concentrations. Additionally, any mass contributed from C_{gain} is assumed to be subtracted from the mass balance by subtracting off the background concentrations, and therefore, the term $Q_{gain}\int_0^t C_{gain}(t)dt$ is eliminated

from Equation 4-18. Applying this assumption, Equation 4-18 is simplified into Equation 4-19. The unknowns in the mass balance now become Q_{loss} and $\int_0^t C_{loss}(t)dt$.

$$M_2 = Q_{loss}\int_0^t C_{loss}(t)dt + Q_1\int_0^t C_{12}(t)dt \quad (4\text{-}19)$$

To solve for Q_{loss}, *Payn et al.* [2009] suggested that if a loss is assumed to occur before a gain (Situation 1), the C_{loss} can be set equal to the concentrations of the response curve at Location 2, that is $\int_0^t C_{loss}(t)dt = \int_0^t C_2(t)dt$. For a gain to be assumed to occur before a loss (Situation 2), they suggested the assumption that the concentration leaving the control volume, C_{loss}, is set equal to the concentration of the measured response curve at Location 1 from Slug #2, that is $\int_0^t C_{loss}(t)dt = \int_0^t C_{12}(t)dt$. With Q_{loss} quantified for both Situation 1 and 2, Q_{gain} is then quantified using Equation 4-20 [*Payn et al.*, 2009] (refer to Appendix B for diagrams illustrating Situations 1 and 2 (Figures B-4 and B-5)).

$$Q_{gain} = \Delta Q - Q_{loss} \quad (4\text{-}20)$$

The variance in the calculated Q_{loss} can again be estimated with the error propagation method and the variance components are associated with the mass injected, the stream discharge previously calculated, integrated chloride concentration response curve, and the background chloride concentration. The sensitivity coefficients (θs) shown in Equation 4-21 are calculated independently for both Situations 1 and 2 (refer to Appendix B for equations used to calculate the θs). The variance estimated for Q_{loss} and net ΔQ are averaged to estimate the variance in Q_{gain}. The estimated 95% confidence

intervals for Q_{gain} and Q_{loss} are then calculated by multiplying the square root of each corresponding variance by 2.

$$\sigma^2_{Q_{loss}} = \theta^2_{M_2}\sigma^2_{M_2} + \theta^2_{Q_1}\sigma^2_{Q_1} + \theta^2_{\int_0^t C_{loss}(t)dt}\sigma^2_{\int_0^t C_{loss}(t)dt} + \theta^2_{\int_0^t C_b dt}\sigma^2_{\int_0^t C_b dt} \quad (4\text{-}21)$$

where:

$\sigma^2_{M_2}$ = the variance of the mass injected from Slug #2, mg^2;

$\sigma^2_{Q_1}$ = the variance of the calculated stream discharge at Location 1 from Slug #1, $L^2\ s^{-2}$;

$\sigma^2_{\int_0^t C_{loss}(t)dt}$ = the variance in the integrated response curve from time = 0 to *t* at Location 1 or 2 from Slug #2, $mg^2\ s^2\ L^{-2}$;

$\sigma^2_{\int_0^t C_b dt}$ = the variance in the integrated background concentration from time = 0 to *t* at Location 1 or 2, $mg^2\ s^2\ L^{-1}$.

Results

Rating Curves

The four rating curves constructed at the Upper and Lower Reach boundaries (stations PT 0, PT 515, PT 692, and PT 1252) were used to estimate net ΔQ at the reach scale, provide information regarding diel fluctuations, and make a comparison to dilution gauging at the reach scale.

The 95% joint confidence region (JCR) constructed for the rating curve parameters *a* and *b* (e.g., Figure 4-4 shows the results for station PT 0) resulted in the estimated 95% confidence bounds of each rating curve (e.g., Figure 4-5 shows the results for station PT 0). Note that the confidence bounds are nonsymmetrical due to the JCR being nonsymmetrical around the least sum of squares (Figure 4-5). The remaining JCRs

and rating curves with estimated 95% confidence bounds are shown in Appendix A (Figures A-5, A-6, A-9, A-10, A-13, and A-14).

The broad elliptical shape of the JCR shows that the model is appropriate for representing the data and the parameter estimation is valid [*Berthouex and Brown*, 2002] (Figure 4-4). The shape of the JCR provides information regarding the interaction between the parameters and the ability of the model to fit the data. To test if variance is constant in this rating curve model, the residuals were analyzed (Figure 4-6). The circled data points in Figure 4-6 indicate variance is not constant in the rating curve model. The residuals are also concluded to not be normally distributed (Figure 4-7). The histogram (Figure 4-7 (a)) indicates the distribution is skewed to the right and the nonlinearity of the probability plot (Figure 4-7 (b)) confirms that the residuals are not normally distributed. The circled residuals in Figure 4-7 (b) indicate these values cause errors in the rating curve. Refer to Appendix A for the remaining residual plots, histograms, and probability plots of the other rating curves. Station PT 515 has constant variance (Figure A-7) with more normally distributed residuals (Figure A-8). Station PT 692 also has constant variance (Figure A-11) with normally distributed residuals (Figure A-12). However, the JCRs for these two stations are elongated ellipses (Figures A-5 and A-9), indicating the parameter estimates for these rating curves may not be appropriate to model the observed data [*Berthouex and Brown*, 2002]. Station PT 1252 has a JCR with a broad shape ellipse (Figure A-9), but non-constant variance (Figure A-15) and residuals that are not normally distributed (Figure A-16). The results from stations PT 515 and PT 692 have only 9 and 7 observations, respectively. This indicates more observations covering a broader range of discharges are necessary to better estimate error and verify assumptions.

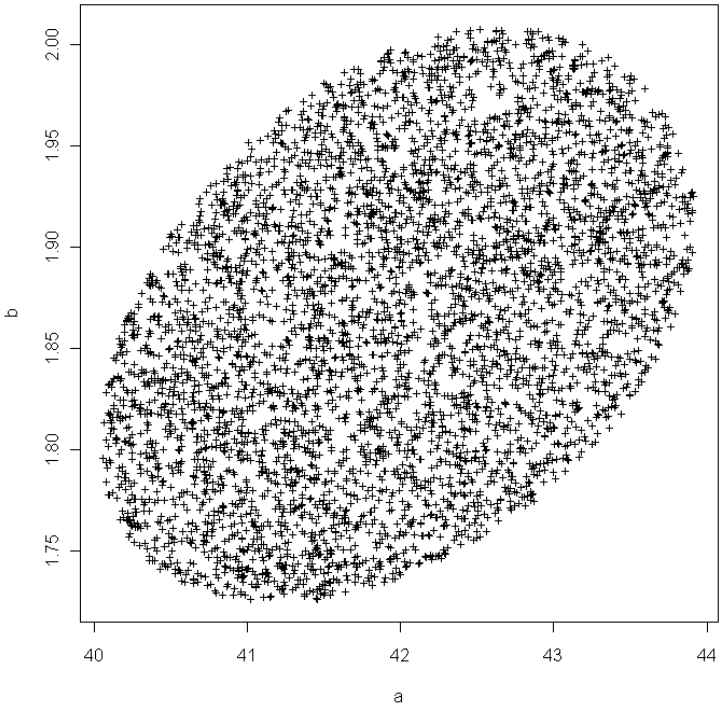

Figure 4-4. Random sample points generated within the estimated 95% JCR for the parameters *a* and *b* of the rating curve constructed at station PT 0.

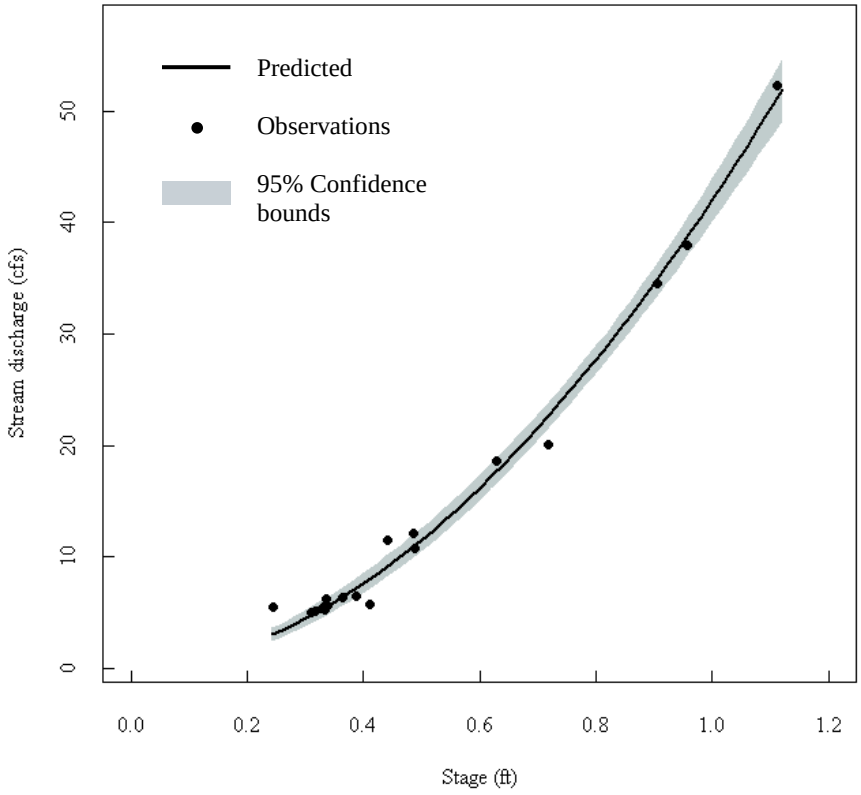

Figure 4-5. The station PT 0 rating curve and estimated 95% confidence bounds.

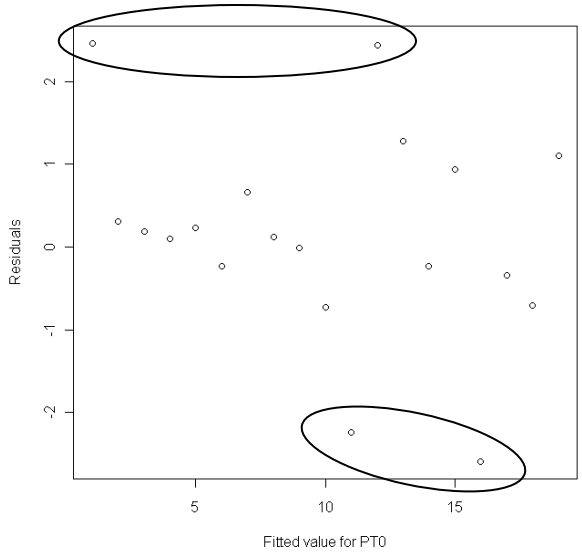

Figure 4-6. Residuals of the rating curve for station PT 0.

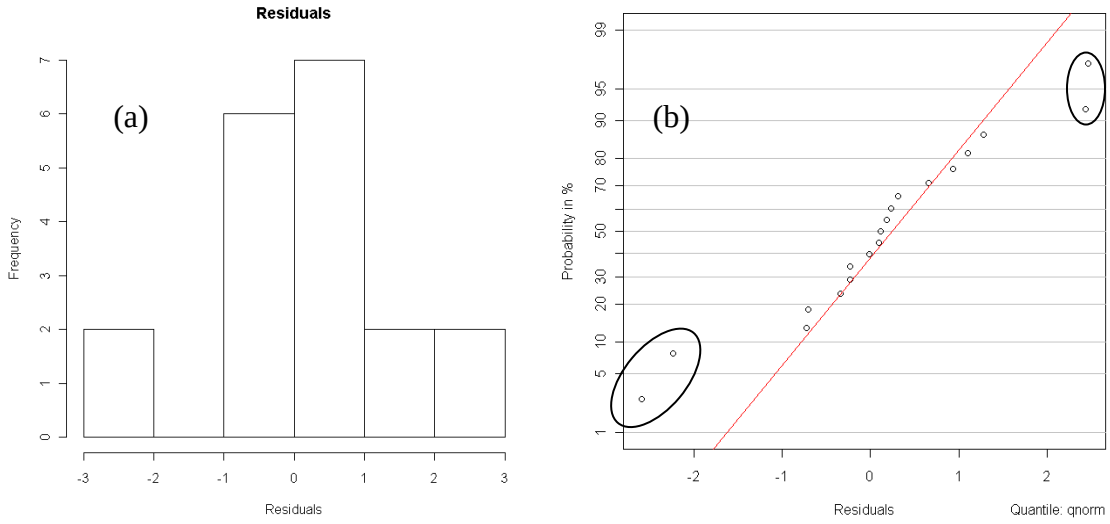

Figure 4-7. (a) Histogram and (b) probability plot of the residuals for station PT 0.

To examine the diel fluctuations of stream discharge estimates at the reach boundaries, five days of predictions are shown along with the time intervals tracer experiments were conducted (Figure 4-8). Station PT 0 was observed to have the largest diel fluctuation of approximately 30% of the total flow within one diel cycle (7/17 0:00 to

7/18 0:00). This fluctuation is approximately 10% during the tracer experiment time periods (shaded regions in Figure 4-8). This possibly added to the error in dilution gauging used to quantify an overall stream water balance for the Upper Reach. However, the error caused by this fluctuation is assumed to be negligible for water balances quantified for individual sub-reaches due to slug travel times being relatively short.

For comparison with the dilution gauging results at the reach scale, rating curve predictions at the time dilution gauging was performed near the corresponding stations are shown in Table 4-1. The Upper Reach was observed to have a significant net gain in stream discharge while the Lower Reach did not have a significant change.

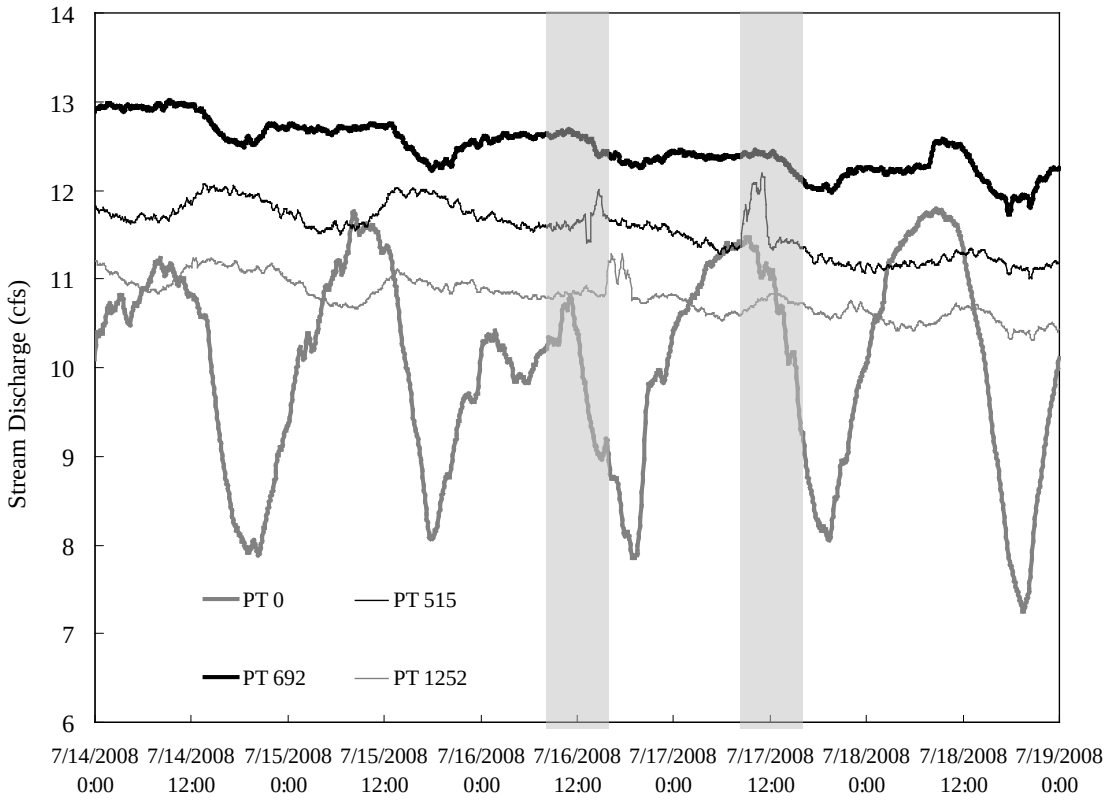

Figure 4-8. Five days of high frequency rating curve predictions at the Upper and Lower Reach boundaries. Gray bars show time intervals when tracer experiments were conducted to complete water balance calculations.

Table 4-1. Net %Δ*Q* From Rating Curve Predictions With % Error at Time Intervals Dilution Gauging was Performed

Reach	Station	Date and time	Stage, *Z* (ft)	*Q* (cfs)	*Q* (L s-1)	Net %Δ*Q*	% Error in *Q* Upper bound	% Error in *Q* Lower bound
Upper	PT 0	7/17/09 13:30	0.47	10.5	296.5		7.9	7.2
	PT 515	7/17/09 9:40	0.52	12.2	345.8	16.6	2.8	3.1
Lower	PT 692	7/16/09 15:20	0.72	12.1	343.6		8.9	8.6
	PT 1252	7/16/09 9:45	0.56	10.8	305.0	-11.2	12.0	13.3

Note that the error is not constant under different flow conditions where an increase in discharge results in an increase in the error in the predictions (e.g., Figure 4-5). This shows that estimating uncertainty with JCRs provides a better representation of the error in the predictions rather than more traditional methods of taking the standard deviation of all residuals and applying it to all discharge predictions.

Dilution Gauging Techniques

Variance in Data Collection Methods

The variance in each discharge estimate from the data collection is estimated from the combined variances in (1) the chloride mass injected, (2) the integrated response curve, and (3) the measured background chloride concentration.

Variance in Mass Injected

Each tracer slug mass of 600 g of NaCl (364 g of chloride) injected was measured in the laboratory. The variance in mass of each slug injected is estimated to be 0.62 g^2 chloride which gives an error of 0.79 g for the mass, *M*, used in Equation 4-2 to estimate discharge. This is only 0.2% of the total mass injected and is therefore considered a negligible source of error to the total error in discharge calculations.

Variance in Integrated Response Curve

The instrument error associated with measuring in situ specific conductance (SC) tracer responses is included in the error of each response curve that is integrated to estimate stream discharge (refer to Figure B-2 in Appendix B). Before Working-Hotelling confidence bands were constructed for each of the four calibration curves (refer to Figure B-3 in Appendix B), the confidence intervals of the slopes and intercepts of each straight line model were determined to test if the curves were statistically different. The slopes of all four calibration curves are statistically the same, confirming that the calibrations curves from the field instruments are appropriate for this study. However, the intercepts are not all statistically the same. This confirms that by correcting each SC response curve to zero prior to calculating discharge and using only the slopes of the calibration curves, the contribution of the variance associated with subtracting off the background could be another source of error. The confidence intervals of the linear model parameters are shown in Appendix B (Table B-8).

The 90% confidence interval for the true SC response based upon one future observation is $y \pm 9.9$ μS cm^{-1} for the Upper Reach and is $y \pm 8.7$ μS cm^{-1} for the Lower Reach and are used to estimate the 95% confidence intervals of the predicted chloride concentrations with the calibration curve confidence bands as shown in Figure 4-9. The sample variances and degrees of freedom are different for calibration curves made to represent the Upper and Lower Reach separately; therefore, calculations of each reach were made independently. The Working-Hotelling confidence bands for the Lower Reach calibration curve are shown as an example along with the procedure to find the confidence interval of the predicted chloride concentrations (Figure 4-9).

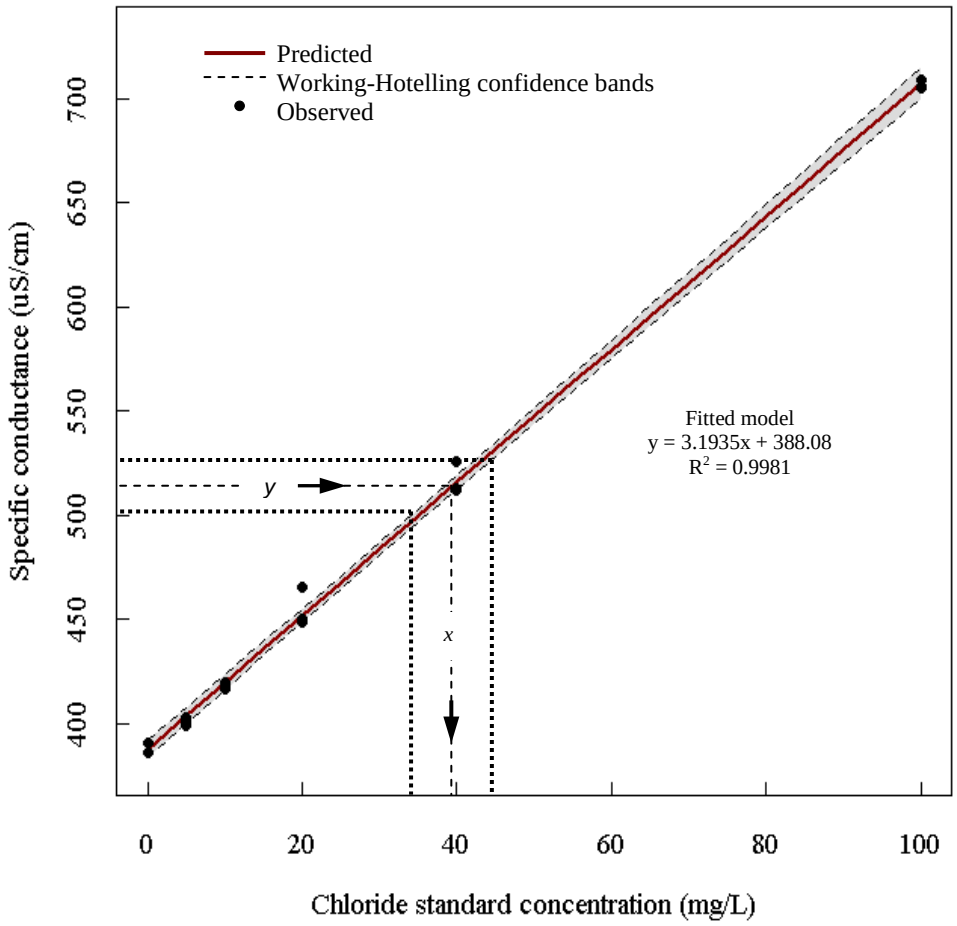

Figure 4-9. Example Working-Hotelling 95% confidence bands and 90% confidence of SC to obtain chloride confidence bounds for the Lower Reach tracer experiments. An example of predicting *x* from *y* is shown with the arrows.

Using the combined error from the instruments and the Working-Hotelling confidence bands, the confidence bounds of each chloride response curve was estimated (Figure 4-10). These confidence bounds were used to estimate the variance associated with the integrated response curve (refer to Equation 4-9).

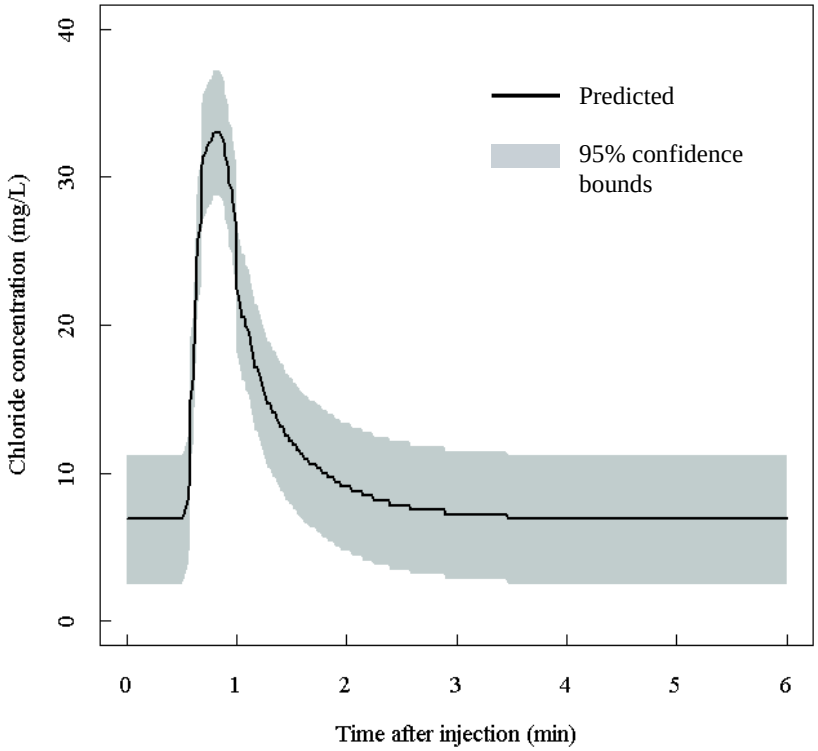

Figure 4-10. Example 95% confidence bounds of predicted chloride concentrations response curve.

Variance in Background Concentrations

The results of the sum of squares and mean squares by completing an ANOVA of the measured background chloride concentrations were used to estimate each component of variance (Table 4-2). For site locations, the critical *F*-value from the upper 5% *F* Distribution is $F_{14,6,0.05} = 2.85$. The calculated *F*-value is 131.6 and is much greater than 2.85 providing evidence that the variation between locations is not random and significantly contribute to the total variance. For specimens (independent grab samples for the same location), the calculated F-value is 23.3 and the critical *F*-value from the *F* Distribution is $F_{9,6,0.05} = 3.37$. This indicates that variation between specimens is not random and that the stream water at each location may not be homogenously mixed.

Table 4-2. Analysis of Variance for Chloride Concentration Measurements

Source of variation	Sum of squares	Degrees of freedom	Mean square	F ratio
Average	1158.79	1		
Locations (L)	24.852	14	1.78	131.6
Specimens (S)	2.8185	9	0.31	23.2
Tests (T)	0.0810	6	0.01	
Total	1186.54	30		

The variance due to replicate tests representing the variance in the laboratory analysis procedure is the smallest contributor to the total variance (refer to Appendix B for all calculations made to complete the ANOVA for background chloride concentrations (Table B-7)). The percent recoveries (%Rs) of spiked samples were within accuracy requirements and relative percent recoveries (RPDs) were within precision requirements according to EPA Method 300.0 (refer to Appendix B for a quality control chart illustrating %Rs (Figure B-1) and the RPDs (Table B-5)). The variance components estimated from the mean squares in Table 4-3 are $\sigma_T^2 = 0.01\, mg^2\ L^{-2}$, $\sigma_S^2 = 0.10\ mg^2\ L^{-2}$, and $\sigma_L^2 = 0.24\ mg^2\ L^{-2}$. The total variance in chloride concentration from a random grab sample is estimated to be 0.35 $mg^2\ L^{-2}$. However, the site specific background chloride concentration was measured at each location where corresponding tracer response curves were observed and therefore, is assumed that the variance component between locations, σ_L^2, does not contribute to the overall variance in background concentrations that contribute to the variance in the stream discharge calculations. The variance component of locations was estimated only to show there is variability between locations, which indicates variable gains and losses are likely occurring. Excluding σ_L^2, the variance of a particular background chloride concentration measurement applied to determining the total variance of Equation 4-2 is

$\sigma_y^2 = \sigma_T^2 + \sigma_S^2 = 0.11\, mg^2\ L^{-2}$. Any variability in background concentration laterally across the stream at a particular site location was addressed with replicate specimens and any variability in the laboratory procedure was addressed with replicate tests.

Variance in Field Injection Method

To determine the total variance with each discharge estimate, the variance component of the injection method must also be estimated. This variance is associated with the complete mixing assumption used throughout the tracer experiments. The assumption was tested by measuring a slug injection with three instruments placed laterally across the stream in the Upper Reach (Figure 4-11 (a)) and the Lower Reach (Figure 4-11 (b)).

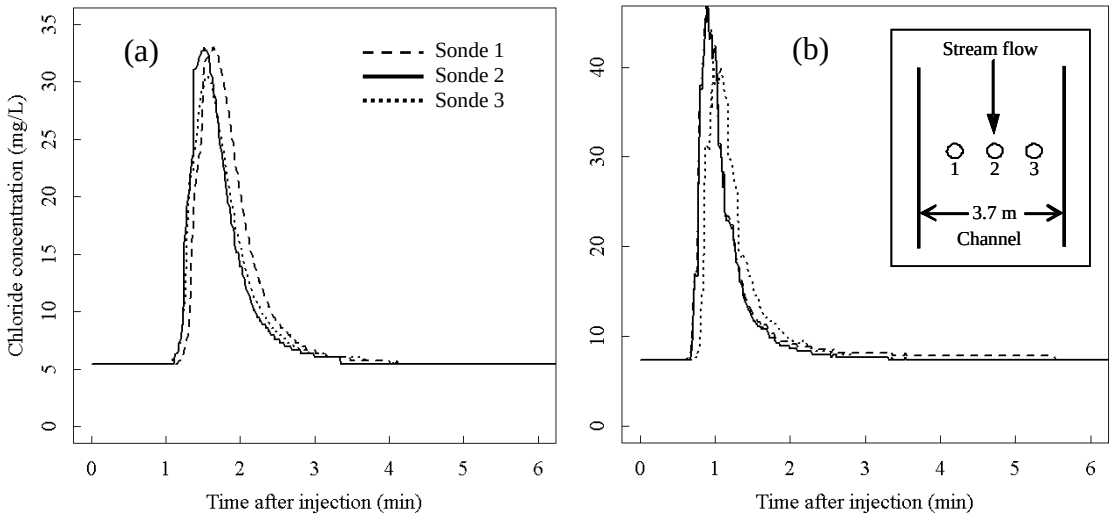

Figure 4-11. Example of three response curves measured in situ to determine variance in the injection method for the (a) Upper Reach and the (b) Lower Reach.

The pooled variance of each injection due to slug mixing is 133.4 L^2 s^{-2} (refer to Table B-9 in Appendix B). Using the standard error and probability value from the *t* distribution, the 95% confidence interval for a discharge estimate based on the injection method is ±26.2 L s^{-1}.

Total Variance and Error in Dilution Gauging

The total variance from both the data collection method and the injection method of each discharge estimate at the sub-reach boundaries resulted in a mean error with estimated 95% confidence of 8.2% for the Upper Reach and 8.0% for the Lower Reach (Table 4-3). The data collection method comprises only a mean of 1.0% for the Upper Reach and 0.9% for the Lower Reach error to each discharge estimate. The injection method contributes a mean of 7.1% error for the Upper Reach and 7.1% error for the Lower Reach in each discharge estimate (Table 4-3). The injection method is clearly the largest contributor to error in discharge calculations (refer to Tables B-10 and B-11 in Appendix B for these calculations made for each sub-reach boundary).

Of the total variance associated with the data collection method, the largest variance component is the response curve integral which contributes a mean of 78.6% to

Table 4-3. Contribution of Each Variance Component to the Total Variance in *Q* from the Data Collection Method of the Upper and Lower Reach and the Total % Error in *Q* with Estimated 95% Confidence

Reach		Variance Component			% error	% error	Total %
		$\theta^2 \mathrm{Var}(M)$	$\theta^2 \mathrm{Var}(\int C(t)\mathrm{d}t)$	$\theta^2 \mathrm{Var}(\int C_b \mathrm{d}t)$	in *Q* from	in *Q* from	error in
		% of $\sigma^2_{Q,Data}$	% of $\sigma^2_{Q,Data}$	% of $\sigma^2_{Q,Data}$	data with 95% confidence	injection with 95% confidence	*Q* with 95% confidence
Upper	Average	**18.7**	**78.6**	**2.7**	**1.0**	**7.1**	**8.2**
	StDev	2.3	2.3	0.1	0.1	0.6	0.5
Lower	Average	**23.1**	**73.5**	**3.4**	**0.9**	**7.1**	**8.0**
	StDev	2.7	2.6	0.1	0.1	0.5	0.5

the total variance for the Upper Reach shown in Table 4-3. The next largest contributor to the total variance is the mass injected with a contribution of 18.7% to the total data collection variance. The contribution of the integrated background concentration curve is the lowest contributor with only 2.7% (i.e., 0.027*1.0% = 0.027% of the total error in discharge from subtracting off the background concentration). This indicates that variance associated with subtracting off the background concentration is negligible. For the Lower Reach, the integrated response curve is also the largest variance component with a contribution of 73.5% of the total variance in the data collection method shown in Table 4-3. The variance component of the injected mass is 23.1%.

With the error in discharge estimates completed with dilution gauging techniques, the estimates can now be compared to the rating curve predictions at the reach scale (Figure 4-12). The Upper Reach shows no significant change based on dilution gauging while the rating curve predictions show a gain is likely occurring. For the Lower Reach, the rating curve predictions indicate no significant change is occurring while the dilution gauging results suggest a slight gain is occurring. However, the site specific discharge estimates from each method are statistically the same, suggesting that neither method reliably detected groundwater exchange at this scale (Figure 4-12).

The stream discharges estimated at the sub-reach boundaries suggest there are varying discharges throughout the two reaches where the Lower Reach appears to have more variation (Figure 4-13) and these were not detected at the reach scale. Incorporating error, however, shows that there are only a few locations where significant differences in stream discharge may be occurring. To better understand the extent of the groundwater exchanges occurring, net ΔQ at the sub-reach scale was quantified.

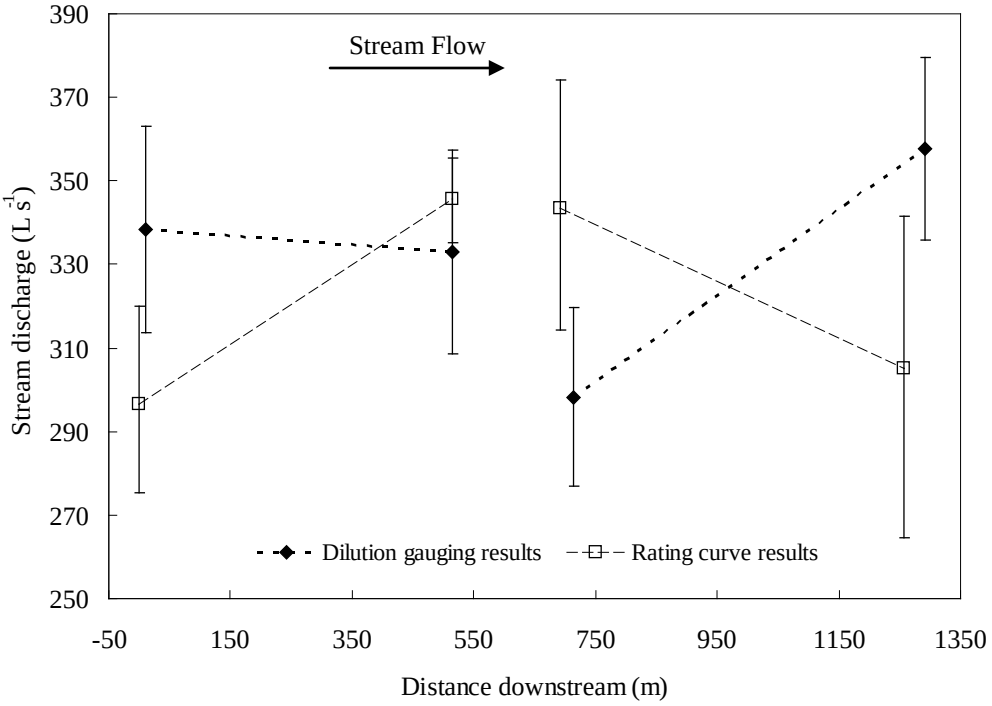

Figure 4-12. Dilution gauging results compared to rating curve results with estimated 95% confidence intervals at the Upper and Lower Reach boundaries.

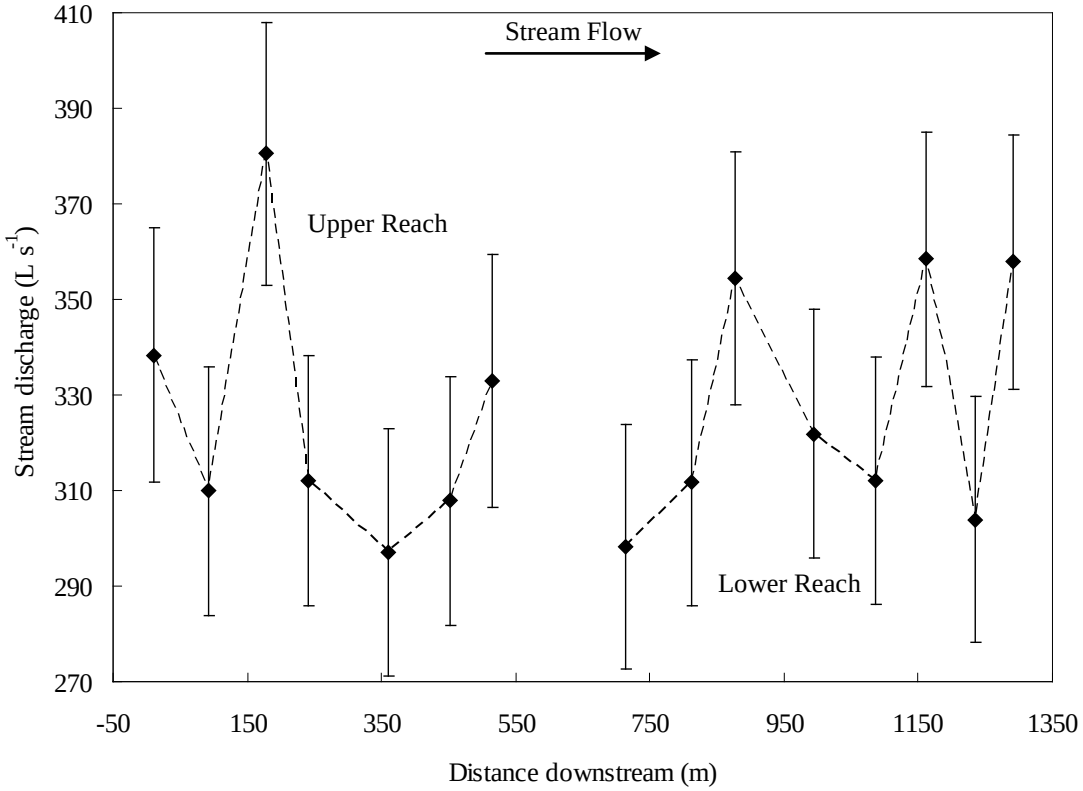

Figure 4-13. Sub-reach scale dilution gauging results with estimated 95% confidence intervals.

Net Change in Stream Discharge and Tracer Mass

The net percent change in stream discharge, net %Δ*Q*, ranged from -18.0% to 22.8% for the Upper Reach (Table 4-4) and -15.2% to 17.7% for the Lower Reach (Table 4-5). The net %Δ*Q* was calculated as the percent change from the discharge at the upstream sub-reach boundary. The mean error with estimated 95% confidence in these estimates for the Upper Reach is net %Δ*Q* ±8.2% (Table 4-4) and for the Lower Reach is net %Δ*Q* ±8.1% (Table 4-5). Therefore, in the Upper Reach any net %Δ*Q* greater than ±8.2% is a significant change and in the Lower Reach any net %Δ*Q* greater than ±8.1% is a significant change.

The percent of unrecovered tracer mass, %Δ*M*, for each sub-reach ranges from -24.8% to 22.2% for the Upper Reach (Table 4-6) and -18.1% to 8.5% for the Lower Reach (Tables 4-7). The mean error in these estimates with estimated 95% confidence for the Upper Reach is %Δ*M* ±6.9% and for the Lower Reach is %Δ*M* ±6.7%. The largest variance component in these estimates (98%) is due to the discharge estimate used to quantify the mass recovered and the smallest is due to the integrated response curves and can be considered negligible (refer to Appendix B for all mass recovery calculations and error estimates (Tables B-15, B-15, B-16, and B-17)).

In the Upper Reach, net changes in stream discharge from upstream discharge are only significant in Sub-reaches #2 and #3 and changes in tracer mass are significant in Sub-reaches #2, #4 and #5 (Figure 4-14). However, a positive %Δ*M* (+22.2% in Table 4-6) indicates that an error occurred somewhere in the data collection method (shown with the dashed box in Figure 4-14). A positive mass recovered should not occur because any gain in mass is assumed to be eliminated from the mass balance by subtracting the

background concentration from each response curve at the downstream sub-reach boundary (i.e., in a purely gaining reach, net %Δ*Q* should be positive and %Δ*M* should be zero). In Sub-reaches #4 and #5, no significant change in discharge was observed, but a negative change in mass was significant. This indicates that gains and losses are likely occurring together in these reaches.

Table 4-4. Net %Δ*Q* with Estimated 95% Confidence Intervals for the Upper Reach

Sub-reach number	Sub-reach interval (m)	Length of sub-reach (m)	Δ*Q* (L s-1)	Error in Δ*Q* (L s-1)	% Error in Δ*Q*	%Δ*Q* from upstream *Q*	Error in %Δ*Q*
1	11 to 92	80	-28.4	26.4	-92.8	**-8.4**	±7.8
2	92 to 178	86	70.6	26.8	37.9	**22.8**	±8.6
3	178 to 240	62	-68.4	26.8	-39.2	**-18.0**	±7.0
4	240 to 360	119	-15.0	26.0	-173.5	**-4.8**	±8.3
5	360 to 452	93	10.7	26.0	242.8	**3.6**	±8.7
6	454 to 515	63	25.1	26.3	104.6	**8.2**	±8.5
						Average	±**8.2**
						StDev	0.65

Table 4-5. Net %Δ*Q* with Estimated 95% Confidence Intervals for the Lower Reach

Sub-reach number	Sub-reach interval (m)	Length of sub-reach (m)	Δ*Q* (L s-1)	Error in Δ*Q* (L s-1)	% Error in Δ*Q*	%Δ*Q* from upstream *Q*	Error in %Δ*Q*
7	713 to 813	100	13.4	25.7	192.0	**4.5**	±8.6
8	813 to 877	64	42.7	26.2	61.3	**13.7**	±8.4
9	877 to 995	118	-32.5	26.2	-80.8	**-9.2**	±7.4
10	995 to 1091	92	-9.9	25.9	-263.0	**-3.1**	±8.1
11	1091 to 1161	74	46.4	26.2	56.4	**14.9**	±8.4
12	1160 to 1235	74	-54.5	26.2	-48.0	**-15.2**	±7.3
13	1235 to 1291	56	53.9	26.1	48.5	**17.7**	±8.6
						Average	±**8.1**
						StDev	0.55

Table 4-6. %Δ*M* and Estimated 95% Confidence Intervals for the Upper Reach

Sub-reach number	Measurement location (m)	Slug travel distance (m)	$\%M_{12}$	%Δ*M*	Error in %Δ*M* with 95% confidence
1	92	140	94.1	**-5.9**	±7.1
2	178	109	122.2	**22.2**	±5.9
3	240	87	95.7	**-4.4**	±7.1
4	360	145	83.3	**-16.7**	±7.4
5	452	145	75.2	**-24.8**	±7.2
6	515	99	102.3	**2.3**	±6.6
				Average	±**6.9**
				StDev	0.6

Table 4-7. %Δ*M* and Estimated 95% Confidence Intervals for the Lower Reach

Sub-reach number	Measurement location (m)	Slug travel distance (m)	$\%M_{12}$	%ΔM	Error in %Δ*M* with 95% confidence
7	813	146	98.4	**-1.7**	±7.0
8	877	105	94.0	**-6.0**	±6.3
9	995	163	87.1	**-12.9**	±6.8
10	1091	148	81.9	**-18.1**	±7.1
11	1160	111	108.5	**8.5**	±6.2
12	1235	106	86.1	**-14.0**	±7.2
13	1291	83	95.3	**-4.7**	±6.2
				Average	±**6.7**
				StDev	0.5

In the Lower Reach, Sub-reaches #8, #9, #11, #12, and #13 had significant changes in stream discharge and Sub-reaches #9, #10, #11, and #12 had significant changes in mass (Figure 4-15). However, a positive %Δ*M* (+8.5% in Table 4-8) was observed in Sub-reach #11, again indicating an error occurred somewhere in the data collection method. Sub-reach #10 did not have a significant change in discharge, but a significant change in mass. This also indicates gains and losses are occurring together in this sub-reach. To complete a water balance more representative of the exchanges occurring, gross gains and gross losses were quantified.

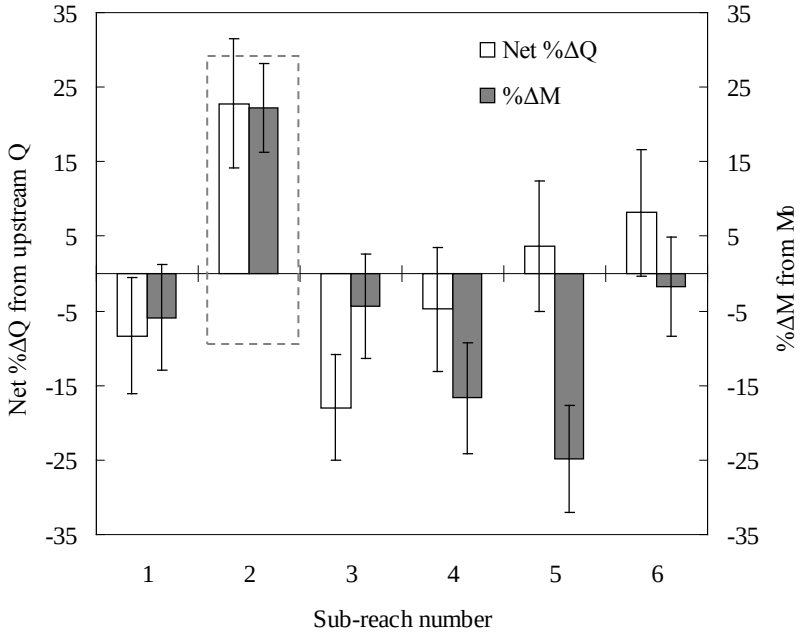

Figure 4-14. Net %Δ*Q* and %Δ*M* for the Upper Reach with estimated 95% confidence intervals. The highlighted sub-reach indicates an error in calculations.

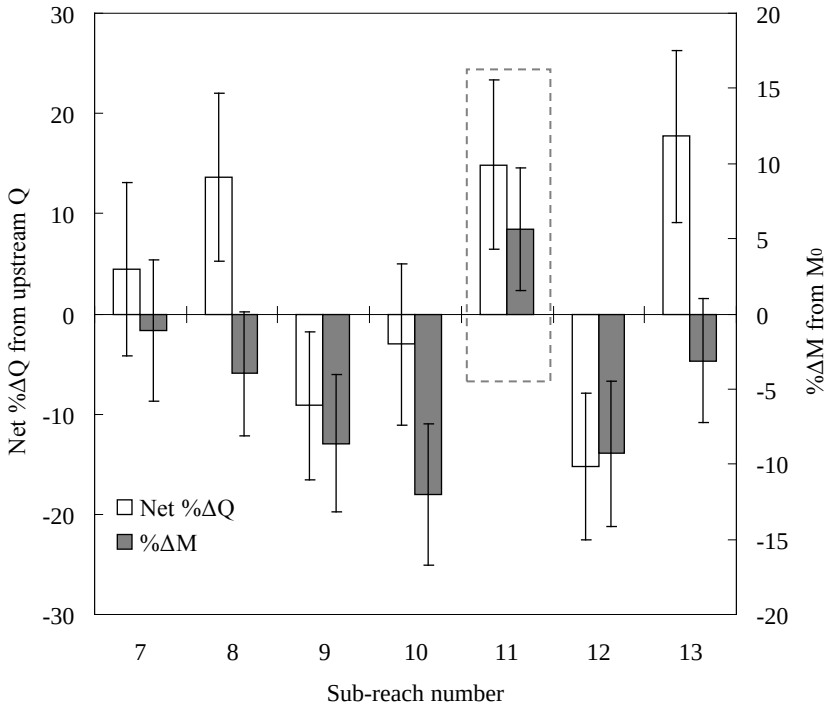

Figure 4-15. Net %Δ*Q* and %Δ*M* for the Lower Reach with estimated 95% confidence intervals. The highlighted sub-reach indicates an error in calculations.

Gross Gains and Gross Losses

Using the net ΔQ and ΔM, gross gains, Q_{gain}, and gross losses, Q_{loss}, were quantified in the Upper and Lower Reaches. The Q_{gain} and Q_{loss} were quantified for both situations where a loss occurs before a gain (Situation 1) and a gain occurs before a loss (Situation 2) in the Upper Reach (Table 4-8) and the Lower Reach (Table 4-9). The order of gains and losses cannot be clearly determined and, therefore, differences in calculations made for both situations are treated as error contributed from assumptions. Additionally, estimated 95% confidence intervals were estimated from the variance in variables used to quantify gross changes.

The largest component of variance from the variables used to calculated Q_{loss} is from the stream discharge estimate at Location 1 (Q_1) (refer to Appendix B for all calculations of variance components used to determine the variance in Q_{loss} (Table B-18 and B-19)). The total mean estimated 95% confidence intervals are $\%Q_{loss}$ ±8.7% and $\%Q_{gain}$ ±9.4% for the Upper Reach (Table 4-8). For the Lower Reach, the estimated 95% confidence intervals are $\%Q_{loss}$ ±7.7% and $\%Q_{gain}$ ±8.3% (Table 4-9). Notice that the error contribution due to the order assumption is the same for both $\%Q_{loss}$ and $\%Q_{gain}$. This occurs because the same net ΔQ is used to calculate Q_{gain} for both situations (refer to Equation 4-20). The percent gain or loss was also determined as the percent change from the discharge at the upstream sub-reach boundary.

In the Upper Reach, significant $\%Q_{gain}$ and $\%Q_{loss}$ were observed to concurrently occur in Sub-reaches #4 and #5 while no net $\%\Delta Q$ was observed (Figure 4-16). This shows that the Q_{gain} and Q_{loss} cancelled each other to get a non-detectable net ΔQ. A significant $\%Q_{gain}$ was also observed in Sub-reach #6 where a net $\%\Delta Q$ was not present.

Table 4-8. Upper Reach $\%Q_{loss}$ and $\%Q_{gain}$ from Upstream Q with Error from the Assumption of Situation 1 or 2 and from Variables That Combine for the Estimated 95% Confidence Intervals

	Situation 1		Situation 2			Situation 1		Situation 2			
Sub-reach number	$\%Q_{loss}$	$\%Q_{gain}$	$\%Q_{loss}$	$\%Q_{gain}$	Assumption Error in $\%Q_{loss}$ and $\%Q_{gain}$	Variables Error in $\%Q_{loss}$	Error in $\%Q_{gain}$	Error in $\%Q_{loss}$	Error in $\%Q_{gain}$	Total error in $\%Q_{loss}$	Total error in $\%Q_{gain}$
1	-5.9	-2.5	-5.7	-2.7	±0.2	6.9	7.4	6.5	7.2	±6.4	±7.0
2	22.2	0.6	22.3	0.5	±0.1	7.4	8.1	7.2	8.0	±7.1	±7.9
3	-4.4	-13.6	-3.7	-14.2	±0.6	7.1	7.1	5.6	6.5	±5.2	±5.9
4	-16.7	11.9	-19.0	14.2	±2.4	6.4	7.4	7.1	7.7	±9.4	±10.1
5	-24.8	28.4	-34.2	37.8	±9.4	5.6	7.3	7.4	8.1	±16.8	±17.5
6	-1.8	10.0	-2.0	10.2	±0.2	6.7	7.7	7.2	7.9	±7.4	±8.1
					Average	**6.7**	**7.5**	**6.9**	**7.6**	**±8.7**	**±9.4**
					StDev	0.6	0.3	0.5	0.6	3.8	3.8

Table 4-9. Lower Reach $\%Q_{loss}$ and $\%Q_{gain}$ from Upstream Q with Error from the Assumption of Situation 1 or 2 and from Variables That Combine for the Estimated 95% Confidence Intervals

	Situation 1		Situation 2			Situation 1		Situation 2			
Sub-reach number	$\%Q_{loss}$	$\%Q_{gain}$	$\%Q_{loss}$	$\%Q_{gain}$	Assumption Error in $\%Q_{loss}$ and $\%Q_{gain}$	Variables Error in $\%Q_{loss}$	Error in $\%Q_{gain}$	Error in $\%Q_{loss}$	Error in $\%Q_{gain}$	Total error in $\%Q_{loss}$	Total error in $\%Q_{gain}$
7	-1.7	6.1	-1.8	6.2	±0.1	7.1	7.9	7.4	8.0	±7.5	±8.1
8	-6.0	19.7	-7.2	20.9	±1.3	6.1	7.3	7.1	7.8	±8.3	±9.0
9	-12.9	3.8	-13.5	4.3	±0.6	6.2	6.8	6.1	6.9	±6.8	±7.4
10	-18.1	15.0	-21.4	18.3	±3.3	6.0	7.1	6.8	7.5	±10.2	±10.8
11	8.5	6.4	9.0	5.9	±0.5	6.9	7.7	7.1	7.8	±6.6	±7.3
12	-13.9	-1.3	-13.7	-1.5	±0.2	6.4	6.9	6.2	6.8	±6.0	±6.5
13	-4.8	22.6	-6.0	23.7	±1.2	6.3	7.5	7.3	8.0	±8.4	±9.1
					Average	**6.4**	**7.3**	**6.9**	**7.5**	**±7.7**	**±8.3**
					StDev	0.4	0.4	0.5	0.5	1.4	1.4

This suggests that completing a water balance in terms of gross changes can be more representative of the exchanges occurring. However, the assumed error that occurred in Sub-reach #2 from a positive ΔM was carried over to the gross change calculations in Sub-reaches #1, #2, and #3 resulting in the exchanges quantified to be inconclusive (shown with dashed box in Figure 4-16). These results are inconclusive due to a positive $\%Q_{loss}$ observed in Sub-reach #2 and a negative $\%Q_{gain}$ observed in Sub-reach #3.

In the Lower Reach, significant $\%Q_{gain}$ and $\%Q_{loss}$ were observed to occur together in Sub-reach #10 while no net $\%\Delta Q$ was observed (Figure 4-17). Sub-reaches #8 and #13 were observed to have significant $\%Q_{gain}$ and no significant $\%Q_{loss}$. These sub-reaches had visible surface seep inflows (refer to Figure 4-2 for locations of surface seeps). There were no significant changes observed in Sub-reach #7 and a significant $\%Q_{loss}$ was observed in Sub-reach #9. Again, the error indicated with a positive ΔM that

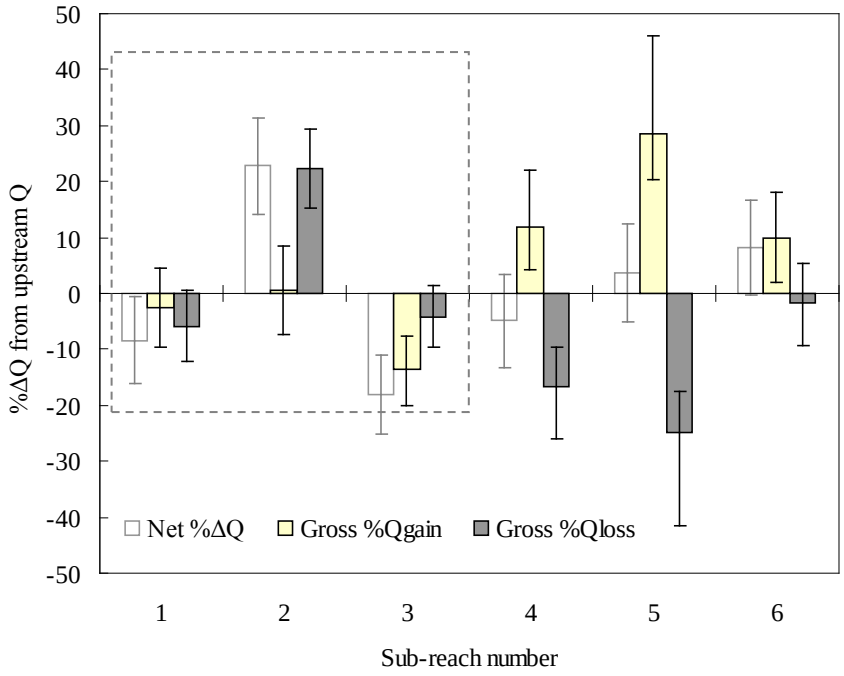

Figure 4-16. $\%Q_{gain}$ and $\%Q_{loss}$ for the Upper Reach with estimated 95% confidence intervals. Net changes are also shown.

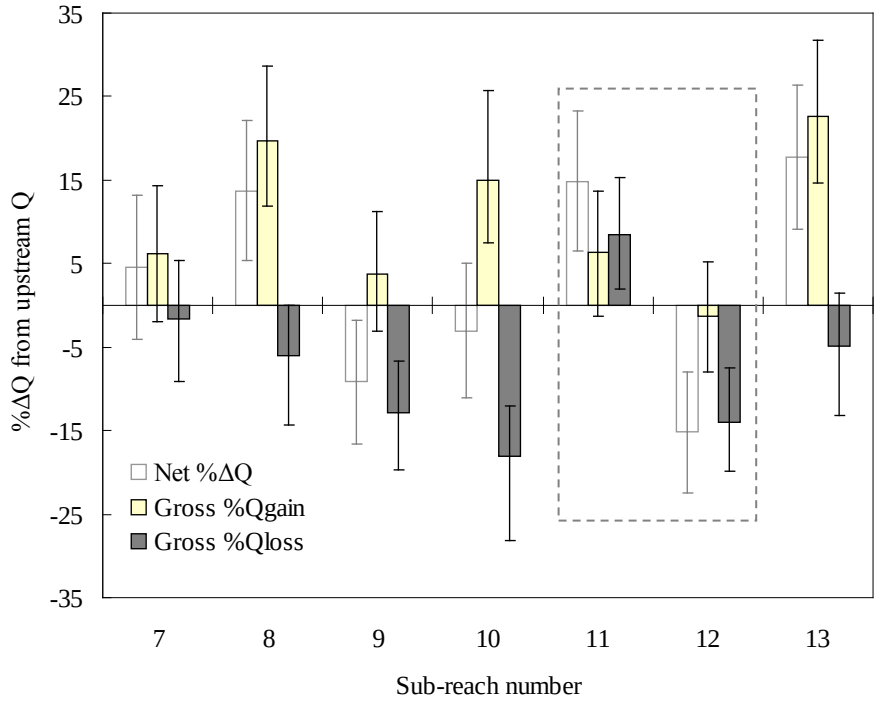

Figure 4-17. $\%Q_{gain}$ and $\%Q_{loss}$ for the Lower Reach with estimated 95% confidence intervals. Net changes are also shown.

occurred in Sub-reach #11 was carried over to the gross change calculations for Sub-reaches #11 and #12 (shown with the dashed box in Figure 4-17). Even with a detailed error analysis of water balance calculations, there are still shortcomings to dilution gauging techniques that cannot be identified, but are likely related to not meeting the required assumptions of the method.

Discussion

Comparing discharge estimates at the reach scale with rating curve predictions and dilution gauging techniques proved to not reliably detect surface water-groundwater exchanges occurring in this system at this scale due to corresponding estimates between both methods being statistically the same. This proved that conducting error analyses for

these methods is important to test the reliability of each to detect small changes. Additionally, this proved that groundwater exchange must be analyzed at a finer spatial scale to better predict solute mass movement.

Performing dilution gauging at the sub-reach scale indicated that surface water-groundwater exchange is highly spatially variable in this system. The first order error analysis of the water balance results was necessary to support more accurately predicting mass movement and provided evidence that the groundwater exchanges were not as extensive as originally believed. For example, net changes were initially observed in every sub-reach, but when applying error to these calculations, significant net changes were only observed in six of the thirteen sub-reaches. Quantifying a gross water balance was also shown to be necessary to better understand the extent of groundwater exchange. This was observed in Sub-reaches #4, #5, and #10 where no significant net changes were observed, but significant gross changes occurred (Figures 4-16 and 4-17).

The method of using a 95% JCR to estimate error in rating curve predictions proved to be better than more traditional methods of applying a constant error to all predictions. The JCR being nonsymmetrical around the least sum of squares, resulting in upper and lower confidence bounds to the rating curve being nonsymmetrical (refer to Figure 4-5). This ultimately provides a better description of the error in predictions (e.g., as the stage increases, the error in predictions increases for each rating curve used in this study).

The first order error analysis of dilution gauging indicates that this method is slightly more accurate for estimating stream discharge than the rating curves. However, the assumptions associated with dilution gauging are difficult to meet and verify. Even

with a detailed first order error analysis, assumptions made to quantify a water balance are likely the largest sources of error (refer to Chapter 3 for more detail). Therefore, rating curve predictions were initially used as a check to assure assumptions for dilution gauging were reasonable. The approach to the error analysis in dilution gauging techniques to estimate a water balance had a distinct advantage. Estimating each independent variance component provided information regarding the largest contributors. The error contributed by the data collection methods was only 1% of the discharge estimate, providing evidence that if careful data collection is implemented, then this is a negligible source of error in discharge calculations. However, a step that proved to be important for estimating error was testing the completely mixed assumption by placing three instruments laterally across the stream that contributed a mean of 7% error to discharge calculations. This source of error is significant and should be estimated for each study system. This component of variance was estimated by only two slug injections and may not be representative. To improve this lack of understanding, more tests of travel distances and appropriate measurement locations (e.g., in pools and riffles) should be completed.

The advantages to using rating curves with continuous stage data are that high frequency discharge estimates provide diel fluctuation information (Figure 4-8) and boundary condition information for testing the steady state flow assumption required for dilution gauging techniques and also provide a check that other assumptions were reasonably met. In this study, the stream discharge at station PT 0 was found to change by ~10% (with the mean error estimated to be 7.6% shown in Table 4-1) during the time period tracer experiments were performed. This indicates additional error in the net and

gross water balances for the entire Upper Reach occurred. However, this error is considered negligible in individual sub-reach water balances based on relatively short travel times of slug injections for one sub-reach. The diel fluctuations during tracer experiments in the Lower Reach appeared to be a negligible source of error in water balance calculations (Figure 4-8). High frequency discharge estimates also provide seasonal flow variation information that can be used to determine optimal time periods to conduct tracer experiments to capture a wider range of flow conditions and the corresponding surface water-groundwater interactions (refer to Appendix C for 18 months of high frequency discharge estimates at the reach boundaries (Figure C-1)).

Even with a robust error analysis in dilution gauging techniques, there were some shortcomings that could not be identified. Positive ΔM observed in Sub-reaches #2 and #11 indicated an error occurred somewhere in the method. It is hypothesized that this occurred due to: (1) the tracer slug not completely mixing before measurements were taken or (2) the background SC measured in the response curves was not representative of the actual instream background SC due to a lack of lateral mixing.

To attempt to omit this error from the water balance of the Upper Reach, Sub-reaches #1, #2, and #3 were combined and treated as one sub-reach. This was made possible by measuring the response of the slug injected upstream of Sub-reach #1 and measured at the downstream boundary of Sub-reach #3. The ΔM for each of the four sub-reaches resulted in significant negative changes in the first three sub-reaches with no significant net ΔQ observed in any of the sub-reaches (Figure 4-18). Lumping together the three sub-reaches provided more reasonable results.

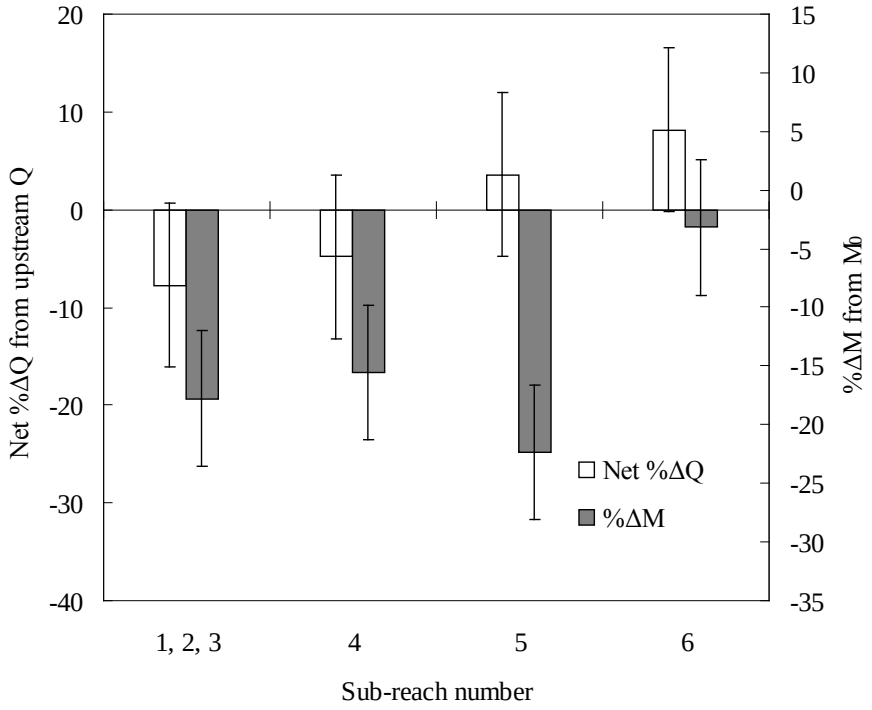

Figure 4-18. Net %Δ*Q* and %Δ*M* with estimated 95% confidence intervals for the Upper Reach with Sub-reaches #1, #2, and #3 combined.

The newly calculated gross gains and losses appear to be more representative of the exchanges in the Upper Reach (Figure 4-19). The first three sub-reaches all had significant Q_{gain} and Q_{loss}. This again confirms the importance of quantifying gross changes because quantifying only net changes would not detect any exchange occurring in the Upper Reach.

Sub-reaches #11 and #12 were also combined and treated as one sub-reach. The Δ*M* for each of the six sub-reaches are now negative, suggesting that the error in the data collection was omitted (Figure 4-20). A significant Δ*M* was only observed in Sub-reaches #9, #10, and combined #11 and #12. Additionally, net Δ*Q* was only observed in Sub-reaches #8, #9, and #13.

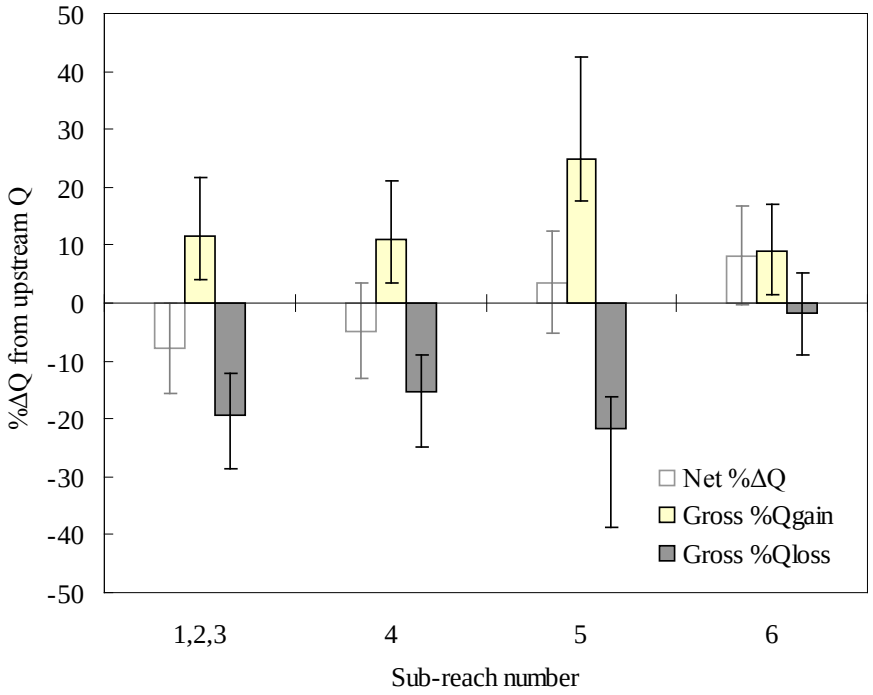

Figure 4-19. %Q_{gain} and %Q_{loss} with estimated 95% confidence intervals for the Upper Reach with Sub-reaches #1, #2, and #3 combined. Net changes are also shown.

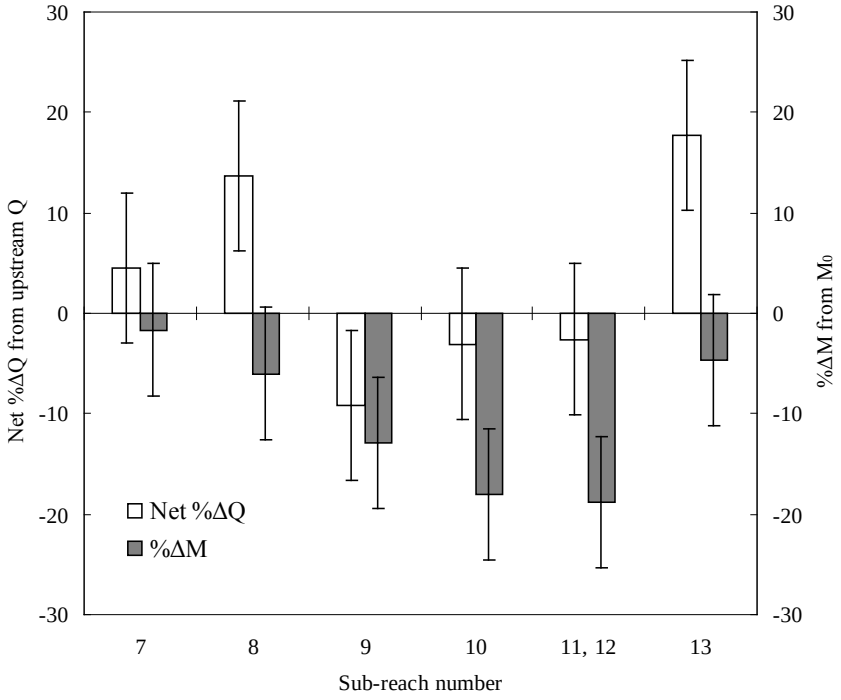

Figure 4-20. Net %Δ*Q* and %Δ*M* with estimated 95% confidence intervals for the Lower Reach with Sub-reaches #11 and #12 combined.

The gross gains and gross losses also appear to be more representative of the exchanges in the Lower Reach (Figure 4-21). The combined Sub-reach #11 and #12indicate a gain and a loss are now occurring with a net ΔQ non-detectable. This illustrates the importance of observing tracer responses at more than one sub-reach boundary in case of the event of an error in the data collection. Combining sub-reaches will likely provide sufficient information regarding a water balance used to support solute transport modeling.

Even though using dilution gauging techniques have a large advantage for estimating gross exchanges, these are only described for flow conditions at one discrete time period and additionally requires a large investment of time and labor. This study shows that the assumptions associated with dilution gauging techniques are difficult to

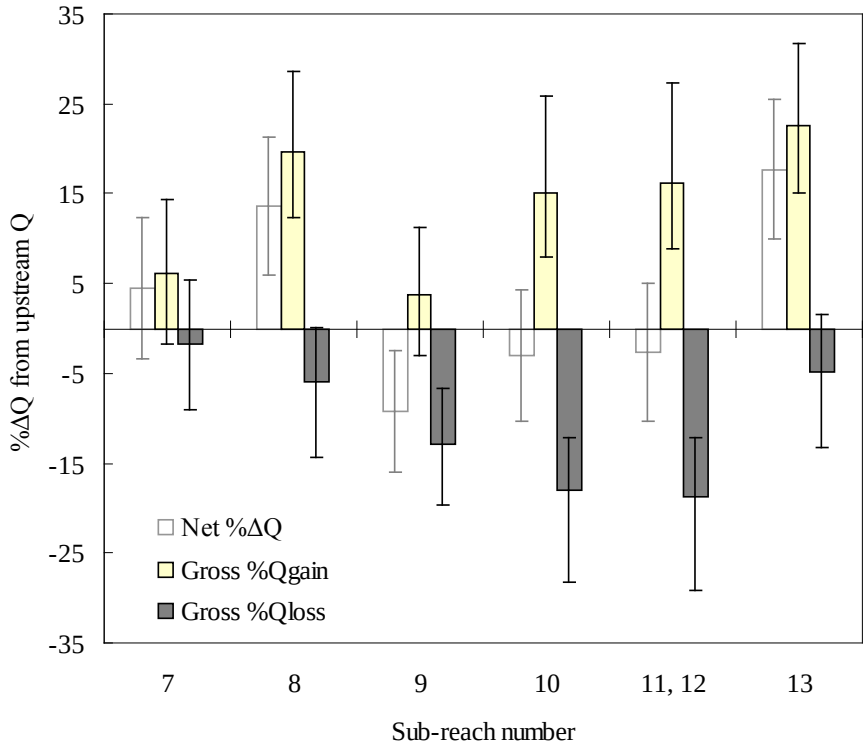

Figure 4-21. $\%Q_{gain}$ and $\%Q_{loss}$ with estimated 95% confidence bounds for the Lower Reach with Sub-reaches #11 and #12 combined. Net changes are also shown.

meet and verify. Additionally, the measured gains and losses are likely a combination of flows (e.g., long hyporheic flow combining with groundwater discharge) and behave as both point and distributed flows.

Conclusions

Neither the rating curve method nor the dilution gauging method was capable of detecting groundwater exchange at the reach scale due to the discharge estimates at the reach boundaries being statistically the same. When looking at exchanges at a finer spatial scale the two study reaches at Curtis Creek were shown to have highly spatially variable surface water-groundwater exchanges. However, the extent of groundwater exchange could not be accurately described without an error analysis. Net changes were detected to occur in every sub-reach, but significant net changes only occurred in half of the sub-reaches. Gross changes were then necessary to quantify to complete a more representative water balance. Significant gross exchanges were observed in five sub-reaches that did not have significant net changes.

A distinct conclusion made by completing a first order error analysis of dilution gauging results was that error due to the data collection method was only 1% of the discharge estimate and therefore, is considered insignificant. Although, the variation in mixing following a slug injection was shown to be a significant source of error in discharge estimates contributing a mean of 7%. In this system, the total error in the dilution gauging method was estimated to be 8% with 95% confidence.

The error analysis performed for the rating curve predictions provided a better understanding of the reliability of predictions. According to the stage-discharge data

used to construct rating curves, error in predictions is a function of stream discharge rather than more traditional methods applying a constant error to all predictions. Rating curve predictions may also provide some insight into whether assumptions for dilution gauging were reasonable.

CHAPTER 5

CONCLUSIONS

Characterizing and quantifying groundwater exchange processes in this research proved to difficult due to interactions being highly complex and spatially variable. This research demonstrated the reliability of common data collection strategies used to quantify groundwater exchanges through comparative and error analyses.

A reach scale net water balance with the two methods of rating curve predictions and dilution gauging techniques provided limited information regarding surface water-groundwater exchanges. High frequency discharge estimates with the use of rating curves and continuous stage data provided useful stream discharge fluctuation information. This information is necessary to understand the variability of stream discharge of longer periods of time and should be used concurrently with dilution gauging. Another advantage to using rating curves is that stream discharge can be estimated to see large variations in discharge caused by storm and snow melt events. The approach to the error analysis in rating curve predications provided a better understanding of how error changes as stream discharges fluctuate due to the confidence bounds being nonsymmetrical.

An error analysis was required to determine the reliability of both rating curves and dilution gauging to detect small changes in stream discharge caused by groundwater exchange at the reach scale. Neither method was capable of detecting exchanges at this scale due to discharges being statistically the same. This confirmed the need for stream gauging at a finer spatial scale.

The two study reaches were shown to have highly spatially variable surface water-groundwater interactions at the sub-reach scale. However, the extent of groundwater exchange could not be accurately described without a detailed error analysis. At the sub-reach scale, true exchanges could not be verified without an error analysis in dilution gauging techniques. An advantage to the error analysis in dilution gauging is that components of variance were estimated separately which provided evidence that error due to data collection can be considered negligible if careful implementation is exercised. However, testing the completely mixed assumption proved to be an important step to better anticipate this variance component and was found to be a significant source of error. Additionally, the assumptions required to complete perform discharge calculations are difficult to meet and verify and are likely the largest sources of error.

An advantage of using dilution gauging is that tracer mass recoveries can be used to quantify gross gains and losses occurring simultaneously within one sub-reach. These calculations provided more information regarding the water balance used to support more accurate solute transport predictions. A disadvantage of dilution gauging techniques is that information on surface water-groundwater interactions can only be provided at discrete time periods and may not capture variations in interactions caused by different flow conditions. Additionally, data collection is time and labor intensive.

Comparing information extracted from groundwater table and stream water surface elevations, VHGs, and *K* estimates to water balance calculations provided general trends in the variability in groundwater movement and exchange that were useful to support and test the water balance calculations. The groundwater table contours and

profiles of discrete elevation data indicated that surface water-groundwater interactions are complex and highly spatially variable with groundwater entering the stream channel on one side and exiting on the other. These data alone were not adequate to determine locations where dominant groundwater gains and losses occurred, but tested if the point flow assumption was appropriate. This assumption was found to may not have been reasonable and further testing is required to verify.

The spatial scale in which data were collected proved to be important when attempting to understand and predict solute mass movement. This study also provided evidence that collecting one data type is not enough to effectively describe stream water-groundwater interactions occurring. Researchers must be careful about what data types are collected, and at which spatial scale, to describe these interactions.

CHAPTER 6

ENGINEERING SIGNIFICANCE

In the fields of Environmental Engineering and Water Resources, there has been a need for improved understanding and prediction of the effects of physical stream transport processes on mass movement. This research demonstrated the reliability and utility of common data types used to characterize and quantify surface water-groundwater exchanges processes. However, at some locations data different types provided conflicting information. The interactions of these processes are often highly complex and spatially variable and this study illustrated that collecting one data type is not adequate to accurately characterize and quantify these interactions. This contributes to other studies by providing information regarding the most appropriate method to use for more accurately predicting mass movement.

The importance of providing a better understanding of physical processes it is necessary for supporting instream transport modeling. Predicting and modeling the transport of a pollutant through a river or stream leads to appropriate management strategies and environmental policy. This study justified the quantification of these processes at different spatial scales is highly important. For example, studies completed at larger spatial scales may be missing smaller scale processes that are greatly influencing mass transport and may later bias management decisions.

Surface water-groundwater exchange processes are particularly important to understand because of their role in biogeochemistry, water quality, and water supply. In the past, these processes have proven to be difficult to measure and predict. This research demonstrates the reliability of approaches used to characterize and quantify

groundwater exchange processes that include estimating a water balance. An error analysis was shown to be necessary in water balance results to more completely predict mass movement. The approach to estimating error provided information regarding improvement of experimental design to reduce error in future experiments. For example, when careful data collection is implemented for dilution gauging, the corresponding source of error was found to be negligible. Evidence was also provided that the assumptions are likely the largest contribution to the overall error and need to be tested and verified.

CHAPTER 7

RECOMMENDATIONS FOR FUTURE RESEARCH

1) Higher resolution of wells, water surface measurement locations, and piezometers should be installed. The resolution in this study was not high enough to accurately characterize groundwater and hyporheic exchange. However, installation of wells proved to be time and labor intensive.
2) Conduct tracer experiments during different flow periods to capture a broader range of conditions. The water balance estimated in this study represented one discrete time period and does not provide information of exchange processes during different time periods or flow conditions.
3) Conduct pump tests to determine *K* values and select more wells to develop a better understanding of surface water-groundwater interactions. *K* could not be estimated in nearly half of the wells where slug tests were performed. Additionally, *K* should be estimated in more wells to gain a better understanding of the spatial variability in the surrounding aquifer.
4) For tracer experiments, use a tracer that has little or no background present in the system (e.g., fluorescein or bromide). This may eliminate the occurrence of observing a positive mass loss in water balance calculations and reduce unforeseeable errors.
5) Install stilling wells around pressure transducers. This would reduce noise in continuous stage data and reduce this component of error that could not be quantified.

6) Collect more stage-discharge observations for a better rating curve and estimation of uncertainty. Two of the rating curves in this study were hypothesized to not reliably predict stream discharge and error due to a limited number of observations used to construct those curves.
7) Complete a better analysis of the variance caused by incomplete mixing in dilution gauging results. This study estimated this variance component with only two separate slug injections and may not have accurately captured this variance.
8) Better quantify groundwater concentration entering and exiting the stream channel by collecting longitudinal concentration profiles and installing deep piezometers and more groundwater observation wells.

REFERENCES

American Public Health Association (1999), *Standard Methods for the Examination of Water and Wastewater*, 20th ed., pp. 2-44–2-46, edited by Water Environment Federation, United Book Press, Inc., Baltimore, Maryland.

Baxter, C., F. R. Hauer, and W. W. Woessner (2003), Measuring groundwater-stream water exchange: New techniques for installing and estimating hydraulic conductivity, *American Fisheries Society, 132*, 493-502.

Beale, E. M. L. (1960), Confidence regions in non-linear estimation, *Journal of the Royal Statistical Society*, *22*(1), 41-88.

Becker, M. W., T. Georgian, H. Ambrose, J. Siniscalchi, and K. Fredrick (2004), Estimating flow and flux of ground water discharge using water temperature and velocity, *Journal of Hydrology*, *296*, 221-233.

Bencala, K. E. (1983), Simulation of solute transport in a mountain pool-and-riffle stream with a kinetic mass transfer model for sorption, *Water Resources Research*, *19*(3), 732-738.

Bencala, K. E. (2005), Hyporheic exchange flows, *Encyclopedia of Hydrological Sciences*, *3*, 1733-1740.

Bencala, K. E., R. E. Rathbun, A. P. Jackman, V. C. Kennedy, G. W. Zellweger, and R. J. Avanzino (1983), Rhodamine WT Dye Losses in a Mountain Stream Environment, *Water Resources Bulletin*, *19*(6), 943-950.

Bencala, K. E., and R. A. Walters (1983), Simulation of solute transport in a mountain pool-and-riffle stream: A transient storage model, *Water Resources Research*, *19*(3), 718-724.

Berthouex, P. M., and L. C. Brown (2002), *Statistics for Environmental Engineers*, 489 pp., CRC Press LLC, Boca Raton, Florida.

Briggs, M. A., M. N. Gooseff, C. D. Arp, and M. A. Baker (2009), A method for estimating surface transient storage parameters for streams with concurrent hyporheic storage, *Water Resources Research*, in print.

Cey, E. E., D. L. Rudolph, G. W. Parkin, and R. Aravena (1998), Quantifying groundwater discharge to a small perennial stream in southern Ontario, Canada, *Journal of Hydrology*, *210*, 21-37.

Chapra, S. C. (1997), *Surface Water-Quality Modeling*, 844 pp., McGraw-Hill Companies, Inc., Boston.

Choi, J., J. W. Harvey, and M. H. Conklin (2000), Characterizing multiple timescales of stream and storage zone interaction that affect solute fate and transport in streams, *Water Resources Research*, *36*(6), 1511-1518.

Covino, T. P., and B. L. McGlynn (2007), Stream gains and losses across a mountain-to-valley transition: Impacts on watershed hydrology and stream water chemistry, *Water Resources Research*, *43*, W10432, doi:10.1029/2006WR005544.

Dierberg, F. E., and T. A. DeBusk (2005), An evaluation of two tracers in surface-flow wetlands: Rhodamine-WT and lithium, *Wetlands*, *25*(1), 8-25.

Findlay, S. (1995), Importance of surface-subsurface exchange in stream ecosystems: The hyporheic zone, *Limnology and Oceanography 40*(1), 159-164.

Gooseff, M. N., and B. L. McGlynn (2005), A stream tracer technique employing ionic tracers and specific conductance data applied to the Maimai catchment, New Zealand, *Hydrological Processes*, *18*, doi:10.1002/hyp.5685.

Harvey, J. W., M. H. Conklin, and R. S. Koelsch (2003), Predicting changes in hydrologic retention in an evolving semi-arid alluvial stream, *Advances in Water Resources*, *26*, 939-950.

Harvey, J. W., J. E. Saiers, and J. T. Newlin (2005), Solute transport and storage mechanisms in wetlands of the Everglades, south Florida, *Water Resources Research*, *41*, W05009, doi: 10.1029/2004WR003507.

Harvey, J. W., and B. J. Wagner (2000), Quantifying hydrologic interactions between streams and their subsurface zones, in *Streams and Ground Waters*, edited by J. B. Jones and P. J. Mulholland, pp. 3-44, Academic Press, San Diego.

Harvey, J. W., B. J. Wagner, and K. E. Bencala (1996), Evaluating the reliability of the stream tracer approach to characterize stream-subsurface water exchange, *Water Resources Research*, *32*(8), 2441-2451.

Jencso, K. G., B. L. McGlynn, M. N. Gooseff, S. M. Wonzell, K. E. Bencala, and L. A. Marshall (2009), Hydrologic connectivity between landscapes and stream: Transferring reach- and plot-scale understanding to the catchment scale, *Water Resources Research*, *45*, W04428, doi:10.1029/2008WR007225.

Kasahara, T., and S. M. Wondzell (2003), Geomorphic controls on hyporheic exchange flow in mountain streams, *Water Resources Research*, *39*(1), 1005, doi:1029/2002WR001386.

Kelson, R. (2007), 5 Meter Auto-Correlated Elevation Model (DEM), May 2008, http://gis.utah.gov/elevation-terrain-data/5-meter-auto-correlated-elevation-model-dem, Utah Automated Geographic Reference Center, Salt Lake City, Utah.

Kennedy, E. J. (1983), Computation of continuous records of streamflow, *Techniques of Water-Resources Investigations of the U.S. Geological Survey, Book 3, Chapter A13*, 53 pp., U.S. Geological Survey, Alexandria, Virginia.

Kerry, J., A. Binley, N. Crook, and J. W. N. Smith (2007), Temporal and spatial variability of groundwater-surface water fluxes: Development and application of an analytical method using temperature time series, *Journal of Hydrology*, *336*, doi:10.1016/j.jhydrol.2006.12.003.

Kilpatrick, F. A., and E. D. Cobb (1985), Measurement of discharge using tracers, *U. S. Geological Survey Techniques of Water-Resources Investigations Report, Book 3, Chapter A16*, 52 pp., U.S. Geological Survey, Alexandria, Virginia.

Landon, M. K., D. L. Rus, and F. E. Harvey (2001), Comparison of instream methods for measuring hydraulic conductivity in sandy streambeds, *Groundwater*, *39*(6), 870-885.

Lapin, L. L. (1997), *Modern Engineering Statistics*, 583 pp., Wadsworth Publishing Company, Belmont, California.

Marsh-McBirney (1990), *FLO-MATE Model 2000 Portable Flowmeter Instruction Manual*, 15 pp., Marsh-McBirney Inc., Frederick, Maryland.

McCalpin, J. P., B. J. Solomon, and J. A. McBride (2001), Amplified Earthquake Ground-Motion and Surface-Fault-Rupture Hazards for the Logan Quadrangle, Central Cache Valley, Utah, *Map Plate 1D*, Utah Geological Survey, Salt Lake City, Utah.

Neilson, B. T. (2006), Dynamic stream temperature modeling: Understanding the causes and effects of temperature impairments and uncertainty in predictions, Ph.D. dissertation, 179 pp., Utah State University, Logan.

Neilson, B. T., S. Chapra, D. K. Stevens, and C. Bandaragoda (2009a), Identifying transient storage zones using solute and temperature observations: Part 1 - Solute, *Water Resources Research*, in review.

Neilson, B. T., D. K. Stevens, S. C. Chapra, and C. Bandaragoda (2009b), Data collection methodology for dynamic temperature model testing and corroboration, *Hydrological Processes*, *23*, 2902-2914.

Neilson, B. T., D. K. Stevens, S. Chapra, and C. Bandaragoda (2009c), Identifying transient storage zones using solute and temperature observations: Part 2 - Temperature and solute, *Water Resources Research*, in review.

Ohaus (2002), *Instruction Manual Navigator Balances*, 48 pp., Ohaus Corporation, Pine Brook, New Jersey.

Payn, R. A., M. N. Gooseff, D. A. Benson, O. A. Cirpka, J. P. Zarnetske, W. B. Bowden, J. P. McNamara, and J. H. Bradford (2008), Comparison of instantaneous and constant-rate stream tracer experiments through non-parametric analysis of resident time distribution, *Water Resources Research*, *44*, W06404, dio: 10.1029/2007WR006274.

Payn, R. A., M. N. Gooseff, B. L. McGlynn, K. E. Bencala, and S. M. Wondzell (2009), Longitudinal distribution of channel water balance through summer discharge recession in a Rocky Mountain headwater stream, Montana, USA, *Water Resources Research*, in press.

Ramaswami, A., J. B. Milford, and M. J. Small (2005), *Integrated Environmental Modeling Pollutant Transport, Fate, and Risk in the Environment*, 678 pp., John Wiley & Sons, Inc., Hoboken, New Jersey.

Rantz, S. E. (1982), Measurement and computation of streamflow: Volume 1. Measurement of stage and discharge, *U.S. Geological Survey Water Supply Paper 2395*, 34 pp., U.S. Geological Survey, Denver, Colorado.

Ruehl, C., A. T. Fisher, C. Hatch, M. L. Huertos, G. Stemler, and C. Shennan (2006), Differential gauging and tracer tests resolve seepage fluxes in a strongly-losing stream, *Journal of Hydrology*, *330*, 235-248.

Runkel, R. L. (1998), One dimensional transport with inflow and storage (OTIS): A solute transport model for streams and rivers, *Water-Resources Investigation Report 98-4018*, U.S. Geological Survey, Denver, Colorado.

Runkel, R. L., and K. E. Bencala (1995), Transport of reacting solutes in rivers and streams, in *Environmental Hydrology*, edited by V. P. Singh, pp. 137-164, Kluwer Academic Publishers, Dordrecht, The Netherlands.

Schmid, B. H. (2004), Simplification in longitudinal transport modeling: Case of instantaneous slug releases, *Journal of Hydrological Engineering*, *9*(4), 319-324.

Stewart, J. (1998), *Calculus Concepts and Contexts*, 991 pp., Brooks/Cole Publishing Company, Pacific Grove, California.

Stream Solute Workshop (1990), Concepts and methods for assessing solute dynamics in stream ecosystems, *Journal of the North American Benthological Society*, *9*(2), 95-119.

Trimble (2009), Trimble R8 GNSS Receiver Datasheet, Dayton, Ohio.

U.S. Geological Survey (2007), NHD GEODATABASE, May 2008, http://nhdgeo.usgs.gov/viewer.htm, U.S. Geological Survey, Lakewood, Colorado.

Utah Division of Wildlife Resources (2001), Curtis Creek Stream Alteration Project, Hardware Ranch, Utah.

Wagner, B. J., and J. W. Harvey (1997), Experimental design for estimating parameters of rate-limited mass transfer: Analysis of stream tracer studies, *Water Resources Research*, *33*(7), 1731-1741.

Weber, W. J. J., and F. A. DiGiano (1996), *Process Dynamics in Environmental Systems*, 943 pp., John Wiley & Sons, Inc., New York.

Winter, T. C., J. W. Harvey, O. L. Franke, and W. M. Alley (1998), Groundwater and surface water: A single resource, *U.S. Geological Survey Circular*, *1139*, 79 pp., Denver, Colorado.

YSI (2006), *6-Series Multiparameter Water Quality Sondes User Manual*, pp. O-12, YSI Incorporated, Yellow Springs, Ohio.

Zellweger, G. W. (1994), Testing and comparison of four ionic tracers to measure stream flow loss by multiple tracer injection, *Hydrological Processes*, *8*, 155-165.

APPENDICES

APPENDIX A

Rating Curves and Supporting Information

Velocity-area technique [*Rantz*, 1982]:

$$Q = \sum_{i=1}^{n} \left(X_{i+1} - X_i\right)\left(U_i Y + U_{i+1} Y_{i+1}\right)/2 \qquad \text{(A-1)}$$

where:
X_i = the distances to successive velocity measurements from the edge of water, ft;
U_i = the velocity measurement at each depth interval, ft s^{-1};
Y_i = the vertical depth at each interval, ft.

Table A-1. Stage and Discharge Data for Location 0 m (Station PT 0)

PT 0 Depth (ft)	Q0 Discharge (cfs)	PT 0 Depth (ft)	Q0 Discharge (cfs)
0.244	5.48	0.410	5.71
0.310	5.03	0.441	11.55
0.317	5.10	0.485	12.16
0.330	5.40	0.488	10.77
0.333	5.62	0.628	18.56
0.334	5.19	0.718	20.04
0.337	6.17	0.905	34.53
0.338	5.66	0.956	37.93
0.364	6.35	1.111	52.25
0.388	6.45		

```
> nls0=nls(m0,data=Data, start=list(a=48,b=2.6))
> overview(nls0)
------
Formula: Q0 ~ a * PT0^b
Parameters:
Estimate Std. Error t value Pr(>|t|)
a 42.01954    0.66909    62.8   <2e-16 ***
b  1.86749    0.05159    36.2   <2e-16 ***
---
Signif. codes:  0 ‘***’ 0.001 ‘**’ 0.01 ‘*’ 0.05 ‘.’ 0.1 ‘ ’ 1
Residual standard error: 2.444 on 17 degrees of freedom
Number of iterations to convergence: 5
Achieved convergence tolerance: 3.703e-07
------
Residual sum of squares: 29.4
------
Asymptotic confidence interval:
      2.5%     97.5%
a 40.607881 43.431195
b  1.758643  1.976334
------
Correlation matrix:
         a         b
a 1.0000000 0.3437794
b 0.3437794 1.0000000
```

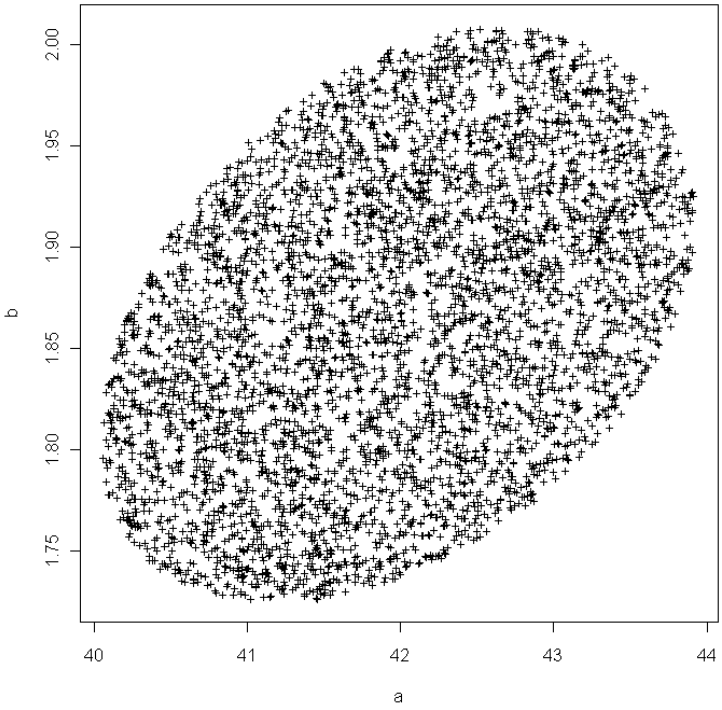

Figure A-1. Random sample points generated within the estimated 95% JCR for the station PT 0 rating curve parameters *a* and *b*.

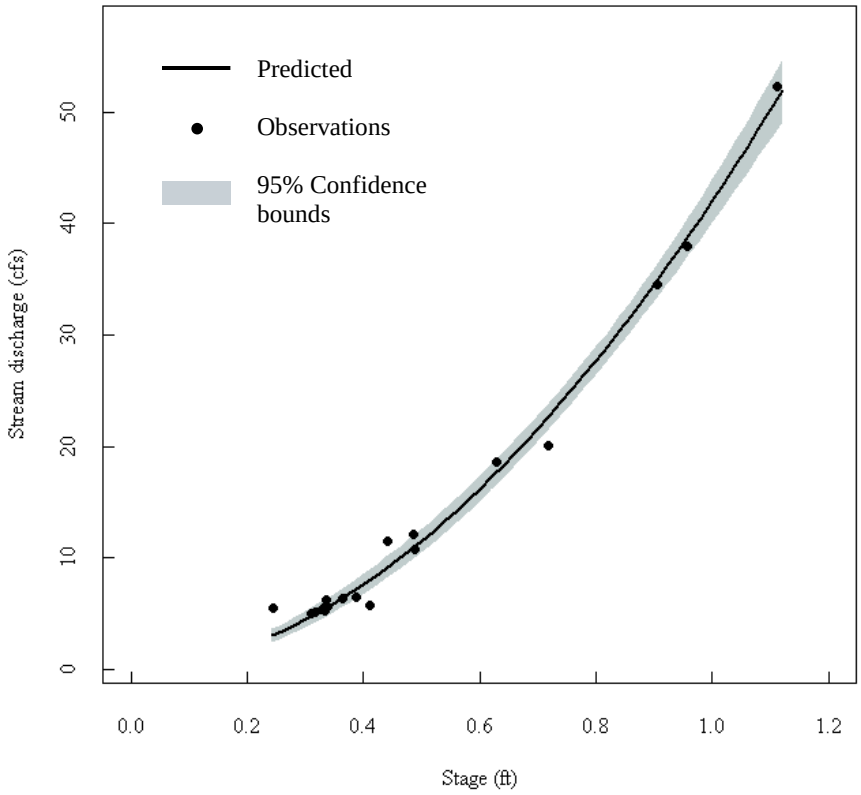

Figure A-2. The station PT 0 rating curve and estimated 95% confidence bounds.

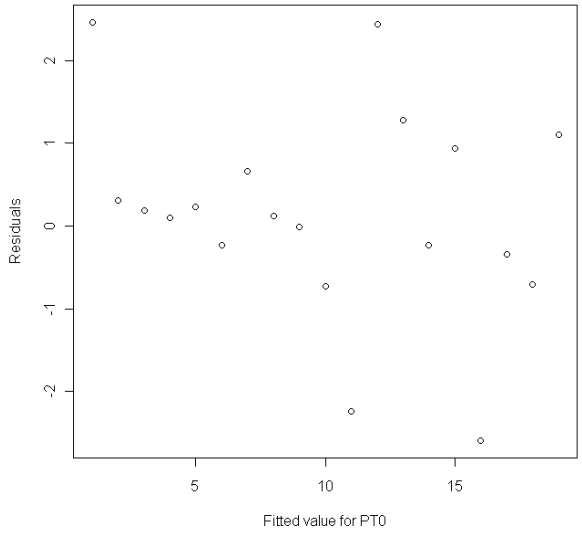

Figure A-3. Residuals of the station PT 0 rating curve parameters.

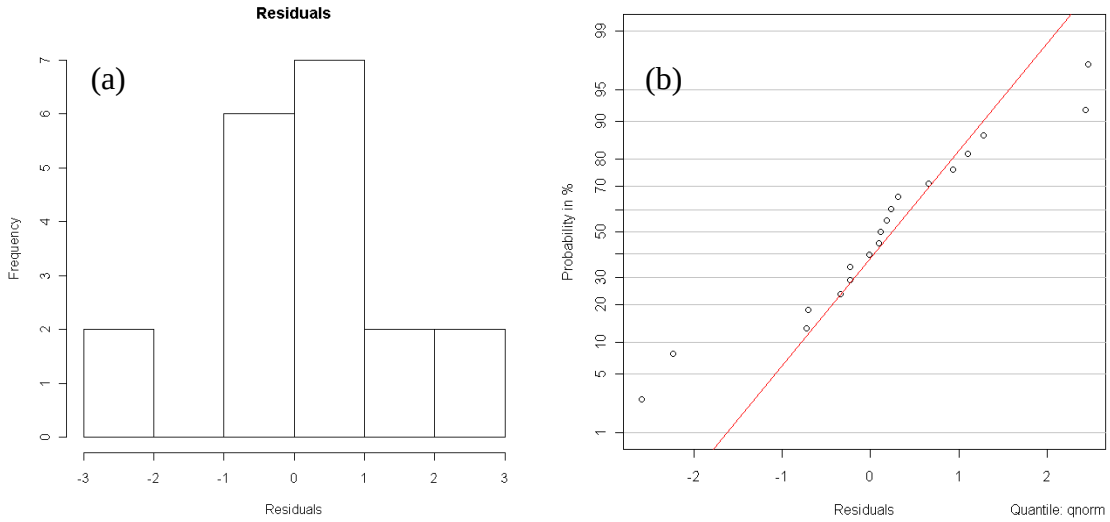

Figure A-4. (a) Histogram and (b) probability plot of the residuals for station PT 0.

Table A-2. Stage and Discharge Data for Location 515 m (Station PT 515)

PT515 Depth (ft)	Q515 Discharge (cfs)
0.395	6.79
0.413	7.42
0.520	11.91
0.523	12.33
0.534	12.85
0.692	21.41
0.716	23.12
0.723	22.81
0.760	25.57

Formula: Q515 ~ a * PT515^b
Parameters:
  Estimate Std. Error t value Pr(>|t|)
a 44.28805   0.61408   72.12 2.59e-11 ***
b 1.99282   0.03486   57.16 1.32e-10 ***

Signif. codes: 0 ‘***’ 0.001 ‘**’ 0.01 ‘*’ 0.05 ‘.’ 0.1 ‘ ’ 1
Residual standard error: 0.3587 on 7 degrees of freedom
Number of iterations to convergence: 4
Achieved convergence tolerance: 2.167e-06

Residual sum of squares: 0.473

Asymptotic confidence interval:
      2.5%   97.5%
a 42.835974 45.740119
b 1.910379 2.075261

Correlation matrix:
         a   b
a 1.0000000 0.9370637
b 0.9370637 1.0000000

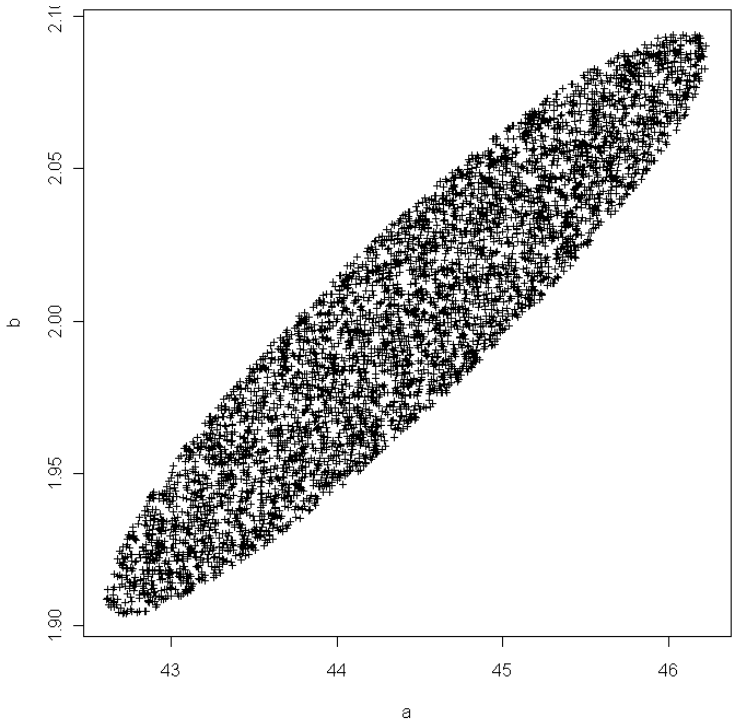

Figure A-5. Random sample points generated within the estimated 95% JCR for the station PT 515 rating curve parameters.

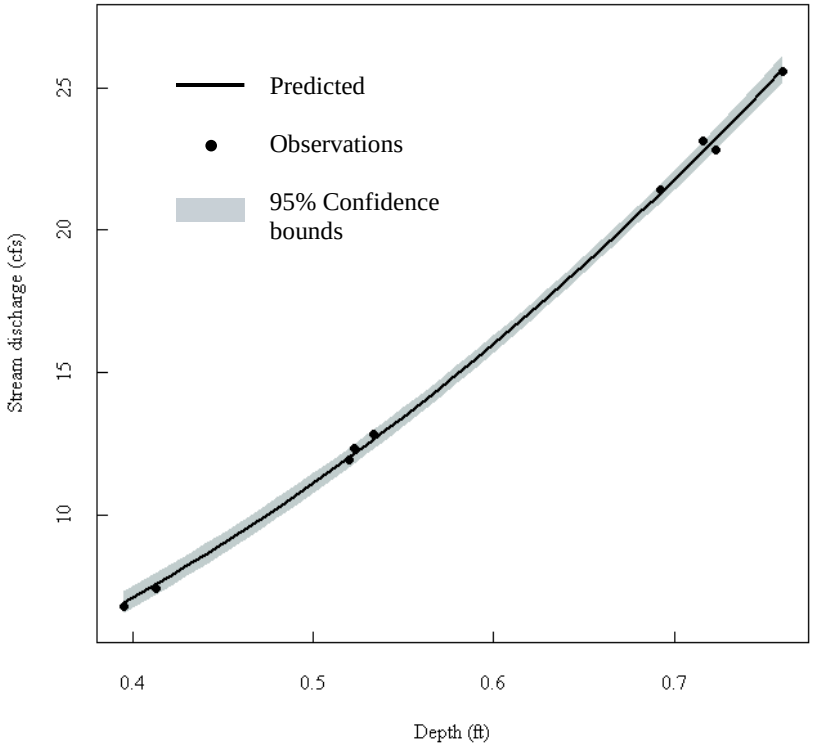

Figure A-6. The station PT 515 rating curve and estimated 95% confidence bounds.

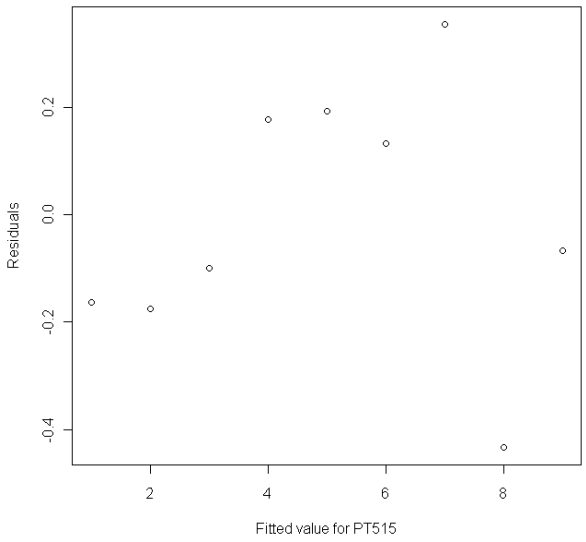

Figure A-7. Residuals of the station PT 515 rating curve.

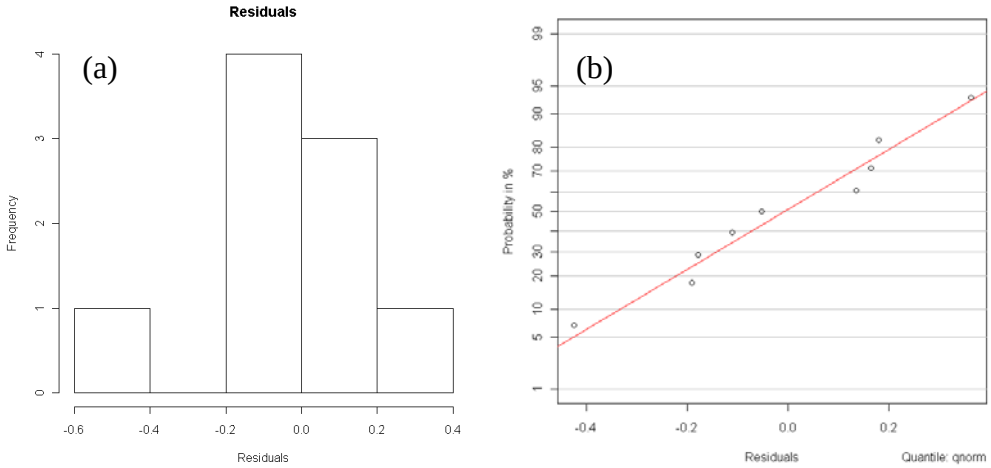

Figure A-8. (a) Histogram and (b) probability plot of the residuals for the station PT 515 rating curve.

Table A-3. Stage and Discharge Data for Location 692 m (Station PT 692).

PT692 Depth (ft)	Q692 Discharge (cfs)
0.588	6.25
0.626	8.32
0.733	12.91
0.739	13.74
0.899	20.69
0.958	25.14
0.975	25.83

```
------
Formula: Q692 ~ a * PT692^b
Parameters:
  Estimate Std. Error t value Pr(>|t|)
a  27.7503     0.5052   54.93 3.78e-08 ***
b   2.5479     0.1040   24.49 2.12e-06 ***
---
Signif. codes:  0 ‘***’ 0.001 ‘**’ 0.01 ‘*’ 0.05 ‘.’ 0.1 ‘ ’ 1
Residual standard error: 1.288 on 5 degrees of freedom
Number of iterations to convergence: 4
Achieved convergence tolerance: 6.977e-07
------
Residual sum of squares: 2.07
------
Asymptotic confidence interval:
       2.5%     97.5%
a 26.451668 29.048964
b  2.280433  2.815280
------
Correlation matrix:
          a         b
a 1.0000000 0.6546934
b 0.6546934 1.0000000
```

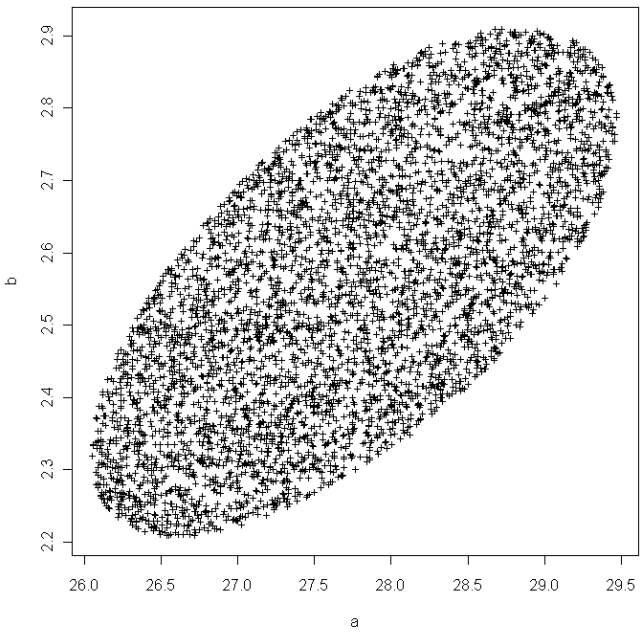

Figure A-9. Random points generated within the estimated 95% JCR for the station PT 692 rating curve parameters.

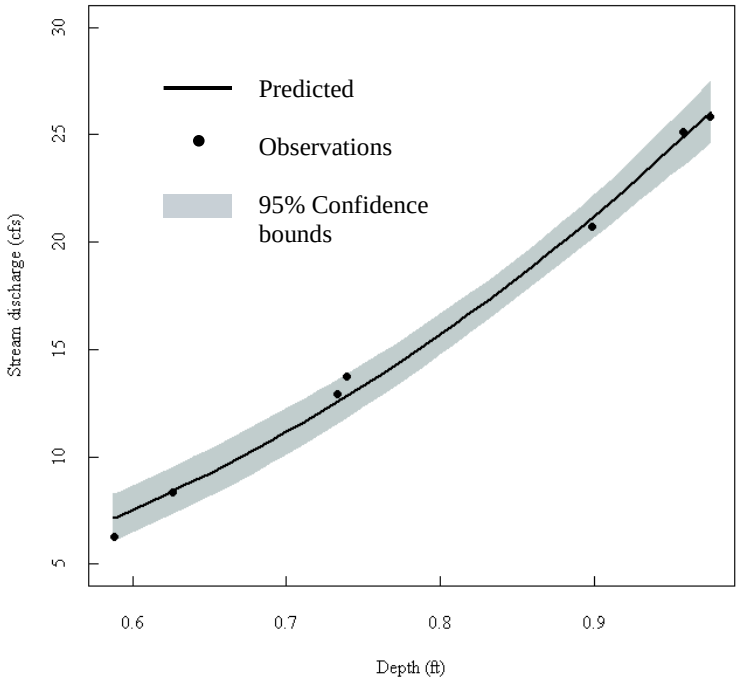

Figure A-10. The station PT 692 rating curve and estimated 95% confidence bounds.

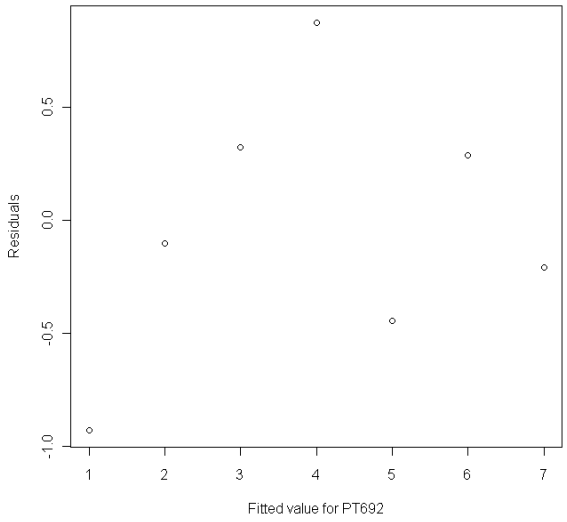

Figure A-11. Residuals of the station PT 692 rating curve.

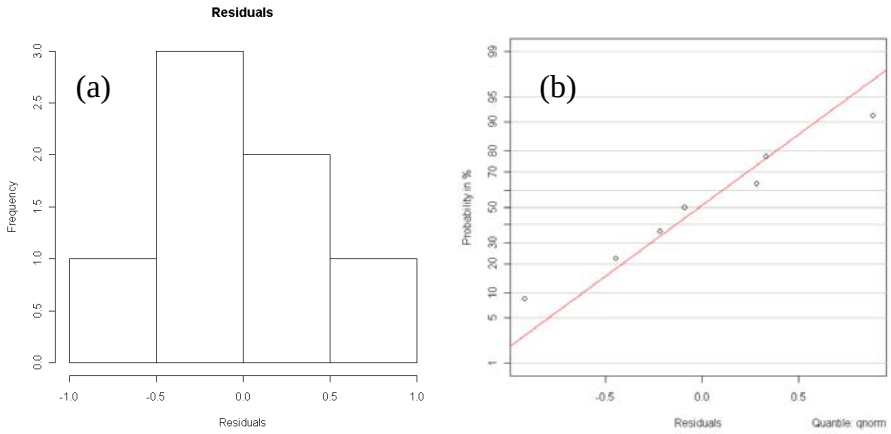

Figure A-12. (a) Histogram and (b) probability plot of the residuals for station PT 692.

Table A-4. Stage and Discharge Data for Location 1252 m (Station PT 1252).

PT 1252 Depth (ft)	Q1252 Discharge (cfs)	PT 1252 Depth (ft)	Q1252 Discharge (cfs)
0.449	6.12	0.515	7.51
0.457	5.56	0.564	11.77
0.457	6.31	0.732	21.95
0.458	5.97	0.787	22.43
0.459	6.31	0.885	38.99
0.469	6.48	0.920	40.84
0.477	7.34	1.048	53.31
0.504	7.33		

Formula: Q1252 ~ a * PT1252^b
Parameters:
  Estimate Std. Error t value Pr(>|t|)
a 48.3737   0.8450   57.25 < 2e-16 ***
b   2.5583   0.1094   23.39 5.24e-12 ***

Signif. codes: 0 ‘***’ 0.001 ‘**’ 0.01 ‘*’ 0.05 ‘.’ 0.1 ‘ ’ 1
Residual standard error: 2.632 on 13 degrees of freedom
Number of iterations to convergence: 4
Achieved convergence tolerance: 6.805e-07

Residual sum of squares: 36.8

Asymptotic confidence interval:
      2.5%   97.5%
a 46.548237 50.199087
b 2.321936 2.794627

Correlation matrix:
          a   b
a 1.0000000 0.3212926
b 0.3212926 1.0000000

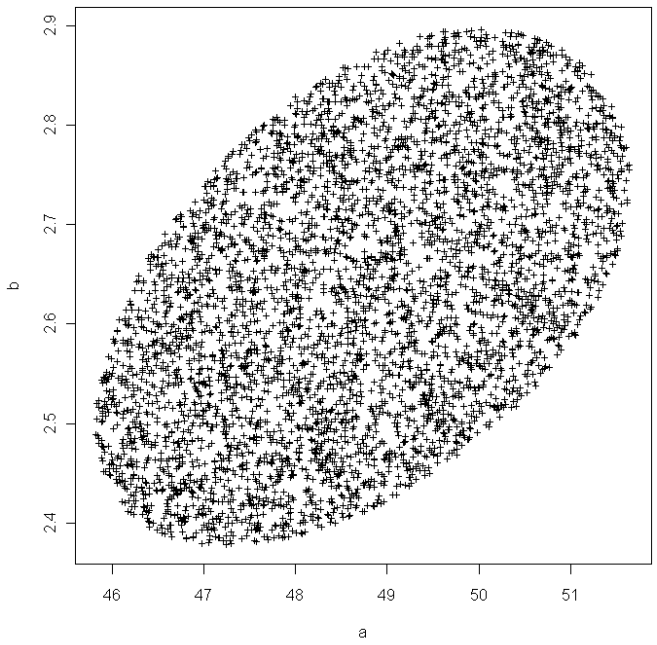

Figure A-13. Random sample points generated within the 95% JCR for the station PT 1252 rating curve parameters.

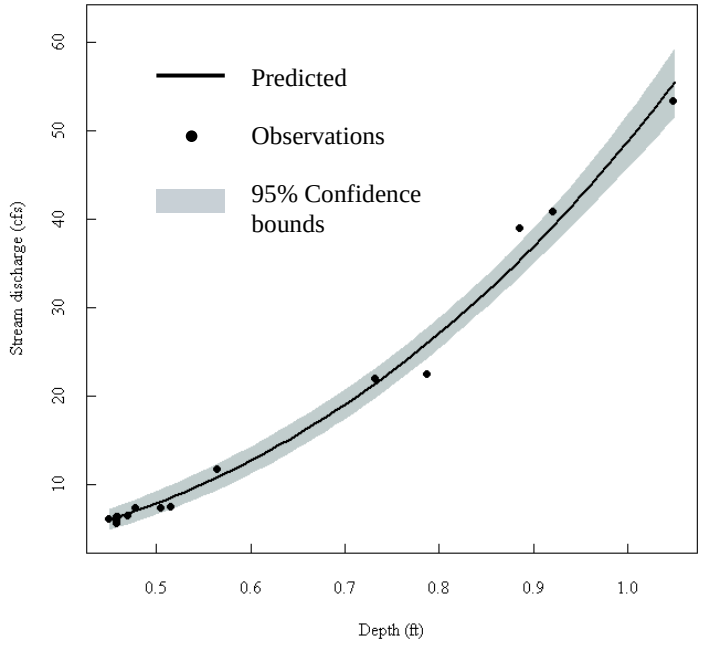

Figure A-14. The station PT 1252 rating curve and estimated 95% confidence bounds.

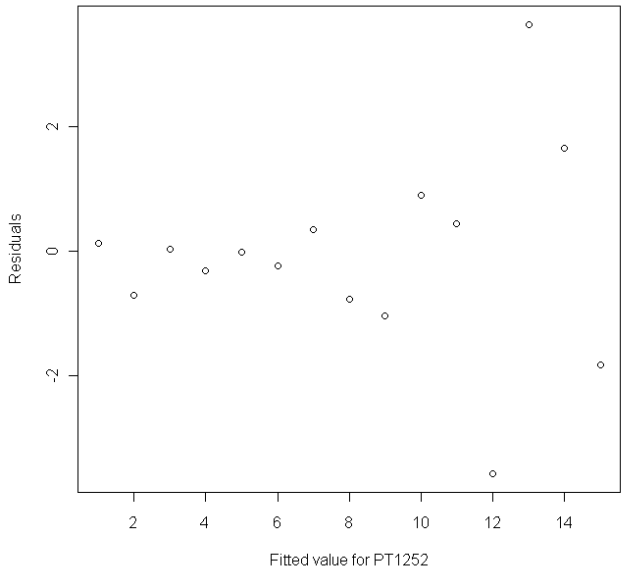

Figure A-15. Residuals of the station PT 1252 rating curve.

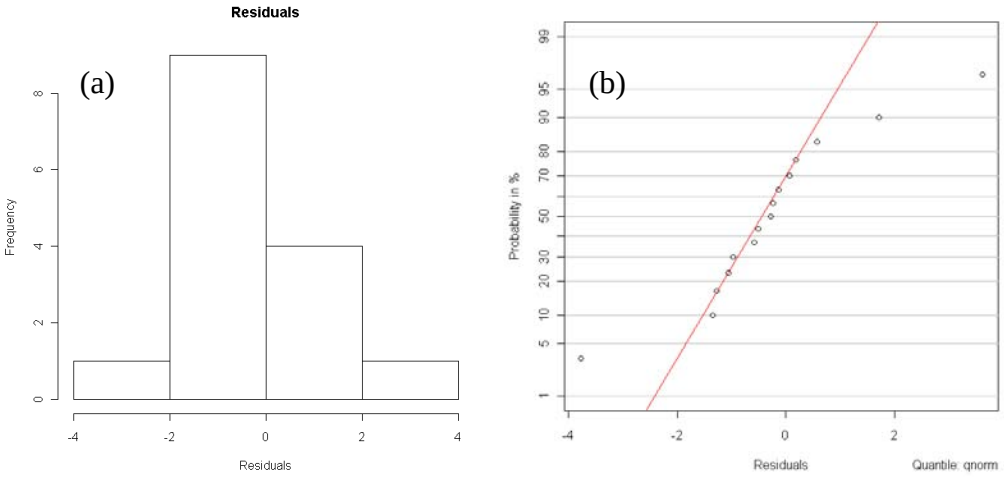

Figure A-16. (a) Histogram and (b) probability plot of the residuals for the station PT 1252 rating curve.

Table A-5. Rating Curve Parameter Estimates with 95% Confidence Intervals.

			Parameter			
Reach	Station	*n*	*a*	95% CI	*b*	95% CI
Upper	PT 0	19	42.02	±1.41	1.87	±0.11
	PT 515	9	44.29	±1.45	1.99	±0.09
Lower	PT 692	7	27.75	±1.30	2.55	±0.27
	PT 1252	15	48.37	±1.83	2.56	±0.24

APPENDIX B

Supporting Information for Dilution Gauging Techniques

Table B-1. Upper Reach Dilution Gauging Results at the Sub-reach Boundaries

Sub-reach number	Injection distance downstream (m)	Measurement location downstream (m)	Slug travel distance (m)	M (g)	$\int C(t)dt - \int C_b dt$ (mg s L^{-1})	Q (L s^{-1})
	-48	11	60	364	1075.9	**338.3**
1	69	92	23	364	1174.6	**309.9**
2	153	178	25	364	956.6	**380.5**
3	215	240	28	364	1166.1	**312.1**
4	307	359	53	364	1225.0	**297.1**
5	416	452	37	364	1182.4	**307.8**
6	452	515	63	364	1152.5*	**333.0***

*Averaged value from three instrument responses placed at a transect

Table B-2. Lower Reach Dilution Gauging Results at the Sub-reach Boundaries

Sub-reach number	Injection distance downstream (m)	Measurement location downstream (m)	Slug travel distance (m)	M (g)	$\int C(t)dt - \int C_b dt$ (mg s L^{-1})	Q (L s^{-1})
	636	713	77	364	1220.2	**298.3**
7	772	813	41	364	1167.7	**311.7**
8	832	877	45	364	1027.2	**354.3**
9	939	995	56	364	1130.8	**321.9**
10	1050	1087	36	364	1166.5	**312.0**
11	1129	1161	31	364	1015.4	**358.4**
12	1208	1235	27	364	1197.5	**303.9**
13	1252	1291	39	364	1018.4*	**357.8***

*Averaged value from three instrument responses placed at a transect

Table B-3. $\%R$, ΔM, and $\%\Delta M$ for the Upper Reach

Sub-reach number	Slug number (measurement location, m)	Slug travel distance (m)	$\int C_{12}(t)dt - \int C_b dt$ (mg s L^{-1})	$\%R$	ΔM (g)	$\%\Delta M$
1	8 (92)	140	1105.4	94.1	-21.4	**-5.9**
2	7 (178)	109	1169.3	122.2	80.9	**22.2**
3	6 (240)	87	1115.4	95.7	-15.8	**-4.4**
4	5 (360)	145	1020.8	83.3	-60.7	**-16.7**
5	4 (452)	145	888.7	75.2	-90.4	**-24.8**
6	3 (515)	99	1073.1	98.2	-6.7	**-1.8**

Table B-4. %*R*, Δ*M*, and %Δ*M* for the Lower Reach

Sub-reach number	Slug number (measurement location, m)	Slug travel distance (m)	$\int C_{12}(t)dt - \int C_b dt$ (mg s L^{-1})	%*R*	Δ*M* (g)	%Δ*M*
7	10 (813)	146	1115.6	98.4	-6.0	**-1.7**
8	8 (877)	105	998.9	94.0	-21.8	**-6.0**
9	7 (995)	163	1160.9	87.1	-47.1	**-12.9**
10	6 (1087)	148	1065.6	81.9	-65.8	**-18.1**
11	4 (1160)	111	972.2	108.5	30.8	**8.5**
12	3 (1235)	106	990.6	86.1	-50.8	**-14.0**
13	2 (1291)	83	1115.6	95.3	-17.0	**-4.7**

Table B-5. Percent Recoveries (%*R*) and Relative Percent Differences (RPD) for Spikes and Replicate Spikes.

Spiked sample number	%*R*		RPD
	1	2	
1	85.3	93.5	6.83
2	92.1	84.9	6.87
3	112.6	111.8	0.48
4	102.4	101.3	0.81
5	114.1	110.9	1.18
6	93.0	101.0	6.50

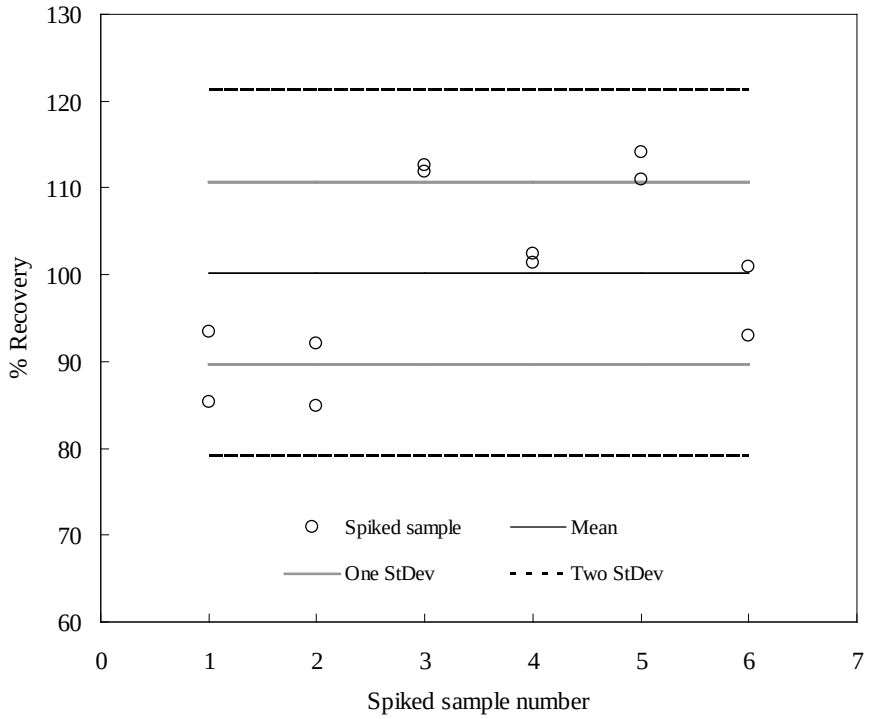

Figure B-1. Quality control chart for IC chloride concentration measurements.

Table B-6. General Analysis of Variance for Estimating Variance Components [*Berthouex and Brown*, 2002].

SS	df	MS	MS estimates
$SS_{ave} = n_L n_S n_T \bar{y}^2$			
$SS_L = n_S n_T \sum_{L=1}^{n_L} (\bar{y}_L - \bar{y})^2$	$n_S - 1$	$MS_L = \frac{SS_L}{n_L - 1}$	$n_S n_T \sigma_L^2 + n_T \sigma_S^2 + \sigma_T^2$
$SS_S = n_T \sum_{L=1}^{n_L} \sum_{S=1}^{n_S} (\bar{y}_L - \bar{y}_S)^2$	$n_L(n_S - 1)$	$MS_S = \frac{SS_S}{n_L(n_S - 1)}$	$n_T \sigma_S^2 + \sigma_T^2$
$SS_T = \sum_{L=1}^{n_L} \sum_{S=1}^{n_S} \sum_{T=1}^{n_T} (y_{LST} - \bar{y}_{LS})^2$	$n_L n_S (n_T - 1)$	$MS_T = \frac{SS_T}{n_L n_S (n_T - 1)}$	σ_T^2
Total $SS = \sum_{L=1}^{n_L} \sum_{S=1}^{n_S} \sum_{T=1}^{n_T} y_{LST}^2$			

$$\sigma_T^2 = MS_T \tag{B-1}$$

$$\sigma_S^2 = \frac{MS_S - MS_T}{n_T} \tag{B-2}$$

$$\sigma_L^2 = \frac{MS_L - MS_S}{n_S n_T} \tag{B-3}$$

where:
MS_T = mean square of replicate tests;
MS_S = mean square of specimens;
MS_L = mean square of locations;
n_T = number of tests;
n_S = number of specimens.

Table B-7. Calculations of Individual Errors e_T, e_S, and e_L and the Sum of Squares Used to Complete an ANOVA

	Sample location			Chloride conc.	Deviations of tests			Deviations of specimens			Deviations of locations	
Site number	downstream (m)	Specimen number	Test number	y (mg L^{-1})	$\bar{y}_S$ (mg L^{-1})	e_T (mg L^{-1})	$(e_T)^2$ (mg^2 L^{-2})	$\bar{y}_L$ (mg L^{-1})	e_S (mg L^{-1})	$(e_S)^2$ (mg^2 L^{-2})	e_L (mg L^{-1})	$(e_L)^2$ (mg^2 L^{-2})
1	11	1	1	5.51	5.51	0.0000	0.0000	5.51	0.0000	0.0000	0.7050	0.4970
2	92	1	1	5.52	5.52	0.0000	0.0000	5.37	-0.1550	0.0240	0.8500	0.7225
		2	1	5.21	5.21	0.0000	0.0000	5.37	0.1550	0.0240	0.8500	0.7225
3	178	1	1	4.21	4.21	0.0000	0.0000	4.21	0.0000	0.0000	2.0050	4.0200
4	240	1	1	4.90	4.88	-0.0200	0.0004	4.95	0.0725	0.0053	1.2625	1.5939
		1	2	4.87	4.88	0.0100	0.0001	4.95	0.0725	0.0053	1.2625	1.5939
		1	3	4.87	4.88	0.0100	0.0001	4.95	0.0725	0.0053	1.2625	1.5939
		2	1	5.17	5.17	0.0000	0.0000	4.95	-0.2175	0.0473	1.2625	1.5939
5	360	1	1	6.53	6.53	0.0000	0.0000	6.55	0.0200	0.0004	-0.3350	0.1122
		2	1	6.57	6.57	0.0000	0.0000	6.55	-0.0200	0.0004	-0.3350	0.1122
6	452	1	1	5.39	5.39	0.0000	0.0000	6.09	0.6950	0.4830	0.1300	0.0169
		2	1	6.78	6.78	0.0000	0.0000	6.09	-0.6950	0.4830	0.1300	0.0169
7	515	1	1	5.50	5.50	0.0000	0.0000	5.44	-0.0650	0.0042	0.7800	0.6084
		2	1	5.37	5.37	0.0000	0.0000	5.44	0.0650	0.0042	0.7800	0.6084
8	713	1	1	5.41	5.41	0.0000	0.0000	6.24	0.8300	0.6889	-0.0250	0.0006
		2	1	7.07	7.07	0.0000	0.0000	6.24	-0.8300	0.6889	-0.0250	0.0006
9	813	1	1	5.77	5.77	0.0000	0.0000	5.77	0.0000	0.0000	0.4450	0.1980
10	877	1	1	6.22	6.22	0.0000	0.0000	6.22	0.0000	0.0000	-0.0050	0.0000
11	995	1	1	6.61	6.61	0.0000	0.0000	6.79	0.1800	0.0324	-0.5750	0.3306
		2	1	6.97	6.97	0.0000	0.0000	6.79	-0.1800	0.0324	-0.5750	0.3306
12	1071	1	1	6.92	6.92	0.0000	0.0000	6.92	0.0000	0.0000	-0.7050	0.4970
13	1160	1	1	7.24	7.24	0.0000	0.0000	6.89	-0.3500	0.1225	-0.6750	0.4556
		2	1	6.54	6.54	0.0000	0.0000	6.89	0.3500	0.1225	-0.6750	0.4556
14	1235	1	1	7.05	7.05	0.0000	0.0000	7.05	0.0000	0.0000	-0.8350	0.6972
15	1291	1	1	7.23	7.29	0.0567	0.0032	7.38	0.0883	0.0078	-1.1600	1.3456
		1	2	7.29	7.29	0.0000	0.0000	7.38	0.0850	0.0072	-1.1600	1.3456
		1	3	7.34	7.29	-0.0500	0.0025	7.38	0.0850	0.0072	-1.1600	1.3456
		2	1	7.26	7.46	0.2033	0.0413	7.38	-0.0883	0.0078	-1.1600	1.3456
		2	2	7.49	7.46	-0.0300	0.0009	7.38	-0.0850	0.0072	-1.1600	1.3456
		2	3	7.64	7.46	-0.1800	0.0324	7.38	-0.0850	0.0072	-1.1600	1.3456
			Average (y)	6.22		SS_T	0.0810		SS_S	2.8185	SS_L	24.8524

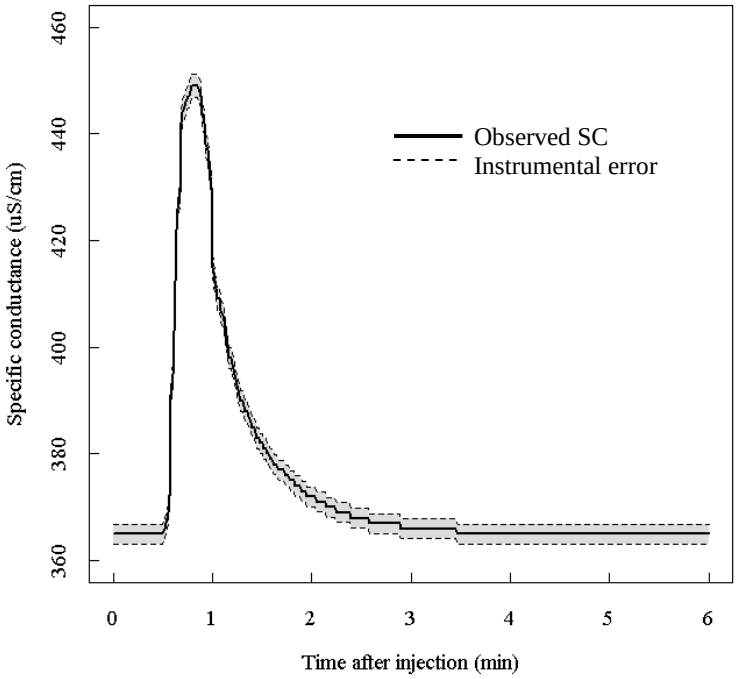

Figure B-2. Example response curve with instrumental error of ±0.5% of the SC reading.

The slopes and intercepts of each calibration curve were tested for statistically equivalency with Equation B-4 [*Berthouex and Brown*, 2002].

$$b_0 \pm t_{\nu,\alpha/2} s \sqrt{\frac{1}{n} + \frac{\bar{x}^2}{\sum (x_i - \bar{x})^2}} \quad \text{and} \quad b_1 \pm t_{\nu,\alpha/2} s \sqrt{\frac{1}{\sum (x_i - \bar{x})^2}} \qquad \text{(B-4)}$$

where:
$t_{\upsilon,\alpha/2}$ = the 95% probability point of the *t* distribution for υ degrees of freedom;
s = the sample standard error, μS cm^{-1};
n = the number of samples;
$\bar{x}$ = the average of the chloride standard concentrations, mg L^{-1};
x_i = the chloride standard concentration.

The Working-Hotelling confidence bands for the Upper Reach

$$s^2 = \sum \frac{(y_i - \hat{y})^2}{n-2} = \frac{416.89 \mu S^2\ cm^{-2}}{16} = 26.06 \mu S^2\ cm^{-2}$$

$$b_0 + b_1 x \pm \sqrt{2F_{2,\nu,\alpha} s^2 \left(\frac{1}{n} + \frac{(x-\bar{x})^2}{\sum (x_i - \bar{x})^2} \right)} = \sqrt{2 * 3.63 * 26.06 \mu S^2\ cm^{-2} \left(\frac{1}{18} + \frac{(x - 29.17 mg\ L^{-1})^2}{21062.5 mg^2\ L^{-2}} \right)}$$

and for the Lower Reach

$$s^2 = \frac{512.79\mu S^2\, cm^{-2}}{22} = 23.31\mu S^2\, cm^{-2}$$

$$b_0 + b_1 x \pm \sqrt{2 * 3.44 * 23.31\mu S^2\, cm^{-2}\left(\frac{1}{24} + \frac{(x - 29.17mg\, L^{-1})^2}{28083.3mg^2\, L^{-2}}\right)}.$$

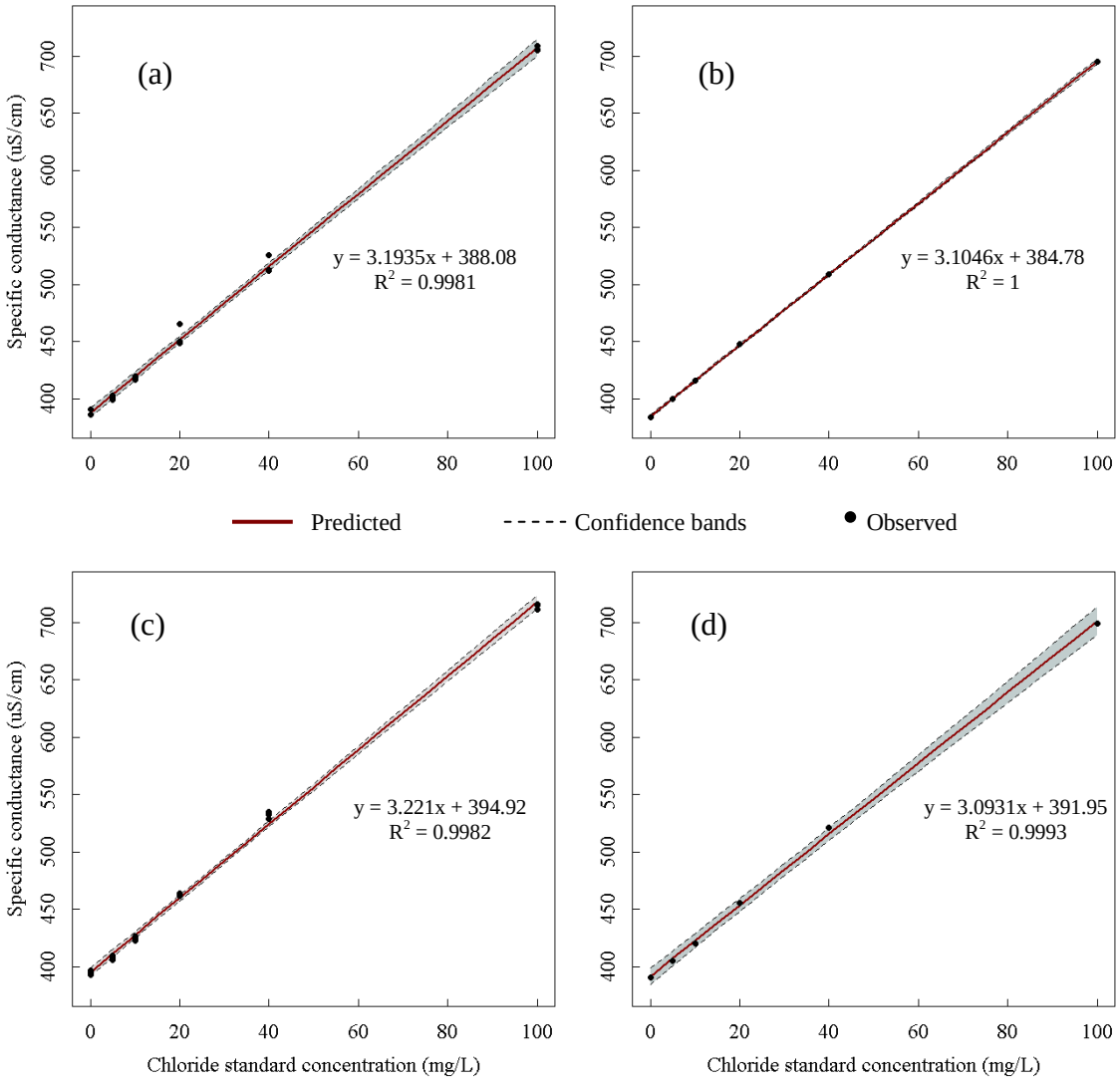

Figure B-3. SC to chloride concentration calibration curves with Working-Hotelling confidence bands for (a) Upper Reach creek water with SC measured with field instruments (b) Upper Reach creek water with SC measured with laboratory conductivity meter, (c) Lower Reach creek water with SC measured with field instruments, and (d) Lower Reach creek water with SC measured with laboratory conductivity meter.

Table B-8. Calibration Curve Parameter Estimates and 95% Confidence Intervals for the Upper and Lower Reach

Reach	Method	n	υ	$t_{\upsilon,0.05/2}$	s^2	Parameter name	Parameter estimate	95% Confidence interval
Upper	Field sonde	18	16	2.12	26.06	b_0 (µS cm^{-1})	388.1	3.352
						b_1 (µS L cm^{-1} mg^{-1})	**3.194**	**0.075**
	SM 2510B	6	4	2.776	0.515	b_0 (µS cm^{-1})	384.8	1.069
						b_1 (µS L cm^{-1} mg^{-1})	**3.105**	**0.024**
Lower	Field sonde	24	22	2.074	23.31	b_0 (µS cm^{-1})	395.6	2.686
						b_1 (µS L cm^{-1} mg^{-1})	**3.222**	**0.060**
	SM 2510B	6	4	2.776	12.13	b_0 (µS cm^{-1})	392.0	5.188
						b_1 (µS L cm^{-1} mg^{-1})	**3.093**	**0.115**

$$\sigma^2_{Q,Data} = \theta^2_M \sigma^2_M + \theta^2_{\int_0^t C(t)dt} \sigma^2_{\int_0^t C(t)dt} + \theta^2_{\int_0^t C_b dt} \sigma^2_{\int_0^t C_b dt} \quad \text{(B-5)}$$

where:

σ^2_M = the variance of the tracer mass injection, mg^2;

$\sigma^2_{\int_0^t C(t)dt}$ = the variance in the integrated response curve, mg^2 s^2 L^{-1};

$\sigma^2_{\int_0^t C_b dt}$ = the variance in the integrated background concentration, mg^2 s^2 L^{-1};

$\theta_M = \dfrac{\partial Q}{\partial M}$, L mg^{-1} s^{-1};

$\theta_{\int_0^t C(t)dt} = \dfrac{\partial Q}{\partial \int_0^t C(t)dt}$, L^2 mg^{-2} s^{-2};

$\theta_{\int_0^t C_b dt} = \dfrac{\partial Q}{\partial \int_0^t C_b dt}$, L^2 mg^{-2} s^{-2}.

$$s_1^2 = \frac{\sum (y_{1i} - \bar{y}_1)^2}{n_1 - 1} \text{ and } s_2^2 = \frac{\sum (y_{2i} - \bar{y}_2)^2}{n_2 - 1} \quad \text{(B-6)}$$

$$s^2_{pool} = \frac{(n_1 - 1)s_1^2 + (n_2 - 1)s_2^2}{n_1 + n_2 - 2} \quad \text{(B-7)}$$

$$s_{\bar{Q}} = s_{pool}\sqrt{\frac{1}{n_1}+\frac{1}{n_2}} \quad \text{(B-8)}$$

$$Q - s_{\bar{Q}} t_{\nu,\alpha/2} < \eta < Q + s_{\bar{Q}} t_{\nu,\alpha/2} \quad \text{(B-9)}$$

where:
y_{1i} = the discharge estimate using response curve *i* in the Upper Reach, L s^{-1};
$\bar{y}_1$ = the mean discharge of the three discharge estimates, L s^{-1};
y_{2i} = the discharge estimate using response curve *i* in the Lower Reach, L s^{-1};
$\bar{y}_2$ = the mean discharge of the three discharge estimates, L s^{-1};
n_1 and n_2 = the number of discharge estimates, in this case each are three;
$s_{\bar{Q}}$ = the standard error, L s-1;
$t_{\upsilon,\alpha/2}$ = the probability value of the t distribution where $\alpha = 0.05$ and $\upsilon = 4$;
η = the true value of *Q*, L s^{-1}.

Table B-9. Estimated Variance of the Slug Injection Method in the Stream Discharge Calculation with 95% Confidence (Two Standard Deviations)

Reach	Slug No.	Measurement location (m)	Travel distance (m)	*M* (g)	$\int C(t)dt - \int C_b(t)dt$ (mg L^{-1} s)	*Q* (L s^{-1})	Mean *Q* (L s^{-1})	s^2_Q (L^2 s^{-2})
	1	515	63	364	1118.5	325.4		
Upper	1	515	63	364	1086.6	335.0		
	1	515	63	364	1075.3	338.5	333.0	45.8
	1	1291	39	364	970.7	375.0		
Lower	1	1291	39	364	1040.8	349.7		
	1	1291	39	364	1043.6	348.8	357.8	221.0
							s^2_{pool}	**133.4**
							s_y	4.7
							$t_{4,0.025}$	2.7776
							$s_y t_{4,0.025}$ (L s^{-1})	**26.2**

$$\sigma^2_{M_{12}} = \theta^2_Q \sigma^2_Q + \theta^2_{\int C(t)_{12}dt}\sigma^2_{\int C(t)_{12}dt} + \theta^2_{\int C_b dt}\sigma^2_{\int C_b dt} \quad \text{(B-10)}$$

where:
$\theta_Q = \frac{\partial M_{12}}{\partial Q} = \int_0^t C_{12}(t) - \int_0^t C_b dt$, mg s L^{-1};

$\theta_{\int C_{12}(t)dt} = \frac{\partial M_{12}}{\partial \int C_{12}(t)dt} = Q$, L s^{-1};

$$\theta_{\int C_{12}(t)dt} = \frac{\partial M_{12}}{\partial \int C_{12}(t)dt} = -Q \text{ , L s}^{-1}.$$

$$Q_{loss} = \frac{Q_1 \int_0^t C_{12}(t)dt}{\int_0^t C_{loss}(t)dt} - \frac{M_2}{\int_0^t C_{loss}(t)dt} \qquad \text{(B-11)}$$

$$\sigma^2_{Q_{loss}} = \theta^2_{M_2}\sigma^2_{M_2} + \theta^2_{Q_1}\sigma^2_{Q_1} + \theta^2_{\int_0^t C_{loss}(t)dt}\sigma^2_{\int_0^t C_{loss}(t)dt} + \theta^2_{\int_0^t C_b dt}\sigma^2_{\int_0^t C_b dt} \qquad \text{(B-12)}$$

where:

$\sigma^2_{M_2}$ = the variance of the mass injected from Slug #2, mg^2;

$\sigma^2_{Q_1}$ = the variance of the calculated stream discharge at Location 1 from Slug #1, L^2 s^{-2};

$\sigma^2_{\int_0^t C_{loss}(t)dt}$ = the variance in the integrated response curve from time = 0 to t at Location 1 from Slug #2, mg^2 s^2 L^{-2};

$\sigma^2_{\int_0^t C_b dt}$ = the variance in the integrated background concentration from time = 0 to t at Location 2 representing C_{loss}, mg^2 s^2 L^{-1};

Situation 1:

$$\theta_{M_2} = \frac{\partial Q_{loss}}{\partial M_2} = \frac{1}{\int_0^t C_2(t)dt} \text{, L mg}^{-1}\text{ s}^{-1};$$

$$\theta_{Q_1} = \frac{\partial Q_{loss}}{\partial Q_1} = \frac{\int_0^t C_{12}(t)dt}{\int_0^t C_2(t)dt};$$

$$\theta_{\int_0^t C_{12}(t)dt} = \frac{\partial Q_{loss}}{\partial \int_0^t C_{12}(t)dt} = \frac{Q_1}{\int_0^t C_2(t)dt} \text{, L}^2\text{ mg};$$

$$\theta_{\int_0^t C_2 dt} = \frac{\partial Q_{loss}}{\partial \int_0^t C_2(t)dt} = -\left(\frac{M_2}{\left(\int_0^t C_2(t)dt\right)^2}\right) - \frac{Q_1 \int_0^t C_{12}(t)dt}{\left(\int_0^t C_2(t)dt\right)^2} \text{, L}^2\text{ mg.}$$

Situation 2:

$$\theta_{M_2} = \frac{\partial Q_{loss}}{\partial M_2} = \frac{1}{\int_0^t C_{12}(t)dt}, \text{ L mg}^{-1}\text{ s}^{-1};$$

$$\theta_{Q_1} = \frac{\partial Q_{loss}}{\partial Q_1} = 1;$$

$$\theta_{\int_0^t C_{12}dt} = \frac{\partial Q_{loss}}{\partial \int_0^t C_{12}(t)dt} = -\left(\frac{M_2}{\left(\int_0^t C_{12}(t)dt \right)^2} \right), \text{ L}^2 \text{ mg}.$$

Examples of commonly used tracers are fluorescent dyes (e.g., rhodamine WT and fluorescein), chloride (Cl^-), bromide (Br^-), lithium (Li^+), and sodium (Na^+) [*Bencala et al.*, 1983; *Dierberg and DeBusk*, 2005; *Zellweger*, 1994]. *Zellweger* [1994] compared four tracers, Cl^-, Br^-, Li^+, and Na^+, and concluded that Cl^- and Br^- are conservative tracers. Li^+ and Na^+ were also found to behave conservatively unless the system has higher pH above neutral.

Fluorescent dyes have been used in a variety of applications in tracer experiments pertaining to both surface water and groundwater systems [*Dierberg and DeBusk*, 2005]. *Bencala et al.* [1983] used rhodamine WT as a tracer dye, but determined that it may have irreversible adsorption depending on the characteristics of the study system (e.g., organic matter content, substrate particle size, and storage features such as woody debris or vegetation). Possible sources of rhodamine WT not behaving conservatively hypothesized are: photodegradation, adsorption onto stream substrate, chemical reactions, volatilization, and uptake by living organisms.

Table B-10. Contribution of Each Variance Component to the Total Variance in Q from the Data Collection Method of the Upper Reach and the Total % Error in Q with Estimated 95% Confidence

Slug	Total	Variance Component						Q	95% conf.	% error	$s_y t_{4,0.025}$	% error	Total %
number	$\sigma^2_{Q,Data}$	θ^2Var(M)	% of	θ^2Var($\int C(t)dt$)	% of	θ^2Var($\int C_b dt$)	% of		$2(\sigma_Q)$,data	in Q from	injection	in Q from	error in
	(L^2 s^{-2})	(L^2 s^{-2})	σ^2_Q	(L^2 s^{-2})	σ^2_Q	(L^2 s^{-2})	σ^2_Q	(L s^{-1})	(L s^{-1})	data	(L s^{-1})	injection	Q
8	3.08	0.537	17.43	2.46	79.81	0.085	2.76	338.3	3.51	1.04	26.19	6.83	7.87
7	2.24	0.451	20.12	1.73	77.21	0.060	2.67	309.9	2.99	0.97	26.19	7.45	8.42
6	4.74	0.680	14.35	3.92	82.77	0.136	2.88	380.5	4.35	1.14	26.19	6.07	7.21
5	2.31	0.457	19.78	1.79	77.56	0.062	2.66	312.1	3.04	0.97	26.19	7.40	8.37
4	1.96	0.414	21.12	1.50	76.26	0.051	2.62	297.1	2.80	0.94	26.19	7.77	8.72
3	2.20	0.445	20.26	1.69	77.08	0.058	2.65	307.8	2.96	0.96	26.19	7.50	8.47
1	2.93	0.468	17.78	2.33	79.50	0.079	2.72	333.0	3.42	1.03	26.19	6.94	7.96
		Average	**18.69**		**78.60**		**2.71**			**1.01**		**7.14**	**8.15**
		StDev	2.341		2.255		0.087			0.069		0.575	0.506

Table B-11. Contribution of Each Variance Component to the Total Variance in Q from the Data Collection Method of the Lower Reach and the Total % Error in Q with Estimated 95% Confidence

Slug	Total	Variance Component						Q	95% conf.	% error	$s_y t_{4,0.025}$	% error	Total %
number	$\sigma^2_{Q,Data}$	θ^2Var(M)	% of	θ^2Var($\int C(t)dt$)	% of	θ^2Var($\int C_b dt$)	% of		$2(\sigma_Q)$,data	in Q from	injection	in Q from	error in
	(L^2 s^{-2})	(L^2 s^{-2})	σ^2_Q	(L^2 s^{-2})	σ^2_Q	(L^2 s^{-2})	σ^2_Q	(L s^{-1})	(L s^{-1})	data	(L s^{-1})	injection	Q
10	1.59	0.418	26.33	1.12	70.43	0.051	3.24	298.3	2.52	0.84	26.19	7.74	8.59
8	1.84	0.456	24.79	1.32	71.88	0.061	3.33	311.7	2.71	0.87	26.19	7.41	8.28
7	2.91	0.589	20.29	2.21	76.20	0.102	3.52	354.3	3.41	0.96	26.19	6.52	7.48
6	2.07	0.486	23.54	1.51	73.08	0.070	3.37	321.9	2.87	0.89	26.19	7.18	8.07
4	1.86	0.457	24.61	1.34	72.08	0.061	3.31	312.0	2.73	0.87	26.19	7.40	8.28
3	3.05	0.603	19.78	2.34	76.70	0.107	3.51	358.4	3.49	0.97	26.19	6.44	7.42
2	1.70	0.434	25.51	1.21	71.24	0.055	3.26	303.9	2.61	0.86	26.19	7.60	8.46
1	3.02	0.600	19.85	2.32	76.65	0.106	3.50	357.8	3.48	0.97	26.19	6.46	7.43
		Average	**23.09**		**73.53**		**3.38**			**0.91**		**7.09**	**8.00**
		StDev	2.700		2.585		0.116			0.054		0.540	0.486

Table B-12. Variance Components from Data Collection in the Dilution Gauging Results for the Upper Reach

Slug number	Q	Var(M)	Var ($\int C(t)dt$)	Var($\int C_b dt$)	θ_M	$\theta_{\int C(t)dt}$	$\theta_{\int Cbdt}$	Variance Component			Var(Q)	95% conf.
								θ^2Var(M)	θ^2Var($\int C(t)dt$)	θ^2Var($\int C_b dt$)	Total σ^2_Q	$2(\sigma_Q)$
	(L s^{-1})	(g^2)	(mg^2 s^2 L^{-2})	(mg^2 s^2 L^{-2})	(L mg^{-1} s^{-1})	(L^2 mg^{-1} s^{-2})	(L^2 mg^{-2} s^{-2})	(L^2 s^{-2})	(L^2 s^{-2})	(L^2 s^{-2})	(L^2 s^{-2})	(L s^{-1})
8	**338.3**	0.622	24.88	0.860	0.00093	-0.314	0.314	0.537	2.46	0.085	3.08	**3.51**
7	**309.9**	0.622	24.85	0.860	0.00085	-0.264	0.264	0.451	1.73	0.060	2.24	**2.99**
6	**380.5**	0.622	24.78	0.862	0.00105	-0.398	0.398	0.679	3.92	0.136	4.74	**4.35**
5	**312.1**	0.622	25.04	0.859	0.00086	-0.268	0.268	0.457	1.79	0.062	2.31	**3.04**
4	**297.1**	0.622	25.43	0.873	0.00082	-0.243	0.243	0.414	1.49	0.051	1.96	**2.80**
3	**307.8**	0.622	24.97	0.859	0.00085	-0.260	0.260	0.445	1.69	0.058	2.19	**2.96**
1	**333.0***	0.622	25.11	0.859	0.00091	-0.304	0.304	0.520	2.33	0.080	2.93	**3.42**

*Averaged value

Table B-13. Variance Components from Data Collection in the Dilution Gauging Results for the Lower Reach

Slug number	Q	Var(M)	Var ($\int C(t)dt$)	Var($\int C_b dt$)	θ_M	$\theta_{\int C(t)dt}$	$\theta_{\int Cbdt}$	Variance Component			Var(Q)	95% conf.
								θ^2Var(M)	θ^2Var($\int C(t)dt$)	θ^2Var($\int C_b dt$)	Total σ^2_Q	$2(\sigma_Q)$
	(L s^{-1})	(g^2)	(mg^2 s^2 L^{-2})	(mg^2 s^2 L^{-2})	(L mg^{-1} s^{-1})	(L^2 mg^{-2} s^{-2})	(L^2 mg^{-2} s^{-2})	(L^2 s^{-2})	(L^2 s^{-2})	(L^2 s^{-2})	(L^2 s^{-2})	(L s^{-1})
10	**298.3**	0.622	18.70	0.860	0.00082	-0.245	0.245	0.418	1.12	0.051	1.59	**2.52**
8	**311.7**	0.622	18.56	0.859	0.00086	-0.267	0.267	0.456	1.32	0.061	1.84	**2.71**
7	**354.3**	0.622	18.60	0.859	0.00097	-0.345	0.345	0.589	2.21	0.102	2.91	**3.41**
6	**321.9**	0.622	18.63	0.860	0.00088	-0.285	0.285	0.486	1.51	0.069	2.07	**2.87**
4	**312.0**	0.622	18.71	0.859	0.00086	-0.268	0.268	0.457	1.34	0.062	1.86	**2.73**
3	**358.4**	0.622	18.76	0.858	0.00098	-0.353	0.353	0.603	2.34	0.107	3.05	**3.49**
2	**303.9**	0.622	18.80	0.859	0.00084	-0.254	0.254	0.433	1.21	0.054	1.70	**2.61**
1	**357.8***	0.622	18.80	0.859	0.00098	-0.351	0.351	0.599	2.31	0.106	3.02	**3.48**

*Averaged value

Table B-14. Supporting Information for Variance in Mass Recoveries in the Upper Reach

Sub-reach number	Slug number (measurement location, m)	M (g)	Var(Q) (L^2 s^{-2})	Var ($\int C_{12}(t)dt$) (mg^2 s^2 L^{-2})	Var($\int C_b dt$) (mg^2 s^2 L^{-2})	θ_Q (L^2 mg^{-2} s^{-2})	$\theta \int C_{12}(t)dt$ (L^2 mg^{-2} s^{-2})	$\theta \int C_b dt$ (L^2 mg^{-2} s^{-2})	Mass recovered (g)	Total σ^2_M (g^2)
1	8 (92)	364	119.3	24.9	0.858	1105.4	309.9	-309.9	342.5	**148.3**
2	7 (178)	364	121.8	24.9	0.858	1169.3	380.5	-380.5	444.9	**170.3**
3	6 (240)	364	119.4	25.0	0.859	1115.4	312.1	-312.1	348.1	**151.0**
4	5 (360)	364	119.0	25.5	0.879	1020.8	297.1	-297.1	303.3	**126.4**
5	4 (452)	364	119.3	25.5	0.879	888.7	307.8	-307.8	273.6	**96.7**
6	3 (515)	364	120.0	25.0	0.860	1073.1	332.9	-332.9	357.3	**141.1**

Table B-15. Supporting Information for Variance in Mass Recoveries in the Lower Reach

Sub-reach number	Slug number (measurement location, m)	M (g)	Var(Q) (L^2 s^{-2})	Var ($\int C_{12}(t)dt$) (mg^2 s^2 L^{-2})	Var($\int C_b dt$) (mg^2 s^2 L^{-2})	θ_Q (L^2 mg^{-2} s^{-2})	$\theta \int C_{12}(t)dt$ (L^2 mg^{-2} s^{-2})	$\theta \int C_b dt$ (L^2 mg^{-2} s^{-2})	Mass recovered (g)	Total σ^2_M (g^2)
7	9 (813)	364	118.9	18.9	0.858	1148.5	311.7	-311.7	357.9	**158.7**
8	8 (877)	364	112.0	18.6	0.858	965.7	354.3	-354.3	342.2	**114.3**
9	7 (995)	364	119.14	18.7	0.858	984.7	321.9	-321.9	316.9	**117.5**
10	6 (1091)	364	118.93	18.6	0.859	955.8	312.0	-312.0	298.2	**110.5**
11	4 (1160)	364	120.12	18.7	0.859	1101.3	358.5	-358.5	394.8	**148.2**
12	3 (1235)	364	118.77	18.7	0.860	1030.6	303.9	-303.9	313.2	**128.0**
13	2 (1291)	364	120.09	18.7	0.856	969.8	357.8	-357.8	347.0	**115.4**

Table B-16. Variance Components of the Total Variance in Recovered Mass, % Change in Mass, and Estimated 95% Confidence Intervals for the Upper Reach

Sub-reach number	Measurement location (m)	Slug travel distance (m)	Total σ^2_M (g^2)	Variance component: $\theta^2\mathrm{Var}(Q)$ (g^2)	% of σ^2_M	$\theta^2\mathrm{Var}(\int C_{12}(t)dt)$ (g^2)	% of σ^2_M	$\theta^2\mathrm{Var}(\int C_b dt)$ (g^2)	% of σ^2_M	$\%M_{12}$	ΔM (g)	$\%\Delta M$	Error in $\%\Delta M$
1	92	140	148.3	145.8	98.3	2.39	1.61	0.08	0.06	94.1	-21.4	**-5.9**	±7.1
2	178	109	170.3	166.5	97.8	3.61	2.12	0.12	0.07	122.2	80.9	**22.2**	±5.9
3	240	87	151.0	148.5	98.3	2.43	1.61	0.08	0.06	95.7	-15.8	**-4.4**	±7.1
4	360	145	126.4	124.0	98.2	2.25	1.78	0.08	0.06	83.3	-60.7	**-16.7**	±7.4
5	452	145	96.7	94.2	97.4	2.41	2.50	0.08	0.09	75.2	-90.4	**-24.8**	±7.2
6	515	99	152.8	150.0	98.1	2.77	1.81	0.10	0.06	102.3	8.2	**2.3**	±6.6
				Average	**98.0**		**1.90**		**0.07**				±**6.9**
				StDev	0.36		0.34		0.01				0.56

Table B-17. Variance Components of the Total Variance in Recovered Mass, % Change in Mass, and Estimated 95% Confidence Intervals for the Lower Reach

Sub-reach number	Measurement location (m)	Slug travel distance (m)	Total σ^2_M (g^2)	Variance component: $\theta^2\mathrm{Var}(Q)$ (g^2)	% of σ^2_M	$\theta^2\mathrm{Var}(\int C_{12}(t)\,dt)$ (g^2)	% of σ^2_M	$\theta^2\mathrm{Var}(\int C_b dt)$ (g^2)	% of σ^2_M	$\%M_{12}$	ΔM (g)	$\%\Delta M$	Error in $\%\Delta M$
7	813	146	158.7	156.9	98.8	1.81	1.14	0.08	0.05	98.4	-6.0	**-1.7**	±7.0
8	877	105	114.3	111.9	97.9	2.34	2.04	0.11	0.09	94.0	-21.8	**-6.0**	±6.3
9	995	163	117.5	115.5	98.3	1.93	1.65	0.09	0.08	87.1	-47.1	**-12.9**	±6.8
10	1091	148	110.5	108.7	98.3	1.81	1.64	0.08	0.08	81.9	-65.8	**-18.1**	±7.1
11	1160	111	148.2	145.7	98.3	2.40	1.62	0.11	0.07	108.5	30.8	**8.5**	±6.2
12	1235	106	128.0	126.2	98.6	1.72	1.35	0.08	0.06	86.1	-50.8	**-14.0**	±7.2
13	1291	83	115.4	112.9	97.8	2.39	2.07	0.11	0.09	95.3	-17.0	**-4.7**	±6.2
				Average	**98.3**		**1.64**		**0.08**				±**6.7**
				StDev	0.35		0.34		0.02				0.46

Table B-18. Supporting Information for the Variance in Q_{loss} from Each Variable of the Upper Reach

Sub-reach number	Q_1 (L s-1)	$\int C_{12}(t)dt - \int C_b dt$ (mg s L^{-1})	$\int C_2(t)dt - \int C_b dt$ (mg s L^{-1})	Var(M_2) (g2)	Var(Q_1) (L2 s-2)	Var ($\int C_{12}(t)dt$) (mg^2 s^2 L^{-2})	Var($\int C_2 dt$) (mg^2 s^2 L^{-2})	θ_{M2} (L mg^{-1} s^{-1})	θ_{Q1} (L^2 mg^{-2} s^{-2})	$\theta_{\int C12(t)dt}$ (L^2 mg^{-2} s^{-2})	$\theta_{\int C2dt}$	Var(Q_{loss}) Total σ^2_Q (L^2 s^{-2})
1	309.9	1105.4	1075.9	0.62	119.3	24.9	24.9	0.00093	1.03	0.29	-0.61	137.8
2	380.5	1169.3	1174.6	0.62	121.8	24.9	24.9	0.00085	1.00	0.32	-0.59	132.3
3	312.1	1115.4	956.6	0.62	119.4	25.0	24.8	0.00105	1.17	0.33	-0.78	180.6
4	297.1	1020.8	1166.1	0.62	119.0	25.5	25.0	0.00086	0.88	0.25	-0.49	99.4
5	307.8	888.7	1225.0	0.62	119.3	25.5	25.4	0.00082	0.73	0.25	-0.42	69.4
6	333.0	1073.1	1182.4	0.62	120.0	25.0	24.9	0.00085	0.91	0.28	-0.52	107.9

Table B-19. Supporting Information for the Variance in Q_{loss} from Each Variable of the Lower Reach

Sub-reach number	Q_1 (L s-1)	$\int C_{12}(t)dt - \int C_b dt$ (mg s L^{-1})	$\int C_2(t)dt - \int C_b dt$ (mg s L^{-1})	Var(M_2) (g2)	Var(Q_1) (L2 s-2)	Var ($\int C_{12}(t)dt$) (mg^2 s^2 L^{-2})	Var($\int C_2 dt$) (mg^2 s^2 L^{-2})	θ_{M2} (L mg^{-1} s^{-1})	θ_{Q1} (L^2 mg^{-2} s^{-2})	$\theta_{\int C12(t)dt}$ (L^2 mg^{-2} s^{-2})	$\theta_{\int C2dt}$	Var(Q_{loss}) Total σ^2_Q (L^2 s^{-2})
7	311.7	1148.5	1220.2	0.62	118.9	18.6	18.7	0.00082	0.94	0.26	-0.48	111.4
8	354.3	965.7	1167.7	0.62	120.0	18.6	18.6	0.00086	0.83	0.30	-0.52	89.2
9	321.9	984.7	1027.2	0.62	119.1	18.7	18.6	0.00097	0.96	0.31	-0.65	119.7
10	312.0	955.8	1130.8	0.62	118.9	18.6	18.6	0.00088	0.85	0.28	-0.52	91.9
11	358.4	1101.3	1166.5	0.62	120.1	18.7	18.7	0.00086	0.94	0.31	-0.56	115.1
12	303.9	1030.6	1015.4	0.62	118.8	18.7	18.8	0.00098	1.01	0.30	-0.66	132.7
13	357.8	969.8	1197.5	0.62	120.1	18.7	18.8	0.00084	0.81	0.30	-0.50	85.5

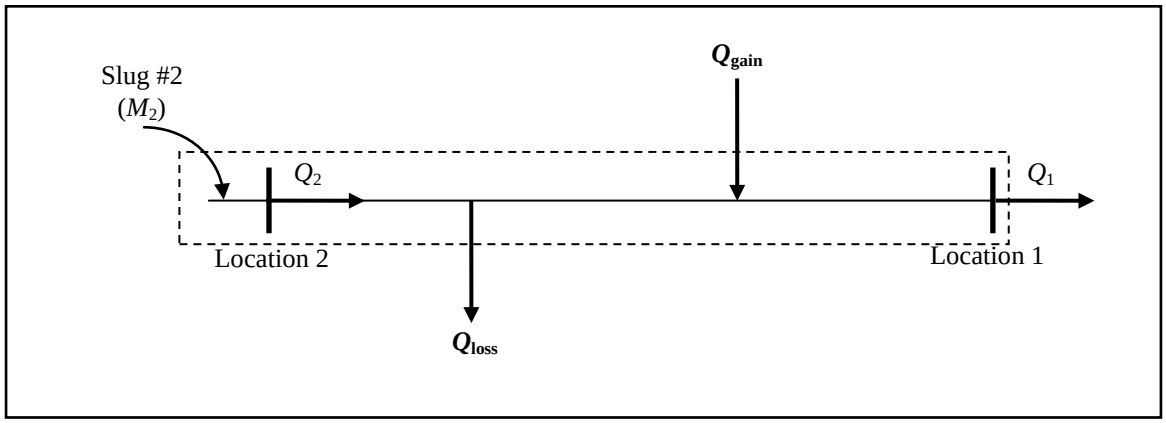

Figure B-4. Diagram (not to scale) of Situation 1: a loss occurring before a gain.

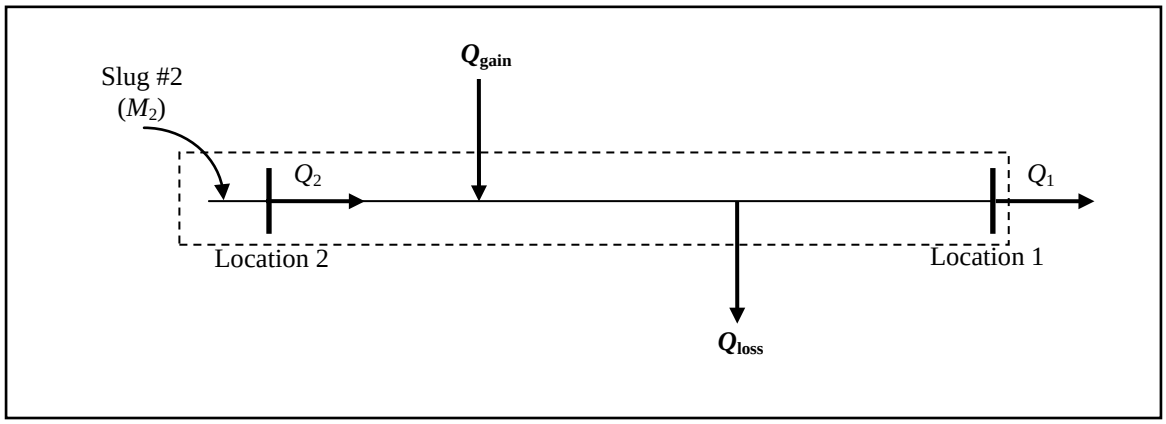

Figure B-5. Diagram (not to scale) of Situation 2: a gain occurring before a loss.

APPENDIX C

High Frequency Discharge Estimates

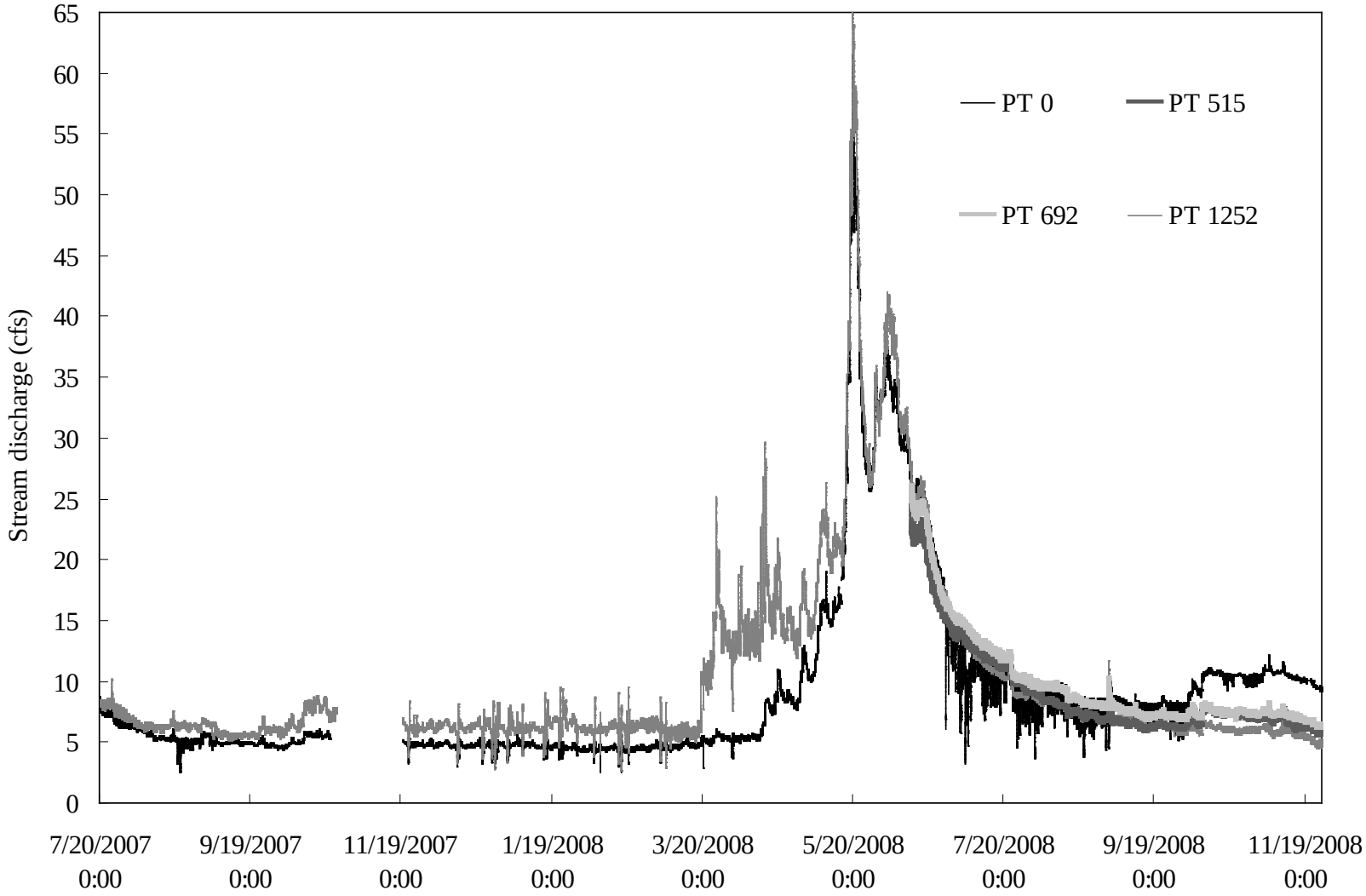

Figure C-1. Eighteen months of high-frequency discharge estimates at the Upper and Lower Reach boundaries.

APPENDIX D

Sub-reach Bottom Slopes and Additional Water Table Contours

Table D-1. Upper Reach Average Bottom Slopes for Each Sub-reach, One Standard Deviation of the Sub-reach Bottom Slopes, and the Overall Average

Reach	Sub-reach Number	Sub-reach interval (m)	Average bottom slope
Upper	1	11 to 92	0.023
	2	92 to 178	0.023
	3	178 to 240	0.032
	4	240 to 360	0.021
	5	360 to 452	0.028
	6	452 to 515	0.013
		Average	0.023
		StDev	0.007

Table D-2. Lower Reach Average Bottom Slopes for Each Sub-reach, One Standard Deviation of the Sub-reach Bottom Slopes, and the Overall Average

Reach	Sub-reach Number	Sub-reach interval (m)	Average bottom slope
Lower	7	713 to 813	0.018
	8	813 to 877	0.018
	9	877 to 995	0.019
	10	995 to 1087	0.010
	11	1087 to 1161	0.013
	12	1161 to 1235	0.020
	13	1235 to 1291	0.011
		Average	0.016
		StDev	0.004

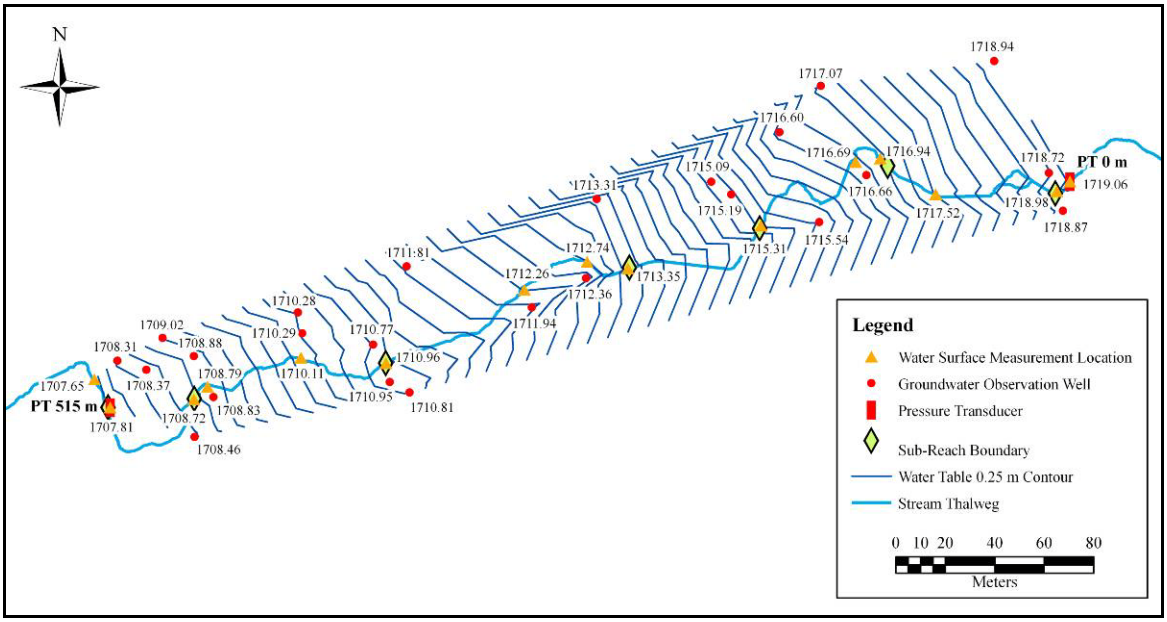

Figure D-1. Discrete head information collected on July 16, 2008 for the Upper Reach.

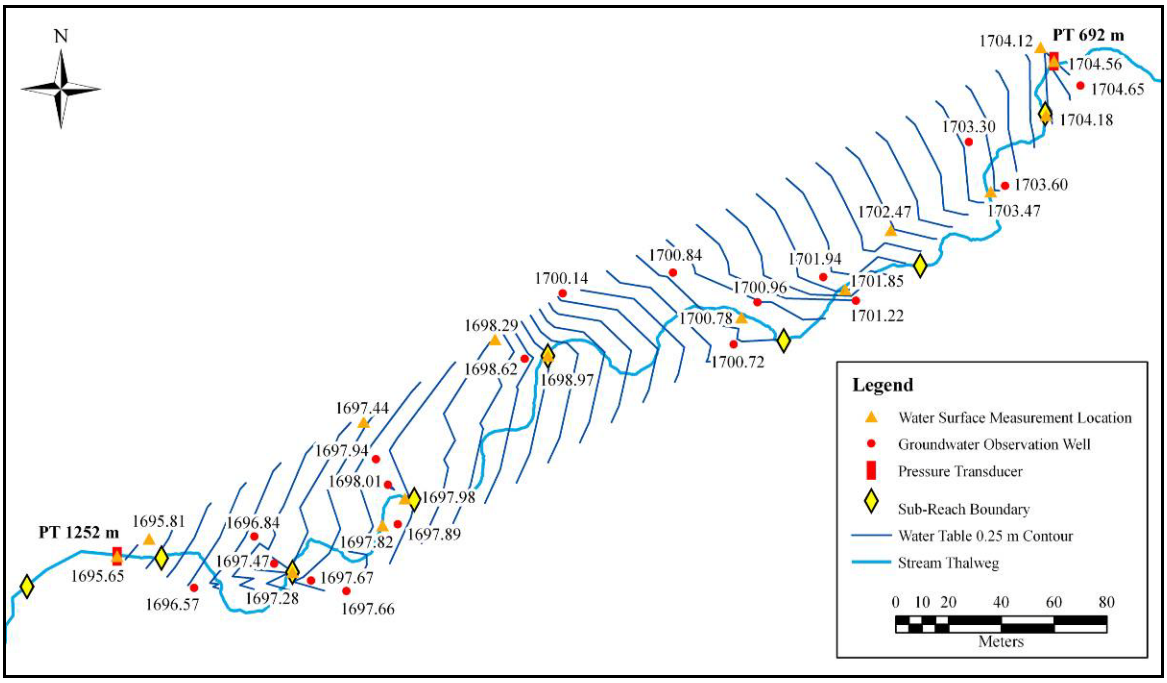

Figure D-2. Discrete head information collected on July 16, 2008 for the Lower Reach.

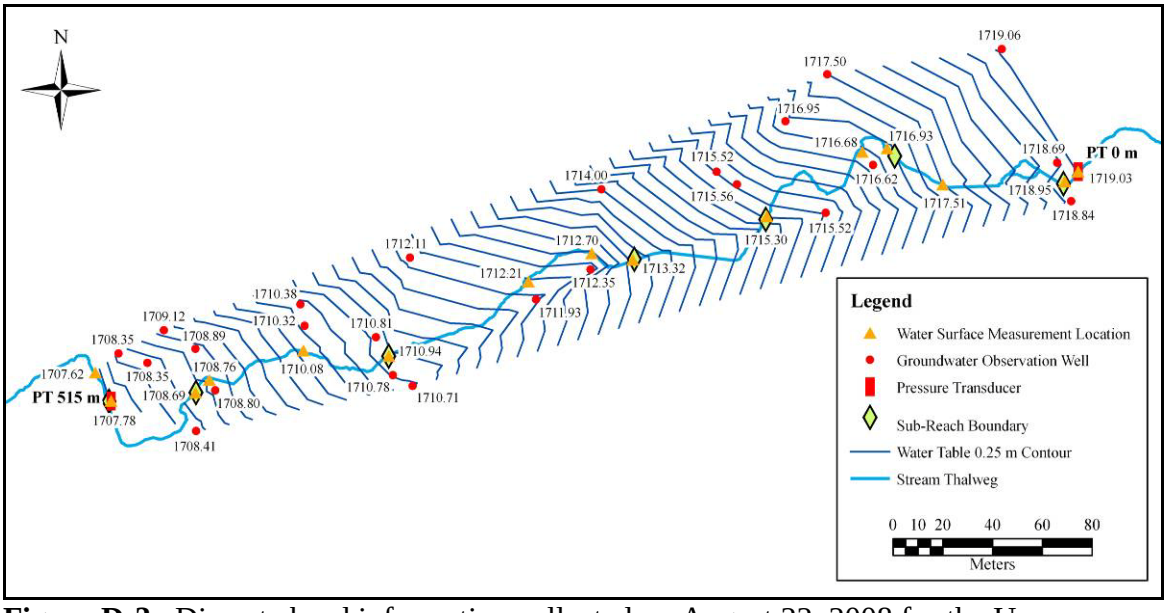

Figure D-3. Discrete head information collected on August 22, 2008 for the Upper Reach.

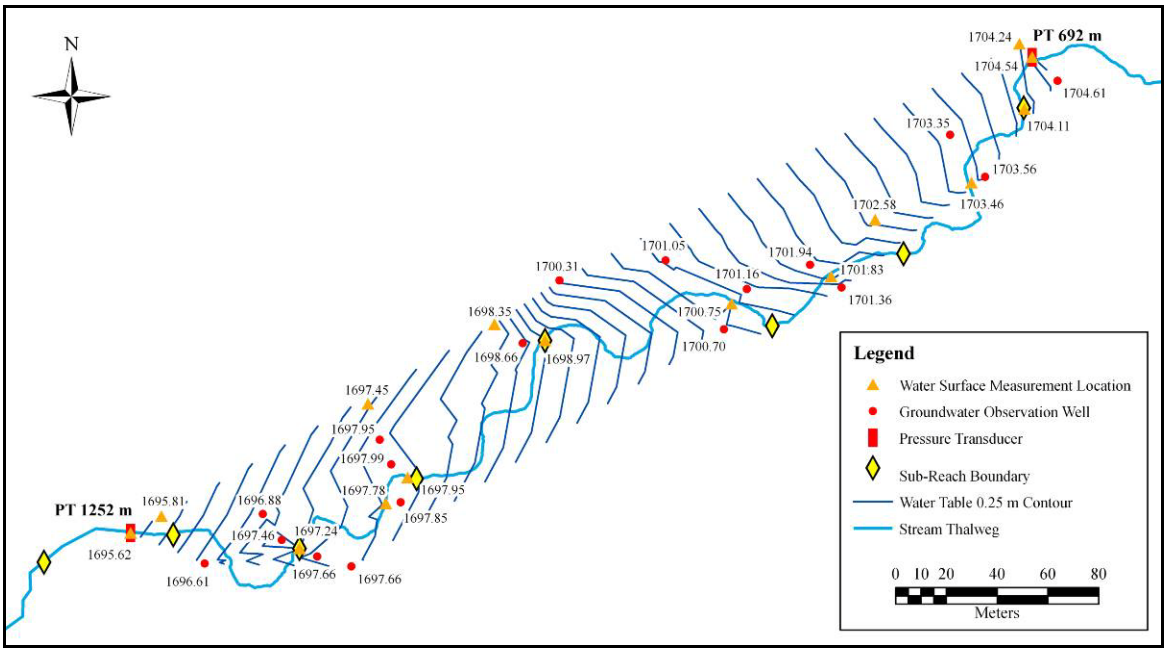

Figure D-4. Discrete head information collected on August 22, 2008 for the Lower Reach.

APPENDIX E

Example Linear Regression Analysis for Hydraulic Conductivity Estimations and Groundwater Quality Parameters

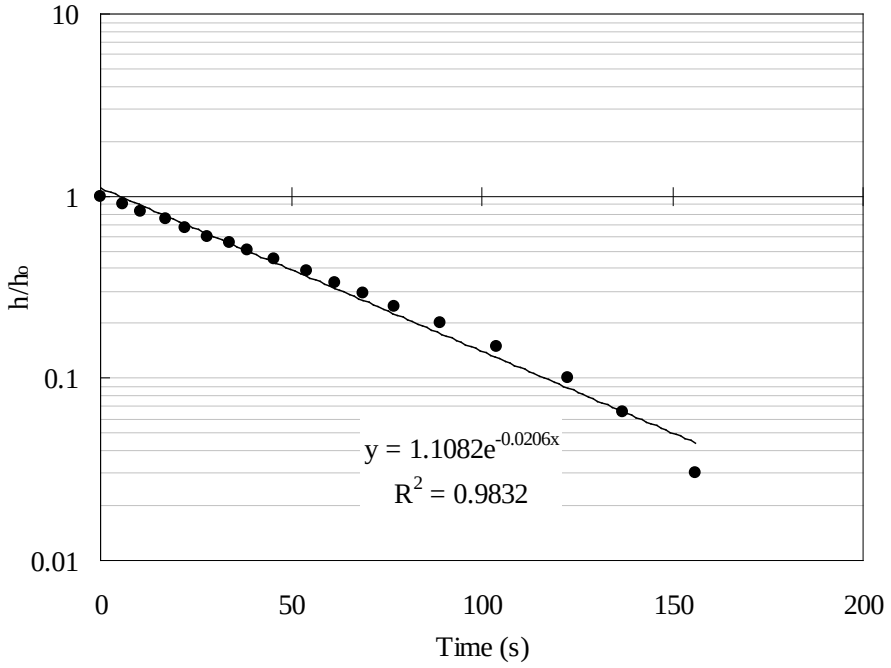

Figure E-1. Linear regression analysis for the hydraulic conductivity of stream location 240 m at a depth of 9 cm.

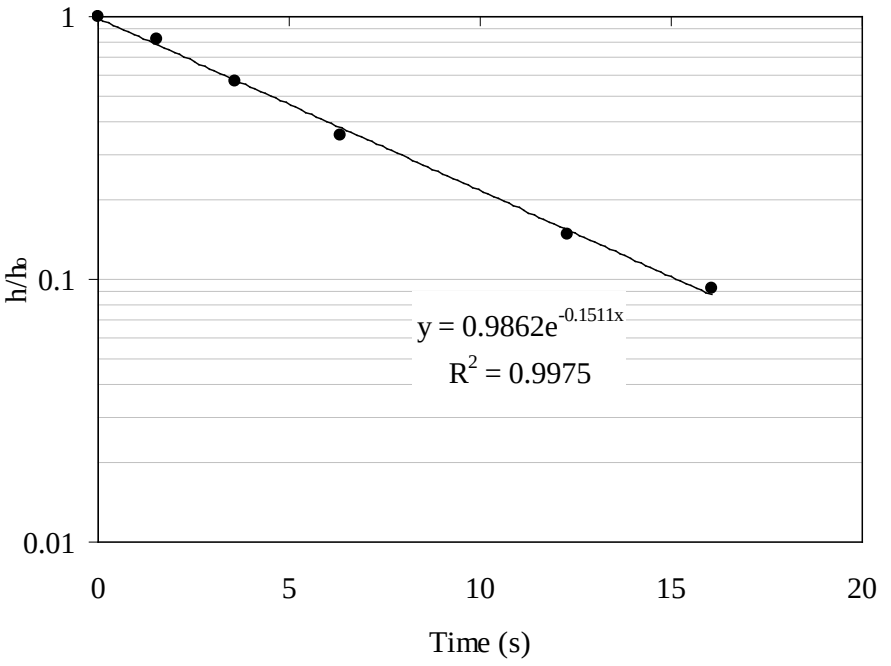

Figure E-2. Linear regression analysis for the hydraulic conductivity of stream location 240 m at a depth of 20 cm.

Table E-1. Upper Reach Groundwater Chloride Concentration, SC, and Temperature

Reach	Sample location	Chloride concentration ($mg\ L^{-1}$)	Laboratory SC ($\mu S\ cm^{-1}$)	Field temperature (°C)
Upper	W1	13.63	534	20.7
	W2	8.07	608	15.9
	W4	7.23	452	15.4
	Surface seep 104 m	9.43	538	11.2
	W7	13.07	650	19.0
	Surface seep 153 m	23.08	510	-
	W8	17.26	604	17.4
	W11	6.12	385	15.4
	W13	8.89	560	16.4
	W16	7.51	476	16.8
	W17	10.58	666	15.4
	W19	9.87	533	14.7
	W20	22.49	704	14.5
	W23	13.27	618	14.5
	Average	12.18	560	15.9
	StDev	5.42	88.3	2.3

Table E-2. Lower Reach Groundwater Chloride Concentration, SC, and Temperature

Reach	Sample location	Chloride concentration ($mg\ L^{-1}$)	Laboratory SC ($\mu S\ cm^{-1}$)	Field temperature (°C)
Lower	W25	252.20	1330	16.2
	W26	61.49	628	14.6
	W27	295.50	1400	15.1
	Surface seep 825 m	19.61	571	12.0
	W29	119.01	1140	16.7
	W30	22.43	613	15.2
	W31	40.35	542	14.6
	W33	20.80	790	16.1
	W34	11.90	573	-
	W36	34.25	516	15.0
	W37	160.15	1020	15.4
	W39	16.28	455	15.9
	W40	15.92	504	14.7
	W42	13.60	464	15.2
	Surface seep 1238 m	19.67	443	12.6
	Average	73.54	733	15.0
	StDev	92.09	327	1.3